Doctoral Dissertation
Doctoral Program in Environmental Engineering (30th Cycle)

Large Scale Simulation of IDEAL CITY under Seismic Scenario

Sebastiano Marasco

******

Supervisor
Prof. Gian Paolo Cimellaro

Doctoral Examination Committee:
Prof. Paolo Bazzurro, Referee, IUSS Pavia
Dr. Paolo Clemente, Referee, ENEA
Prof. Luca Martinelli, Politecnico di Milano
Prof. Pietro Cornetti, Politecnico di Torino
Dr. Marco Domaneschi, Politecnico di Torino

Politecnico di Torino
September 10, 2018

I hereby declare that, the contents and organization of this dissertation constitute my own original work and does not compromise in any way the rights of third parties, including those relating to the security of personal data.

…………………………………..…

Sebastiano Marasco
September 10, 2018

Summary

Widespread urbanization is a recent phenomenon. Cities are centers of economic activity and innovation so that many people are attracted to better jobs positions, services and prospects for improved living conditions. Furthermore, the urban population growth varies considerably worldwide but a common increasing trend is observed in the large cities. Then, modern society is critically dependent on a network of complex and interdependent systems which compose the urban environment. For this reason, urban areas are particularly vulnerable due to the high concentration of people and economic assets, and in many cases, their hazard-prone location.

When a natural disaster such as earthquake strikes an urban area, the majority of the losses in terms of casualties and repair costs are due to the buildings extensive damage and collapse. Therefore, urban buildings portfolio represents the most vulnerable physical system of a built environment.

This thesis presents research conducted in the prediction of the damage experienced by the building stock located in urban areas following a seismic event. A physical simulation model is proposed to assess the seismic capacity of individual building and then estimate the level of damage caused by a pre-defined seismic scenario on the exposed building portfolio. A large scale virtual city, named *IDEAL CITY*, consisting of different buildings categories and infrastructure is designed envisioned as being representative of the typical Italian building stock. An intensive data collection and processing is performed to create a comprehensive building exposure database that provides numerous benefits in estimates of potential damage due to catastrophic events.

The proposed simulation model provides an efficient perspective to estimate the seismic vulnerability of any individual building within a large-scale area subjected to a given seismic scenario.

Acknowledgment

First, I would like to thank my advisor, Prof. Gian Paolo Cimellaro, for making this dissertation possible. Your guidance was necessary every step of the way and I will always appreciate it.

I have several people that I would like to acknowledge that have guided me and supported my ideas. I must thank Prof. Stephen A. Mahin and his research group for their constructive supports on both academic and social level during my period in Pacific Earthquake Engineering Research Center.

The research leading to these results has received funding from the European Research Council under Grant Agreement No. ERC_IDEAL RESCUE_637842 of the project IDEAL RESCUE-Integrated Design and Control of Sustainable Communities during Emergencies.

Lastly, special thanks to my mother, my father, and my brother for their unconditional love and support. No amount of words can express my gratitude for all they have done for me.

I would like to thank Cristina for giving me the ability to keep going, I would not have been able to do this without her.

I would like to dedicate this thesis to my family and Cristina

Contents

List of Tables

List of Figures

Chapter 1

Disaster resilience

1.1 Introduction

According to the World Bank, disasters have killed 58,000 people on average each year and affected another 225 million people worldwide since 1990. The rising of global populations and the massive economic development in areas prone to disasters have increased the chance of catastrophic incidents, which leads to disruption of buildings and infrastructure. Over the years, community resilience has attracted tremendous attention due to the increasing number of natural and man-made disasters. The concept of resilience is multi-dimensional, and therefore involves various subjects of different disciplines. In engineering, resilience is the ability to "withstand stress, survive, adapt, and bounce back from a crisis or disaster and rapidly move on". It can also be defined as "the ability of social units (e.g. organizations, communities) to mitigate hazards, contain the effects of disasters when they occur, and carry out recovery activities in ways to minimize social disruption and mitigate the effectors of further earthquakes". The absence of a concise and methodical approach makes it extremely difficult to evaluate resilience.

In the last decade, earthquake engineers have given more attention to life safety of damaged buildings, while less attention has been given to socio-economic parameters. Nowadays, attention is shifting towards the necessity to focus also on the loss of functionality and the rapidity of recovery of the structure. Shorter recovery processes are possible at the building level if the structure has little or no damage; otherwise it might take months to recover.

Seismic resilience describes the loss and loss recovery required to maintain the function of the system with minimal disruption. According to this statement, Bruneau et al. (2003) claimed that seismic resilience is defined as "the ability of a system to reduce the chances of a shock, to absorb such a shock if it occurs (abrupt reduction of performance) and to recover quickly after a shock (re-establish normal performance)".

The response of a community to a disaster is assessed by taking into account all the subjects, elements, and processes which take place at a given community scale. According to this definition, it is important to define all the attributes of resilience at the community level. In this thesis, specific attention has been paid on the prediction of physical damage on the building portfolio of an urban area. This could be considered as the first essential step of resilience-based approach and it is always considered a challenge to community developers and decision makers.

Despite, the goal of this research is to develop a simulation model to assess the damage to the building portfolio of a large-scale area under a given seismic scenario; it is essential and helpful to introduce the main concepts of resilience.

1.2 Resilience Based Design (RBD)

The resilience definition provided by Bruneau et al. (2003) has been clarified and extended in Cimellaro et al. (2010a). According to them Resilience (R) is defined as a function indicating the capability to sustain a level of functionality or performance of a given building, bridge, lifeline networks, or community, over a period defined as the control time T_{LC}. Analytically, *resilience performance index* is defined as

$$R(\vec{r}) = \int_{t_{OE}}^{t_{OE}+T_{LC}} Q_{TOT}(t)/T_{LC}\, dt \tag{1}$$

where $Q_{TOT}(t)$ is the global performance function of the considered region; T_{LC} is the control time of the period of interest that is usually decided by owners, or society (usually is the life cycle, life span of the system etc.); t_{0E} is the time instant when the event happens; $\vec{r}$ is the vector defining the geospatial coordinate of the system within the selected region where the resilience index is evaluated (Cimellaro et al. 2010b). The time T_{LC} includes the building recovery time, T_{RE} and the business interruption time that is usually smaller compared to the other one. The performance function is the combination of all functionalities related to different facilities, lifelines, etc. for the case when physical infrastructures, resources and services are considered. Schematic representation of disaster resilience is shown in Figure 1.

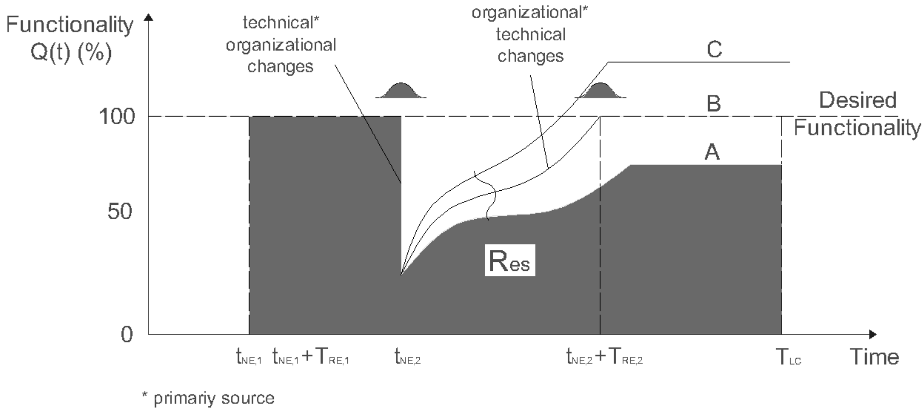

Figure 1. Example of resilience functions (Bruneau *et al*., 2007).

Resilience is graphically defined as the normalized area underneath the performance function of a system (functionality $Q(t)$). The term $Q(t)$ is a non-stationary stochastic process and each ensemble is a piecewise continuous function as the one shown in Figure 1, and it is measured as a dimensionless (percentage) function of time. Consider a single catastrophic event (E), resilience is given by the following equation (Bruneau *et al*., 2007).

$$Q(t)=\left[1\text{-L}\left(\text{I,T}_{\text{RE}}\right)\right]\left[H\left(\text{t-t}_{0\text{E}}\right)-H\left(\text{t-}\left(\text{t}_{0\text{E}}+T_{RE}\right)\right)\right]f_{\text{Rec}}\left(t,t_{0E},T_{RE}\right) \qquad (2)$$

where $L(I,T_{RE})$ is the loss function; $f_{REC}\ (t,t_{0E},\ T_{RE})$ is the recovery function; $H(t_0)$ is the Heaviside step function, T_{LC} is the control time of the system, T_{RE} is the recovery time from event E and; t_{NE} is the time of occurrence of event E. The recovery time T_{RE} and the recovery path are two key components for evaluating resilience, so they should be estimated accurately.

In the seismic engineering field, the seismic performance of the system is measured through a unique decision variable (DV) that combines other variables (economic losses, casualties, recovery time, etc.). Then the functionality of the system is defined by means of the direct and indirect losses caused by the seismic event.

Resilience is considered as a dynamic quantity that changes over time and across space. It can be applied to engineering, economic, social, and institutional infrastructures, and can use various geographic scales. The first in quantifying the resilience performance index (R) is to define the spatial scale (e.g. building, structure, community, city, region, etc.) of the problem of interest. It is also important to mention that the entire recovery process is affected by the spatial scale of the disaster. Huge disasters will have longer recovery processes. The spatial scale will also be used for defining the performance measures that will be considered in defining the global functionality of the system.

The second step is to define the temporal scale (short term emergency response, long term reconstruction phase, midterm reconstruction phase, etc.) of the problem of interest (in the figure below). The selection of the control period

T_{LC} will affect the resilience performance index. Therefore, when comparing different scenarios, the same control period should be considered.

The RBD methodology can be used on a scenario basis or include uncertainties (probabilistic approach) when a particular level of confidence of achieving performance objective is of interest. In the probabilistic approach, the expected value of resilience index (random value) is estimated by considering five types of random variables which are identified by the i*ntensity measure*, *response measure*, *performance measure*, *recovery time measure*, and *resilience index*.

1.3 Dimensions of resilience

Resilience can be enhanced by reducing the likelihood of failure of critical infrastructure (thereby, reducing their impacts) and speeding up the time it takes to make a full recovery. In an effort to enhance these disaster resilience characteristics, researchers at the MCEER (Bruneau, et al. 2003; Bruneau and Reinhorn 2007) have identified four fundamental properties. These are *robustness, resourcefulness, redundancy,* and *rapidity*. Graphical explanation of the robustness and rapidity concept is given in Figure 2.

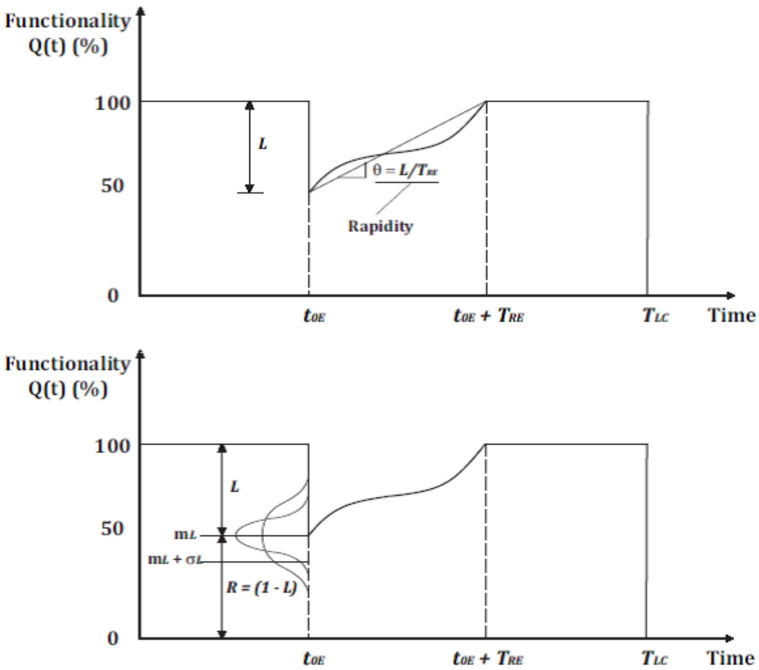

Figure 2. Rapidity (a) and robustness (b) properties.

1.3.1 Robustness

Robustness is the “strength, or the ability of elements, systems or other units of analysis to withstand a given level of stress, or demand without suffering degradation or loss of function” (Bruneau et al., 2003). With respect to infrastructural qualities, NIST defines the robustness as “the inherent strength or resistance in a system to withstand external demands without degradation or loss of functionality”. Practically, the robustness represents the residual functionality right after the extreme event (Figure 2.b) and can be represented by the following relation

$$Robustness = 1 - \tilde{L}(m_L, \sigma_L); \tag{3}$$

where $\tilde{L}$ is a random variable expressed as function of the mean m_L and the standard deviation σ_L.

1.3.2 Rapidity

Rapidity is the "capacity to meet priorities and achieve goals in a timely manner in order to contain losses and avoid future disruption" (Bruneau et al., 2003). According to the NIST report (2015), rapidity is defined as "the speed with which disruption can be overcome and safety, services, and financial stability restored". Mathematically, it represents the slope of the functionality curve (Figure 2.a) during the recovery-time and it can be expressed by the following Equation.

$$Rapidity = \frac{dQ(t)}{dt}; \quad for: t_{0E} \le t \le t_{0E} + T_{RE} \tag{4}$$

An average estimation of the rapidity is given by the ratio between the loss (L) is the loss or drop of functionality right after the event's occurrence and the recovery time (T_{RE}).

1.3.3 Redundancy

Redundancy is "the quality of having alternative paths in the structure by which the lateral forces can be transferred, which allows the structure to remain stable following the failure of any single element" (FEMA 356, 2000). In other words, it describes the availability of alternative resources in the recovery process of a system. In the structural field redundancy also refers to "the multiple availabilities of load-carrying components or multiple load paths which can bear additional loads in the event of failure. If one or more components fail, the remaining structure is able to redistribute the loads and thus prevent a failure of the entire system. Redundancy depends also on the geometry of the structure and the properties of the individual load-carrying elements. Furthermore, Bruneau et al. (2003) defined redundancy as "the extent to which elements, systems, or other units of analysis exist that are substitutable, i.e. capable of satisfying functional requirements in the event of disruption, degradation, or loss of functionality"

1.3.4 Resourcefulness

Resourcefulness is "the capacity to identify problems, establish priorities, and mobilize resources when conditions exist that threaten to disrupt some element, system, or other unit of analysis; resourcefulness can be further conceptualized as consisting of the ability to apply material (i.e., monetary, physical, technological, and informational) and human resources to meet established priorities and achieve goals" (Bruneau et. al., 2003). This is a property that is difficult to quantify, since it mainly depends on human skills and improvisation during the extreme event. Referring to infrastructural qualities, NIST defines resourcefulness as "the capacity to mobilize needed resources and services in emergencies".

Resourcefulness and Redundancy are strongly interrelated. Changes in Resourcefulness and Redundancy will affect the shape and the slope of the recovery curve and the recovery time T_{RE}. Adding resources can reduce time recovery beyond what is expected by the benchmark normal condition. In theory, if infinite resources were available, time recovery would asymptotically approach zero.

1.4 Resilience assessment approaches

The vagueness of the concept of resilience makes it difficult to define but it becomes even more problematic when trying to measure it. Most researchers in the field emphasize that research on measuring community resilience is still in the early stages of development. There is no single or widely accepted method to the measurement issue as the landscape of resilience indicators is messy and increasingly hard to navigate (Cutter et al. 2014). This is particularly the case for community resilience to disasters, since this concept raises not only questions related to the measurement of resilience, but also related to the definition and conceptualizations of communities. Since communities are interconnected system whose indicators may apply to different scales and policy realms and also address different types of shocks.

Assessment and measurement of resilience can be performed according to four different types of approaches:

- *Indices* which quantitatively represent a selected characteristic of the analyzed system. Indices are statistically evaluated and they have to summarize the observations or measurements by aggregating multiple characteristics into a single value.
- *Scorecards* provide an evaluation of performance or progress toward a goal. Example of these approaches is the checklist which identifies a series of questions related to presence or absence of resilience-related items and actions. According to the question's results, a score is produced based on how many often the items are present, used, and so forth.
- *Models* provide a simplified representation of system processes using mathematical expressions which are capable to describe the relationships and the interactions in the real world. Models can be used to characterize resilience of a system for a specific point of view (such as economic, social, etc.) in a computational way or to characterize the resilience of specific places (Renscher et al. 2010).
- *Tools* provide guidance for assessing resilience with sample procedures and survey instruments, or data for use in compilation of indices or scorecards.

Resilience measurement methods can be resumed in:

- *Idiographic (bottom-up)* which are locally generated and customized to particular places (Pfefferbaum et al. 2015). They represent a qualitative methodology which uses localized data that may not be widely available.
- *Nomothetic (top-down)* which is focused on comparisons across varying units of analysis. Bigger spatial units (such as states or nations) are used in this measurement approach, allowing to compare units of analysis using standardized data, what makes these types of resilience indices more appropriate for assessing spatial variability, allocating resources, and/or monitoring progress-all done at state, national, or international scales.

Each type of approach may refer to a small unit (e.g. single building) or large scale (*City level, Region level, Nation level*). This classification reveals the appropriate scale of the resilience assessment and also affects the methods of data collection. Table 1 resumes some of proposed resilience measurement approaches specifying the type, spatial scale, and method.

Table 1. Resilience measurement approaches.

Measure name	Type	Spatial	Method
APIRE	Tool	Country	Top down
BRIC	Index	USA Countries	Top down
CART	Tool	Community	Bottom up
CCRAM	Tool	Community	Bottom up
CDRI	Index	USA Coastal Countries	Top down
Coastal Resilience Index	Score-card	Community	Bottom up
CoBRA	Tool	Community	Bottom up
Community Resilience System	Tool	Community	Bottom up
Community Resilience Index	Index	Community	Top down
CREAT	Tool	Infrastructure	Top down
DFID Resilience	Tool	Country	Bottom up
FAO Livelihoods	Index	Community	Bottom up
Financial System Resilience	Index	Infrastructure	Top down
FM Global Resilience	Index	Infrastructure	Top down
NIST	Tool	Infrastructure	Top down
Oxfam GB	Index	Community	Bottom up
PEOPLES	Tool	Community	Top down

1.5 Resilience framework

A conceptual framework is needed for understanding resilience at community level at each scale. The scale, unit of analysis, and temporal variability are essential issues in a resilience framework. The scale refers to the domain size in which the processes are investigated. While the scale of these processes can be local or global, the unit of analysis varies from the individual to the continental. Whenever local information is available, global comparisons can be carried out through aggregation processes. On the other hands, global information and processes can be downscaled to evaluate the impact of a specific event on the local level.

In addition to the scale and unit of analysis, the temporal variability is another important issue to be considered. In the context of disaster resilience, is fundamental to analyze the disaster with reference to the action rapidity in order to provide the adequate response actions.

Bruneau et al. (2003) identified four types of resilience that should be adequately measured: Technical; Organizational; Social; and Economical, (TOSE). Technical and economical resilience are mainly related to the physical systems, while organizational and social resilience are related to the society and the nonphysical systems. *Technical resilience* describes the capability of a system to perform its functionality. *Organizational resilience* describes the ability of the organization(s) to manage the system. *Social resilience* concerns how well society copes with the loss of services as a result of a blackout. Finally, e*conomic resilience* describes the capability to reduce both indirect and direct economic losses (Rose and Liao, 2005).

1.6 Dimension of resilience framework

The response of a community to a disaster is assessed by taking into account all the subjects, elements, and processes which take place at a given community scale. According to this definition, it is important to define all the resilience dimensions which describe the attributes of resilience at the community level. Generically, the community resilience dimensions can be resumed as below:

- *Physical*. Physical dimension refers to the infrastructures that compose the community's built environment. It incorporates both facilities (housing, commercial, and cultural facilities) and lifelines (food supply, health care, utilities, transportation, and communication networks, medical, financial). Furthermore, lifeline infrastructures include also energy utilities and companies, transportation systems (roads and highways, railroads, airports, and seaports), water distribution network, communication systems, and health care facilities (Renschler et al., 2010).
- *Social/cultural*. According to Norris et al. (2008), "*individuals invest, access, and use resources embedded in social networks to gain returns* ". Thus, social/cultural aspects are important prerequisite to community competence

(Norris et al., 2008) in that it incorporates the array of services that the community has chosen to provide for itself, understanding that community health requires more than good jobs and infrastructure. In the context of disaster resilience, social vulnerability is a pre-existing condition of the community that affects the society's ability to prepare for and recover from a disruptive event.

- *Institutional*. The socio-economic activity is regulated through the governmental system of norms, informal conventions, formal laws, regulations, and procedures (Institutional services). Example of Institutional services is legal and security services (e.g. police, emergency, fire department, military, etc.), public health and hygiene services, and cultural heritage services. These organized governmental services are essential in sustaining communities before, during and after hazardous events.
- *Economic*. The economic dimension refers to a set of decision rules that aligns community's subjects to the financial services, production and employment pattern, and guides the economic decision-making process. The community economic structure is characterized by production of goods and services and their distribution. The impact of an extreme event son the economic dimension is strictly affected to the population employed within the various industries and distributions vector (economic development indicator).
- *Ecological*. While resilience is a critical element of resource management and is necessary to sustain desirable ecosystem states in the face of unknown futures and variable environments, it is not easily assessed. Resilience of a system depends on various factors such as time scale, the actual disturbance, the structure of the system, and control measures or polices that are available to be implemented.

1.7 Outline

The core goal of this research is to develop a simulation model to assess the damage to the building portfolio of a large-scale area under a given seismic scenario. The building exposure database is envisioned as being representative of the typical Italian housing stock. Moreover, the building attributes are collected and manipulated based on the seismic standard construction procedures associated with different periods of construction.

First, a general overview on disaster resilience (Chapter 1) and simulation and models (Chapter 2) are presented. Detailed state of the art on disaster simulation in built environment and description of the available methodologies for damage assessment of building portfolio are provided (Chapter 3).

A virtual city (*IDEAL CITY*) consisting of different buildings categories is designed to be representative of the Italian building stock. Furthermore, the intensive typological-based data processing is described and adopted to create the comprehensive exposure database of the typical Italian housing portfolio (Chapter 4).

A simplified and efficient physical model is presented to simulate the global seismic capacity of any individual building within urban areas (Chapter 5).

To test the proposed simulation model, two different simplified seismic scenarios are defined (Chapter 6).

Nonlinear time history analyses are performed to assess the performance of the buildings, while a seismic response model is proposed to predict the demand parameter associated with the level of damage (Chapter 7).

The integrated large scale simulation environment is implemented and all of its processes are detailed explored (Chapter 8).

The two selected seismic scenarios are applied to the exposed virtual city and the associated outcomes are illustrated. Furthermore, two case studies are assumed to validate both building's capacity model and damage assessment procedure (Chapter 9).

Chapter 2

Simulation and models

2.1 Introduction

Simulation represents the bridge between theory and experiment and it has to be able to describe the operation of a generic system over time, whereas the model is the system itself. A system is defined as a group of objects that are joined together in some regular interactions (named interdependences) toward the accomplishment of some purpose. The system is defined through its boundary between the system and the external environment. A system is composed by different terms:

- entity: object of the system;
- attribute: property of an entity;
- activity: specified time period.

The study of a system is strictly dependent on the collection of variables that describe the system at any time (*state* of the system). The number of collected variables affects the precision in defining the entities of the system. When an *event* occurs within the system (endogenous) or into the environment that affects the system (exogenous), the state of the system might change. Supposing to consider a built environment as system and an earthquake as exogenous event, an example of entities, attributes, and activities are depicted in Figure 3.

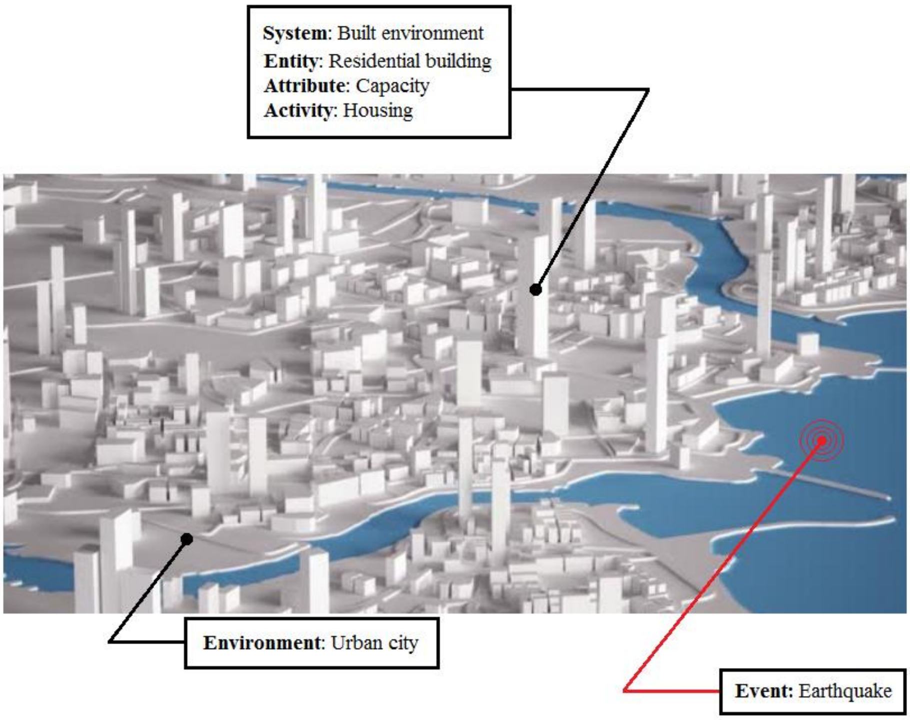

Figure 3. Components of a built environment exposed to a seismic event.

In the example showed in Figure 3, the state variables might be the damage to structural and nonstructural elements.

In a simulation process it is important to understand how the system changes and operates during and after the occurrence of an event. Thus, it is necessary to study the relationships between the components of the system, or in other words to experiment with the system itself. For this purpose, the first key step is represented by the model development that consists in the representation of a system through the definition of its entities, attributes, and activities according to the purpose of the study.

This chapter has been thought to provide useful information related to the simulation modeling. Furthermore, the general practice and theory of simulation are provided in this chapter.

2.2 Types of models

Models are used to represent a system and they can be classified according to different aspects. The first classification is associated with the nature of the relationships which describe the model. For this purpose, the models can be distinguished into *mathematical models* and *physical models*. The first ones express the relationships in terms of formulas. For example, the relationship between the force needed to move an object and the moving distance can be expressed by the work's formula given by the product between the force and the distance (*Work =Force x Distance*). A physical model is a larger or smaller physical representation of an object. In this case, the geometry of the object represents an important factor. Furthermore, a model can be studied over time considering its alteration in a period of time (*dynamic model*). On the contrary, a *static model* represents a system at a particular state in time. Based on the state variables changing, a generic model can be defined as *discrete model* if the state variables change at a discrete set of time steps. When the state variables change continuously over time, the system is named *continuous model*.

Moreover, the classification of the models can be also carried out according to the nature of the variables. When the model contains one or more random variables is named as *stochastic model*, whereas if no random variables are contained, the model is classified as *deterministic model*. Deterministic models have a specified set of inputs which leads to have a unique set of outputs. On the contrary, stochastic models will have random outputs due to the random nature of the input variables. Furthermore, the stochastic models are intended as estimates of the real characteristic of the system's entities, attributes, and activities. This leads to have statistical output measure expressed by average (mean or median) and dispersion parameters. Figure 4 resumes the types of models above discussed.

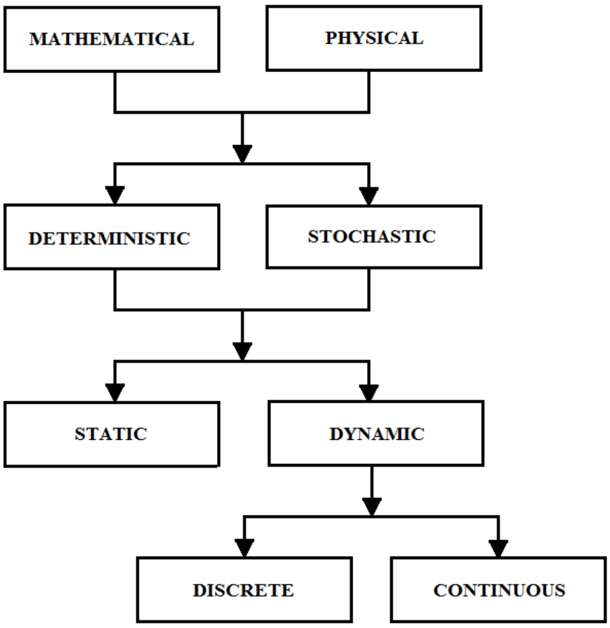

Figure 4. Types of models.

2.3 Simulation process

The simulation process is as much complex as the complexity of the problem. Generally, the steps in a simulation study can be resumed as listed below:

1. *Problem formulation:* the statement of the problem represents the key point of any simulation. The problem's solution is strongly affected by the understanding of the problem itself. Then, all the subjects involved in the simulation process (managers, customers, stakeholders, analysts) must be actively participate and communicate in the problem formulation and understanding.

2. *Objectives and project plan setting:* the simulation has to be capable to give answers to all the questions established at the starting point. Once the objectives are stated, the project plan has to be clearly defined in order to provide an effectiveness of the simulation process. It should include the complete plan in terms of costs, people involved, and time required in each phase.
3. *Model conceptualization:* the conceptualization of the model has to capture the developer's idea. In this stage it is important to abstract the essential features of the problem, and define the basic assumptions which characterize the system. The conceptualization's effort is proportional to the complexity of the system which has to be coherent to the purpose of the study. Also in this stage it is suggested to involve the users in order to increase the quality and confidence of the model.
4. *Data collection:* the entities, attributes, and activities are the basis of the model construction. The required data and their accuracy depend on the complexity of the model. Therefore, the data collection is among the most important and critical simulation steps, then it results time consuming. In addition, the potential use of certain data (e.g. customer records for marketing, public data recorded by a governmental institution, etc.) and any sharing must be disciplined through specific rules. In these cases, the circumstances in which data have been obtained, the notifications given to the data applicant, and the permission obtained must be clearly expressed. Very often, the availability of certain data might be limited or they can result inaccessible.
5. *Model translation:* the real system has to be translated into computer recognizable format in order to be manipulated through specific simulation software managed by programming languages. Many simulation software are available in the market to assist and support in the modeling and analyzing any problem. The modeler can also develop the entire simulation software but some advanced skills of programming languages and knowledge on software architecture are required. The translation of the model into computer recognizable format is performed with reference to three model management processes:
    - *Information storage*. All the collected data have to be stored and managed in order to be accessible at every time.
    - *Algorithm development*. The functionality of the system and its behavior is studied through the development of on-purpose algorithms. An algorithm represents a sequence of actions to be performed in a finite amount of space and time through a given formal language. In the context of simulation, the algorithms allow to control the actions which calculate the functions involved in the assessment of the system's response.
    - *Visualization features*. The visualization of the response of the system to an external action is important for decision makers. The visualization provides a powerful tool to investigate the response of the system and to take decisions about it.

6. *Model Verification*: the computer program has to be verified. The verification phase concerns the debug process. When the input parameters and the logical structure of the model are correctly represented in the computer, the verification is completed.
7. *Model Validation:* the model needs to be compared with the real system. Validation procedure may be performed by using an iterative process which allows enhancing the model until reaching an adequate accuracy.
8. *Implementation:* the simulation model building process affects the outcome of the implementation and then each single phase of the process has to be clearly performed. It is worth highlighting that an invalid model leads to erroneous results which, if implemented, are costly and time consuming.

The consecutive and ordered steps used in a simulation process are resumed in Figure 5.

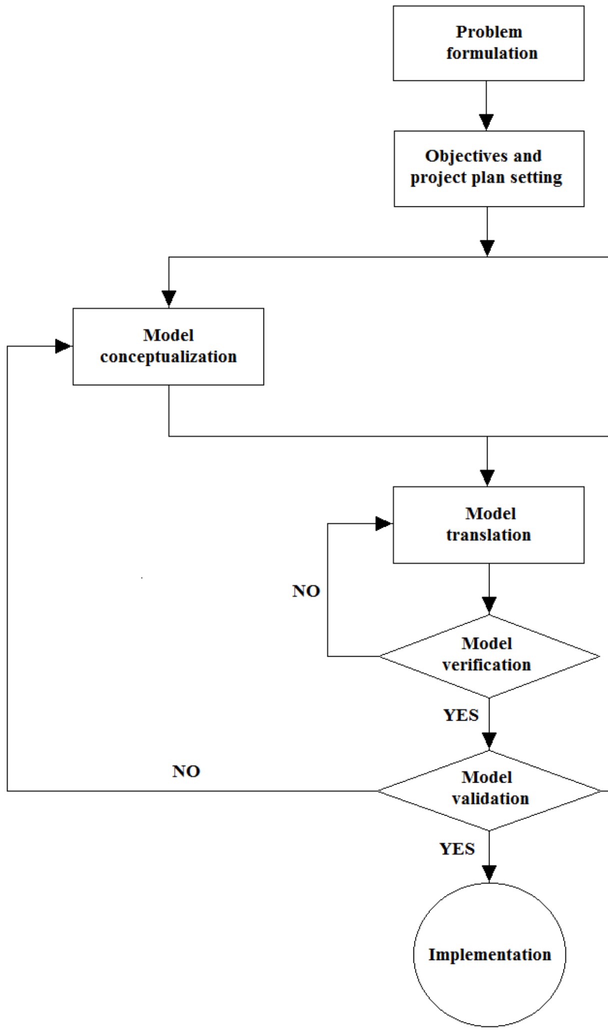

Figure 5. Simulation process flow.

Verification phase consists in correcting model by finding and fixing modeling errors (debugs) through specific techniques. Verification phase may require several iterative loops, which causes some changing in the model translation and further verification phases. Similarly, the validation is aimed to reach adequate model accuracy by comparing the real system to the model. Validation refers to the processes and techniques that the model's developer, customer, and decision makers jointly use to assure that the model represents the real system. Very often, the validation process require a modification in the model building phase (model conceptualization and data collection) in order to reach a certain level of accuracy.

A simple and clear graphical definition of modeling, simulation phases, and activities was provided by the Technical Committee on Model Credibility of the Society for Computer Simulation (Schlesinger, 1979), (Figure 6).

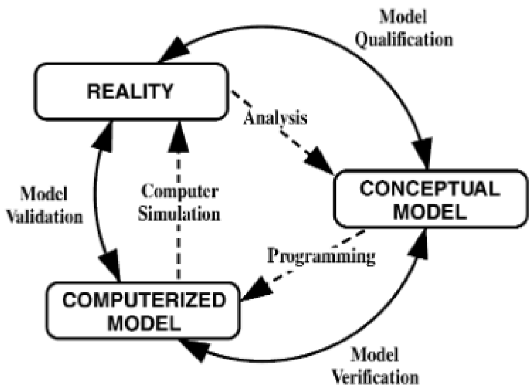

Figure 6. Modeling and simulation phases according to Schlesinger, 1979.

The conceptual model of the real system is developed through specific analysis. Programming is aimed to convert the model conceptualization into a computer recognizable format (computerized model). Then, computer simulation is performed to accurately simulate the real system behavior. The activities which interconnect the simulation phases are grouped into the model qualification, model verification, and model validation.

2.4 Model conceptualization stages

Model conceptualization phase refers to the establishment of the conceptual problem to be solved through simulation. Model conceptualization is achieved by performing the steps below listed:

1. *Specification of physical system*: the first step of model conceptualization is aimed to develop a specification of the physical system and the surrounding environment. The specification of physical system can be resumed in the following steps:
   - system-environment specification
   - scenario abstraction
   - coupled physics specification
   - nondeterministic specification

Specification of the system includes:

- physical event or sequence of events
- element of the system (entities and attributes)
- physical processes (activities)

The complete description of the physical system is made by formulation of the fundamental assumptions associated with its elements, processes, and events. In this phase no mathematical formulation are made, but the model statement is conceptually treated. Furthermore, the event or sequence of events has to be analyzed. This leads to define possible scenarios in the simulation that affects the response of the physical system depending also on the environment's characteristics.

It is also important to define the interactions between the system's elements and system and environment (coupled physics specification). All the nondeterministic characteristics of the physical system and the environment have to be satisfactory treated. The nondeterministic quantities are affected by the uncertainties which have to be considered in the analyses.

2. *Mathematical modeling*: the description of the physical system and process is carried out through mathematical models. The mathematical modeling process can be resumed in the following steps:
   - solving equations specification
   - auxiliary physical equations specification
   - initial or boundary conditions specification
   - nondeterministic values specification

A dynamic physical system is mathematically formulated by complete specification of the system's relationships, and auxiliary and initial conditions of the system. In the case of stochastic variables, the mathematical modeling consists also in the selection of appropriate statistical distributions which describe the random variables. The predictive power of a model depends on identifying the dominant controlling factors and their influences rather than its completeness. Thus, a complex and complete mathematical model is not the better solution in the conceptualization phase. It is suggested to use limited and effective mathematical formulation to describe the system. In other words, the mathematical modeling should be as much as useful and simple. This sentence is confirmed by Box (1979), who claimed that "All models are wrong, some are useful".

2.5 Model translation stages

The real system has to be translated into computer recognizable format. Model translation can be performed through the following two stages:

1. *Discretization and algorithm selection for the mathematical models*: in this stage the mathematical models are converted into a specific form. The continuous mathematic forms have to be discretized to formulate the

mathematical problem in a numerical form which is addressable for computational analysis. The discretization process has to be carried out based on the requirements of *consistency* of the equations, *stability* of the numerical method, and *adequate approximation* between the continuum and discrete system. Moreover, the deterministic and/or stochastic methodologies expressed through sequence of actions, which will be performed in the further analysis, have to be specified. In other words, this stage focuses in the development of the algorithms that control the behavior of the system and its interactions with the surrounding environment.

2. *Computer programming*: the algorithms selected in the previous stage have to be converted into a computer language. This stage is also named as computer programming or coding which allows specifying a given set of instructions aimed to produce specific type of output. These instructions are expressed in a computer formal language (programming language).

2.6 Modeling errors and uncertainties

Each phase of modeling and simulation is affected by uncertainties and errors. The errors can be also defined as recognizable inaccuracy in any phase or activity of modeling and simulation that is not due to the lack of knowledge. Very often, the model and the simulation may show an inaccuracy due to the divergence between the model and the real system. Practical project constraints (such as cost, time schedule, complexity) may impose to accept this divergence (recognizable errors). The characteristics of recognizing errors lead to identify them as acknowledged errors. Moreover, some errors could be not recognized by the modeler, but they are generically recognizable. In these cases, the errors are called unacknowledged errors.

Based on the nature of the error in the modeling process, it is possible to distinguish the following categories of modeling errors:

1. *Project management errors*: modelers, analysts, customers, decision makers, equipment vendors, consultant engineers, etc. are involved in the simulation process (problem formulation and objectives and project plan setting phases). The communications issues between those subjects are crucial for successfully manage the modeling and simulation activities. Very often, unclear communication and people's responsibility may result in errors during the simulation process.
2. *Data Errors*: they refer to the form and completeness of the input data. Very often, the quantity of data required to build a model could result extremely large. Furthermore, the process to collect the input data is bureaucratically complicated and time consuming, then some data are reasonably assumed according to statistical dataset. The accuracy and/or completeness of the collected data are important in limiting the errors.
3. *Data Modeling Errors*: the inappropriate use of the data for modeling can cause data modeling errors. Common example of this kind of errors is

represented by the assumption of an inadequate statistical distribution for stochastic models or uncorrected mathematical formulation which describes the deterministic model.

4. *Logic Modeling Errors*: they are related to the errors committed in the model translation phase. The logic modeling errors are dependent on the languages used at the implementation stage. Naturally, these errors can be reduced by the technical modeler's skill.

The uncertainties are grouped into *aleatory* and *epistemic* accordingly to the nature of the uncertainty itself. The aleatory uncertainty describes the inherent variation associated with the considered system and environment. They are usually quantified by probability distributions characterized by means of own statistical parameters. The epistemic uncertainty is associated with the *inaccuracy in any phase or activity of modeling process that is due to lack of knowledge and alternative modeling assumption*. In the context of modeling and simulation, the source of epistemic uncertainty can be found in incomplete information. The information is classified as incomplete when the data collecting process and the model conceptualization result:

- *vague* that is related to the communication language;
- *nonspecific* which refers to the variety of possible alternatives;
- *dissonant* when conflicting evidences are totally or partially observed.

2.7 Example of simulation and modeling process

The simulation and modeling processes involve in different steps and they are used to predict future events. In this section, an example of long-range trajectory of bullet via atmospheric flight to final impact point is analyzed. The entire simulation phase is discussed to give a more detailed idea of the simulation and modeling process for a physical system.

1. *Problem formulation*: some assumption has to be made to clarify the statement of the problem. For the examined case, the following assumptions are made:
   - The bullet is fired from a rifle attached to a steel support.
   - The free atmospheric flight is considered;
   - The bullet motion depends on moment variations, gravity forces and Magnus effect.

Figure 7 depicts a scheme of the problem statement.

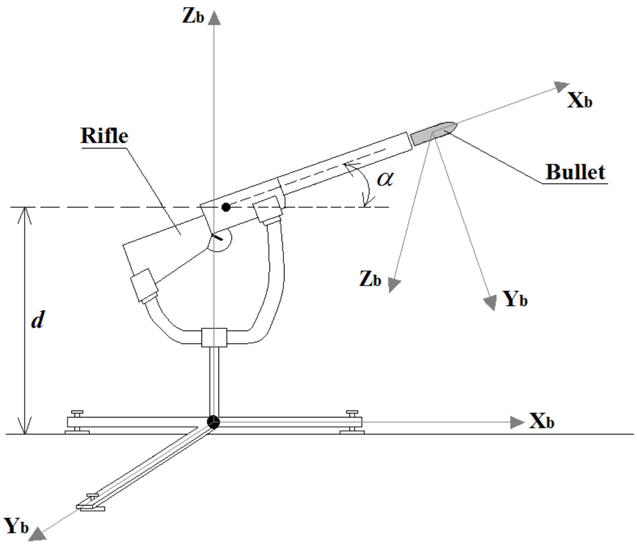

Figure 7. Example of the parameters used to describe the simulation problem.

The fixed reference system is represented by the axes X_G-Y_G-Z_G which have origin at the firing site. The X_b-Y_b-Z_b is a no-roll rotating reference system on the bullet body.

2. *Model conceptualization: specification of physical system*: As previously mentioned, the specification of the physical system and environment is the first step to be addressed. Then, the physical elements which are considered part of the system and the environment have to be carefully defined. Furthermore, the interactions among the system's elements and the environment-system influence have to be defined. This last process is strongly influenced by the engineering judgment and they are not unique. In other words, several possible scenarios must be defined to have a satisfactory description of the reality. For the bullet trajectory estimation, the possible *system-environment specification*, *scenario abstraction*, *coupled physics specification*, and *nondeterministic specification* are resumed in Figure 8.

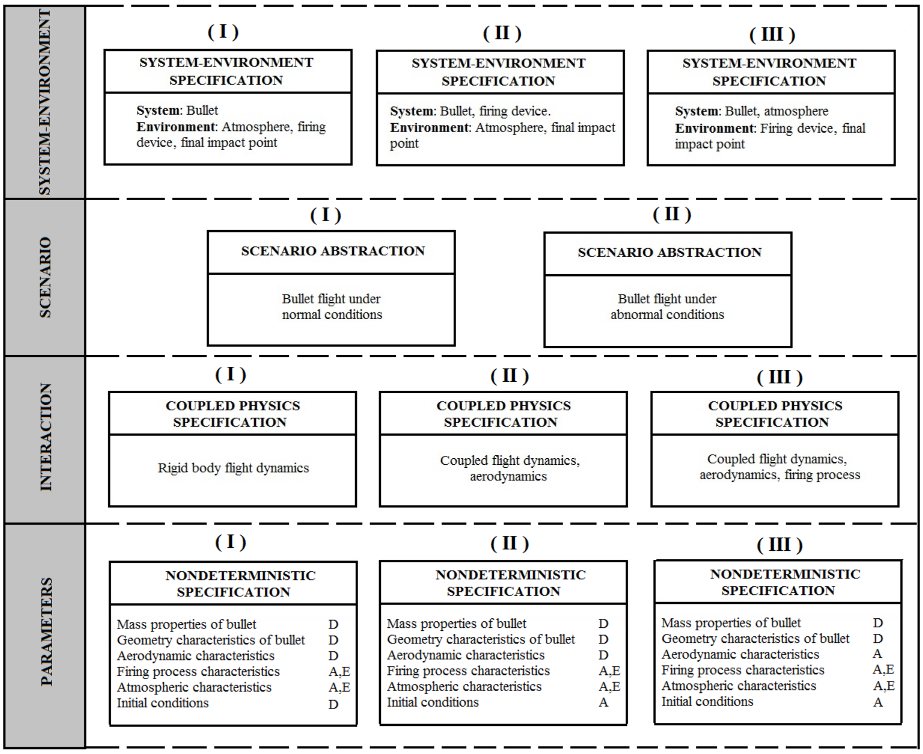

Figure 8. Scheme of the model conceptualization through a set of different system-environment, scenario, interaction, and parameters specification.

The first system-environment specification is the simplest one. Only the bullet is considered as system, whereas the atmosphere, firing device, and final impact point are considered as environment. In the second system-environment specification the elements of the system are the bullet and the firing device, while the atmosphere and the final impact point constitute the environment. In this case the interaction between the bullet and the firing process affects the estimation of the bullet's trajectory. When the bullet traverses the barrel of the gun, minor deformation occurs (set-back deformation) due to the imperfection in rifling within the barrel. The effects of these imperfections may affect the trajectory of the bullet, and then the coupling of the system bullet-firing device is analyzed. In the third system-environment specification the system is composed by the bullet, whereas the atmosphere and the firing device and the final impact point are considered as environment. The flow field around the bullet affects its trajectory, and then the interaction bullet-atmosphere has to be analyzed.

Different scenarios must be investigated to have exhaustive and more accurate results coming from the simulation. For the analyzed example, two different scenarios are assumed based on the weather conditions: normal and abnormal conditions. The first ones refer to the normal weather conditions (e.g. low wind, no rain) whereas the second ones consist in hostile conditions such as strong wind and rain or snow.

The coupled physics specification is aimed to define the interactions among the elements of a physical system. Regarding the considered example, three coupled physics specification are analyzed. The first one assumes the bullet as rigid-body without considering any other coupling, and then the bullet responds only to the forces coming from the environment. The second coupled physics specification couples the flight dynamics (or external ballistic) with the aerodynamic loading, which results in a time dependent fluid (atmosphere-bullet interaction) simulation. The third coupled physics specification refers to a complete coupling of all physics that could exist in the problem. Thus, the coupling among the flight dynamics, aerodynamic loading, and firing process is considered. The firing process refers to the internal ballistic which studies how the energy required to fire the bullet from the rifle is generated. Furthermore, the bullet travel through the rifle barrel affects the simulation of the bullet trajectory.

The last issue to be considered in the model conceptualization is the nondeterministic specification which includes the aleatory and/or epistemic uncertainties in the process. The atmospheric characteristics and the pressure generation within the rifle barrel (firing process characteristics) are considered as stochastic variables because affected by uncertainties. For example, the firing process characteristics depend on the temperature of burning propellant, whereas the atmospheric characteristics are given by the wind direction and velocity and temperature of the air. These parameters are unknown, then statistical model have to be used to estimate the rifle performance and atmospheric conditions. Different set of nondeterministic parameters could be specified based on the level of knowledge. Three different set of nondeterministic parameters are considered. In the first nondeterministic specification the geometric and mass characteristic of the bullet, the aerodynamic characteristics (such as drug and lift force aerodynamic coefficients, Magnus moment aerodynamic coefficient, etc.), and the initial conditions are considered as deterministic (*D*) whereas the firing process characteristics and atmospheric characteristics are assumed as nondeterministic parameters. The initial condition refers to the characteristics of the bullet at the firing site (e.g. initial velocity, distance between the bullet's center of the mass and ground, etc.). The letter *A* and *E* are associated with the aleatory and the epistemic uncertainties, respectively. In the second nondeterministic specification the initial conditions are also considered as aleatory uncertainties. In the third case, the entire set of physical parameters is considered as nondeterministic except the mass and geometry characteristics of the bullet.

3. *Model conceptualization: mathematical modeling:* the free atmospheric bullet flight is evaluated through a six degree of freedom rigid bullet model, where the position and orientation of the bullet at fixed time is given by the three translational components (x,y,z) and three Euler angles (φ, θ, ψ). The velocity of the bullet at each time is also required to predict its trajectory. Thus, three translational ($u, \tilde{v}, w$) and rotational velocities have to be considered in the mathematical modeling. The rotational velocity components are named as yaw ($\tilde{r}$), roll (p), and pitch (q) which causes forces keeping the bullet off a straight axis of flight. Figure 9 shows the six components defining the position and orientation of the bullet and the other six components which refer to the velocity of the bullet.

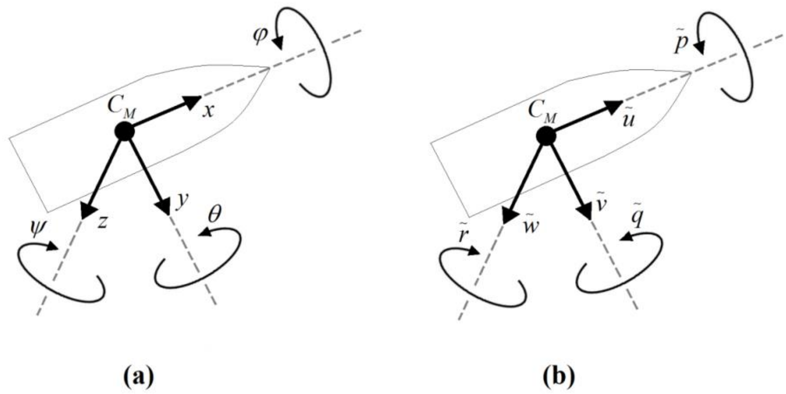

Figure 9. Parameters used to represent the position (a) and orientation (b) of a bullet.

The mathematical model describing the bullet dynamic trajectory consists of twelve first Ordinary Differential Equations (ODEs). These equations express the linear and angular momentum conservation law. The ODEs require a set of additional equations (auxiliary physical equations) which complete the mathematical formulation. Examples of these equations are those ones that describe the environmental excitation conditions and the bullet's aerodynamic conditions expressed by aerodynamic coefficients (e.g. drag force coefficient, lift force coefficient, Magnus moment coefficients, etc.).

Furthermore, the Initial Conditions (ICs) of the system have to be formulated. In the analyzed case, the ICs are expressed by means of the initial firing velocity (V_0), initial spin rate at the rifle muzzle (p_0), orientation of rifle (α), distance between the rifle's center of the mass and the ground (*d*). Naturally, the initial conditions are affected by the aleatory and the epistemic uncertainties. The bullet free trajectory's problem is a well-known physical process, and then the ODEs used to describe the process might be only affected by acknowledged errors. These errors are due to the simplification or approximation of the problem (such as consider the bullet as perfect rigid-body). On the other hand, using high fidelity mathematical models requires high computational costs associated with their solutions.

The last step in the mathematical modeling is represented by the selection of appropriate statistical distributions. Let's suppose to consider the nondeterministic specification *I* showed in Figure 8. In this case the firing process and atmospheric characteristics are assumed as stochastic parameters. The firing process is described by the pressure generated within the rifle barrel which provides an initial velocity to the bullet (V_0), whereas the atmospheric characteristics are expressed by the aerodynamic coefficients. In this example the initial bullet's velocity is supposed to be normally distributed, while the aerodynamic coefficients are expressed through the specified mean values experimentally estimated.

Figure 10 depicts the mathematical modeling process flow used to predict the bullet's trajectory in the free atmosphere.

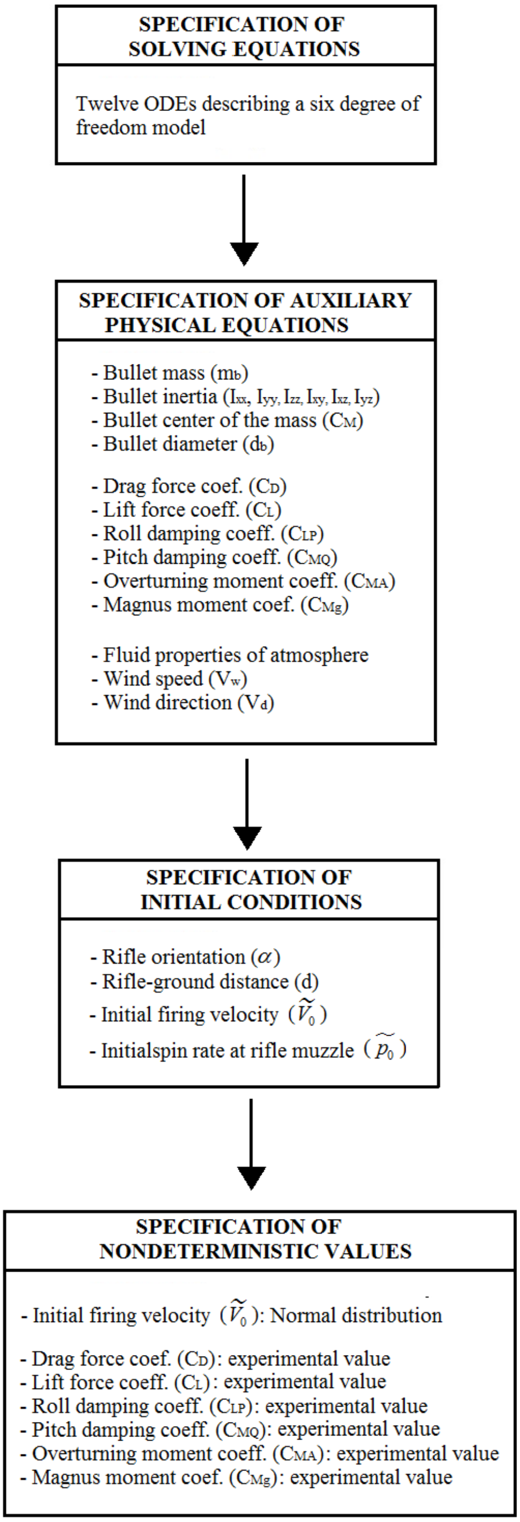

Figure 10. Mathematical modeling process flow to predict the bullet's trajectory in the free atmosphere.

4. *Model translation; discretization and algorithm selection for the mathematical models:* the continuum mathematical model has to be converted in a discrete

form suitable for numerical solution. Consistency of the discretization is necessarily required for reducing the errors.

The discretization involves in the conversion of the initial conditions into the discrete form suitable for solving the problem at each time step. For the bullet flight example, the twelve ODEs are discretized in the time domain and each of them is solved through a 4^{th} order Runge-Kutta numerical method. This numerical method provides a good accuracy and stability.

The nondeterministic variables have to be converted into multiple runs or solution of a deterministic simulation. In other words, the uncertainties and errors are propagated through specific approaches (e.g. Monte Carlo method). Considering the example of bullet flight, the initial firing velocity is assumed as stochastic variables which are normally distributed. Monte Carlo method is used to propagate the uncertainties by choosing discrete values from a set of stochastic variables. Figure 11 illustrates the steps used in the discretization and algorithm selection for the mathematical models.

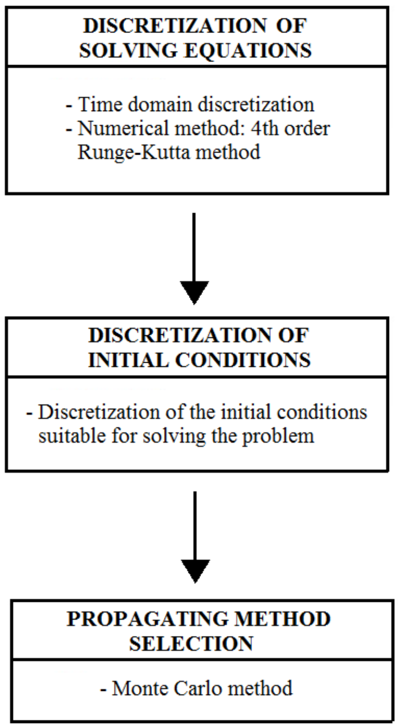

Figure 11. Discretization and algorithm selection for the mathematical model.

The further steps of simulation and modeling process refer to the computer programming and implementation. This paragraph is thought to give detailed information on a simulation case study which does not require specific computer and programming skills.

Chapter 3

Disaster simulation in built environment

3.1 Introduction

Disaster simulation is essentially based on four step processes that are hazard definition, inventory development, damage (or vulnerability) assessment, and loss estimation. These steps are similar to those ones adopted in CATastrophe modeling (CAT) framework (Grossi et al., 2005). Beside the definition of the processes, CAT modeling aims to estimate the probability of loss, whereas disaster simulation also contributes to high-precision disaster prediction.

In the last years, many studies and research projects have focused on risk assessment of physical system subjected to different earthquake scenarios. The European RISK-UE project (Mouroux & Le Brun, 2006) dealt with the assessment of the direct and indirect damages following a scenario earthquake, in order to increase awareness and prepare a “Plans of Action” necessary to effectively reduce the seismic risk. In the context of European projects, the SYNER-G research project (Pitilakis et al., 2014) focused on the systemic seismic vulnerability and risk assessment of complex urban systems. The main goals of the project was to elaborate the fragility relationships for the vulnerability analysis and loss estimation of all elements at risk, for buildings, utility networks, transportation systems, hospitals, and emergency rescue systems. It is also worth mentioning the HAZUS methodology (FEMA, 2011) focuses on the loss estimates for use by decision makers. Extensive national database was developed to contain information on built environment aspects.

Many complex physical systems are studied by developing models and using computationally intensive methods to learn about the behavior of those systems. The simulation process consists in creating and analyzing a prototype of a physical model to predict its performance in the real world. Nowadays, computer-based simulation is the most useful and feasible methodology for reproducing the behavior of systems under external perturbations through appropriate mathematical models. Beside, complex mathematical models may require excessive computational effort, therefore, computer hardware and numerical solvers are critical issues to be considered in the computer-based simulations.

The Integrated Earthquake Simulation (IES) in the NIED project (Hori 2006) was developed to reproduce the earthquake effects in urban environment. The input data was collected into a Geographic Information System (GIS) and then converted in suitable numerical models. IES analyses were organized into parallel computational processes implemented in a K computer.

Tagawa et al. (2015) performed detailed Finite Element (FE) analyses of a full scale four-story steel frame structure subjected to consecutive scaled seismic excitation recorded during Hyogoken-Nanbu earthquake. Parallel Finite Element (FE) software with a dense mesh of solid elements was used to simulate the global structural response of the steel frame using the E-Simulator. This is related to a Japanese project of E-Defense, an organization of the National Research Institute for Earth Science and Disaster Prevention (NIED). The world's largest capacity shaking table is currently operating within E-Defense and was used to validate the results obtained with E-Simulator.

The major advantage of the computer simulation is the reduction in running time. Some other processes may be taken a large time to complete analyses and obtain results. Thus, these kinds of processes require robust analysis which is difficult to perform especially when the operations and the interactions are multiple.

3.2 Built environment

The term *built environment* is used to describe the interdisciplinary field that addresses the design, construction, management, and use of these man-made issues and their relationships with the human activities over time. The human activities are generally defined as all the processes, behaviors and actions in different field (economy, law, public policy, public health, design, engineering, technology, etc.) aimed to manage and regulate a community.

The built environment plays a key role and it needs to be *functional* and *operational* at every time. Therefore, when a disaster (natural or manmade) occurs, the entities and activities of a built environment must be protected in order to limit the total loss and ensure a rapid recovery to the full functionality and operational (disaster resilient environment). Despite this theoretical definition, recent disasters have shown the high vulnerability of built environment. In this regard, disaster impact can be controlled and reduced through an effective disaster management activity. At the same time, reducing the built environment vulnerability means increasing its resilience. The definition of resilient built environment was suggested by Bosher (2008) who claimed that "*built environment is designed, located, built, operated and maintained in a way that* *maximizes the ability of built assets, associated support systems (physical and institutional) and the people that reside or work within the built assets, to withstand, recover, and mitigate for, the impacts of extreme natural and human induced hazards*". Mannakkara and Wilkninson (2013) identified some factors which increase the risk of disasters within a built environment, such as inadequate or insufficient consideration of natural risks, design and constructions processes, neglecting building codes and regulations, illegal occupancy, and structural capacity.

The scale of built environment (National, Regional, or City) affects the completeness of the data used to model the physical system (such as building portfolio, infrastructures, etc.). In the last decades the modernization, industrialization, and the sociological process of rationalization have led to a massive urbanization phenomenon and cities are becoming centers of economic activity and innovation. According to United Nations, half of the world's population lived in urban areas at the end of 2008. Thus, urban areas are particularly vulnerable due to the high concentration of people and economic assets, and in many cases, their hazard-prone location. When a natural disaster such as earthquake strikes an urban area, the majority of the losses in terms of casualties and repair costs are due to the buildings extensive damage and collapse. Coburn et al. (1992) observed a direct proportionality between the mortality per building collapse and the population per building (P/B) ratio. Moreover, the daytime of earthquake occurrence and the building occupancy affect the number of casualties. Generally, among all the building typologies in urban areas, strategic buildings such as hospitals, schools, etc. have rigorous structural requirements in order to ensure full or partial operational of the structure after strong ground motion. On the contrary, the design code is less stringent for residential buildings, even if they are the majority and they have a higher daily occupancy. Based on the aforementioned observations, residential buildings represent the most vulnerable physical system of an urban built environment.

3.3 Building stock vulnerability

As previously mentioned, the building stock of a built environment is particularly important due to highest percentage of loss caused by a seismic event. Furthermore, among the three variables of seismic risk (earthquake hazard, physical systems vulnerability, and level of exposure), the building vulnerability assumes great importance because represents the potential aspect for which the engineering research can intervene, improve and even control the seismic behavior (Vicente et al., 2008). In fact, reducing the level of vulnerability consequently limits the level of physical damage, life loss and economical loss (seismic risk reduction). Thus, determination of the vulnerability of buildings within the existing building portfolio is a high priority task in the seismic risk reduction of urban environment (Ozcebe et al., 2006). Besides, the complexity of the building inventory at urban scale poses the problem of reliability of estimates, given the large existing uncertainties. Current seismic building vulnerability assessment approaches are classified based on their level of complexity. FEMA 310 (1998) provided a three-tiered process for seismic evaluation of existing buildings in any region of seismicity. The simplest level of seismic risk-assessment approach of building stock is essentially based on observation of certain building parameters to be correlated with available post-earthquake damage data. A methodology based on rapid visual screening of the building was proposed by FEMA 154 (1998) to define potential seismic deficiencies in existing buildings (Tier 1) and then identify the correct mitigation strategies.

The second complexity level for building vulnerability assessment methodologies is represented by those approaches based on simplified analysis of buildings (Tier 2 or Preliminary Assessment Methodology, PAM). In these cases, more detailed building data are required (such as structural and nonstructural parameters). According to FEMA 310 (1998) a simplified analysis, limited to linear analysis methods, is performed by taking into account the building deficiencies identified in the first level.

The procedures in Tier 3 employ linear or nonlinear analyses of the building. They require detailed building information such as structural members' dimensions and percentage of reinforcement of all structural members.

3.4 Building stock exposure

It can be recognized how modeling of buildings requires a large amount of data that may not be available or accessible especially for medium or large-scale cities. Nonetheless, data collection and processing are required to create a comprehensive building exposure database that provides a foundation for all catastrophe model loss estimates. The concept of exposure database is widely adopted in catastrophe modeling to manage the natural hazard-induced risk originates in the fields of property.

The Earthquake Engineering Research Institute and the International Association for Earthquake Engineering performed an Internet-based project called World Housing Encyclopedia (WHE) and available at www.world-housing.net (Brzev et al., 2004). The purpose of the WHE is to develop a comprehensive global categorization of characteristic housing construction types through a standardized format that provides basic information on the seismic vulnerability of housing stock.

The widespread usage of Information Technology (IT) and GIS systems has led to characterize the inventory of properties. Geographic coordinates such as latitude and longitude to a property may be identified based on its street address, ZIP code or another location descriptor. Given the building location, other features may be collected such as its construction type, the number of stories in the structure, and its age (Grossi et al., 2005).

Gamba et al. (2009) developed the Building RECognition (BREC) software that collect and manage different building information. This tool was developed by the Remote Sensing Group at the University of Pavia with the aim of extracting some features of built environment at different scales from aerial or satellite high resolution images.

A global building inventory for the U.S. Geological Survey's Prompt Assessment of Global Earthquakes for Response (PAGER) program was developed (Jaiswal & Wald, 2010). The building database was developed using taxonomy of global building types at regional level through three different phases (data acquisition, data aggregation, and data assignment). This global database contains spatial, structural, and occupancy characteristics of buildings.

3.5 Seismic damage simulation methods of building stock

Given the large number of buildings in a built environment, the prediction of the seismic response of the buildings requires the use of simulation methods. In recent three decades, the research activities have been focused on the definition of numerical models aimed to simulate the seismic buildings damage. The simulation models may be based on a statistical (*data-driven*) or physical approach (*physics-driven*). In the first case, the building damage assessment is based on statistical data collected from previous seismic events. Therefore, the accuracy of the data-driven methods is dependent on the available data.

One widely used data-driven method is the Damage Probability Matrix (DPM) which predicts the level of damage for different seismic intensities and buildings typologies (Whitman 1973). The generic DPM component *DPM(DS,I)* represents the probability that a particular Damage State *DS* is reached in the considered building subjected to a given earthquake intensity *I* (Yucemen et al., 2003). For a given intensity level, the sum of the probabilities for different DSs is equal to 1. The Modified Mercalli Intensity (MMI) scale or Peak Ground Acceleration (PGA) can be adopted as seismic intensity scale.

The concept of DPM was widely adopted into the ATC-13 report (Rojahn and Sharpe 1985) to evaluate the earthquake damage data for California that includes the DPMs for 78 different facility types. Later, Dolce et al. (2006) applied a modified version of it to the city of Potenza (Southern Italy), while Eleftheriadou et al. (2013) extended the DPM-based methodology to the building stock in Southern Europe.

The accuracy of the data-driven methods is dependent on the quality and quantity of the data. Some worldwide regions were not hit by destructive earthquakes or the recorded seismic events were not enough to have an adequate statistical population. The enhancement of the computer technologies has led to use of the physics-driven simulations which are capable to predict the seismic damage to the buildings through nonlinear dynamic or static structural analyses of individual system. In case of nonlinear static approach, the Capacity Spectrum Method CSM (Freeman 1998) or N2 method (Fajfar and Gašperšič 1996) may be used. El Ezz et al. (2014) adopted the CSM to assess the seismic damage of Quebec City, Canada. The building inventory of the city was prepared based on construction material, structural type, height, and seismic design level. Each building type was modeled as equivalent Single Degree Of Freedom (SDOF).

Nonlinear static analysis of buildings does not take into account the dynamic characteristics of an earthquake since the seismic excitation is considered as a monotonically increasing function. To overcome this limitation, nonlinear time history analysis may be used. Korkmaz (2009) proposed a combined probabilistic seismic safety approach performing nonlinear time history analyses. This method was applied to unreinforced masonry low-rise buildings to estimate the regional seismic vulnerability of Pakistan. Furthermore, Tang et al. (2011) assessed the collapse resistance of Reinforced Concrete (RC) frame structures representative of the Chinese school stock. A parametric study was conducted by performing Incremental Dynamic Analyses (IDA) (Vamvatsikos et al. 2002) for all the configurations of RC frames designed according to the 2001 Chinese Code (GB 2001). The final collapse resistance of the analyzed RC buildings was evaluated through the Collapse Margin Ratio (CMR) according to ATC-63 (ATC 2009).

Xu et al. (2014) proposed a high-fidelity structural model to predict the seismic damage on buildings in urban areas through time-history analysis. In the context of regional seismic damage simulation, Lu et al. (2017) proposed a shear model for Multi Degree of Freedom (MDOF) systems and a shear-flexure model for tall buildings. Inter-story nonlinear properties were simulated through a tri-linear backbone curve and a single-parameter hysteretic model was proposed to take into account the dynamic degradation of the mechanical properties. All the parameters related to the MDOF models were determined based on the Chinese design codes and the statistical data were gathered from the available results of experimental and analytical studies.

Figure 12 depicts a scheme of the simulation models adopted to assess the response of a large number of buildings within a built environment.

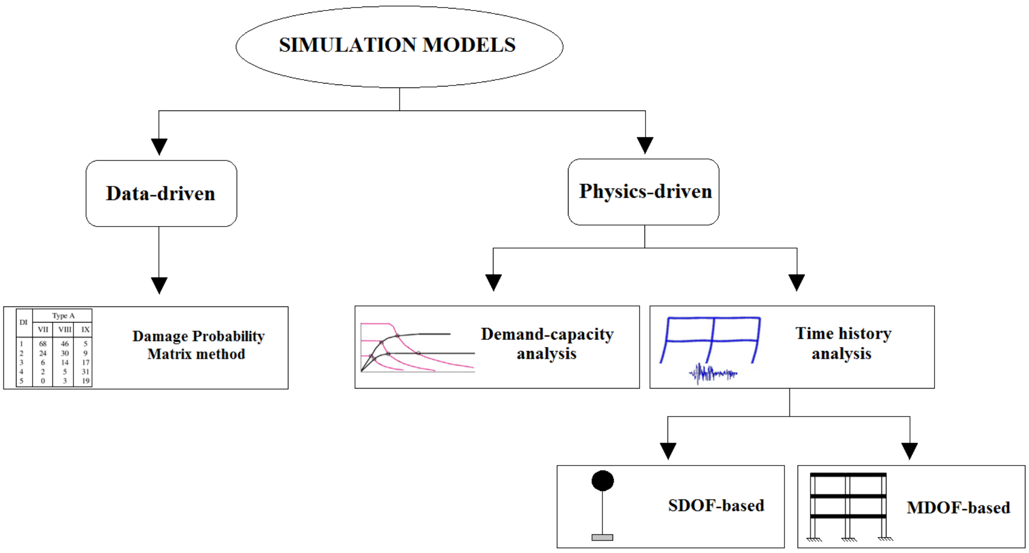

Figure 12. Data-driven and physics-driven simulation models used to assess the buildings response within a built environment.

Data-driven approaches require information from observed data to identify the building typologies and then to estimate the damage level through statistical procedures. On the contrary, the physics-driven approaches assume that a physical model is available and then combine the physical model with collected data to assess the building damage. Both approaches are based on data that are noisy and almost always censored, while modeling stage requires some approximations and assumptions. Therefore, sources of uncertainties are introduced in simulation models. The uncertainties are mostly related to the lack of knowledge on the model's parameters. Therefore, a realistic estimate of the behavior of structural systems requires a probabilistic approach for an appropriate treatment of uncertainties. Two stochastic approaches are currently employed to deal with the available data which compose the exposure database of the analyzed building stock. In the first approach, the measured data are used to estimate the unknown parameters in the form of a Probability Density Function (PDF) based on the available data. This prior distribution is multiplied by the likelihood function which is represented by the PDF of the available data conditional on the known parameters (An et al., 2015). The Bayesian method is an example of model's parameters estimation approach where the posterior probability (probability of A given B, *P(A|B)*) is calculated based on the prior probability (probability of A, *P(A)*), likelihood (probability of observing B given A, *P(B|A)*), and marginal likelihood (probability of B, *P(B)*) (Equation (5)).

$$P(A \mid B) = \frac{P(B \mid A) \cdot P(A)}{P(B)} \tag{5}$$

The second process aims to consider the model's parameters as Random Variables (RVs) defined through a pre-determined PDF. This approach is used when the limited measured data are not enough for defining a consistent prior distribution and likelihood function. Then, different technique can be used to estimate a range of probable values for each parameter. Monte Carlo Simulation (MCS) is among the most diffused technique based on repeated random input sampling to obtain numerical outputs in terms of PDF.

A general overview of the simulation methods used to predict the damage to buildings is illustrated in Figure 13. The blue lines refer to the logical path for the physics-driven approach, while the red ones are associated with the data-driven approach. In both cases, three main stages are identified: *building data*, *building response*, and *damage assessment*.

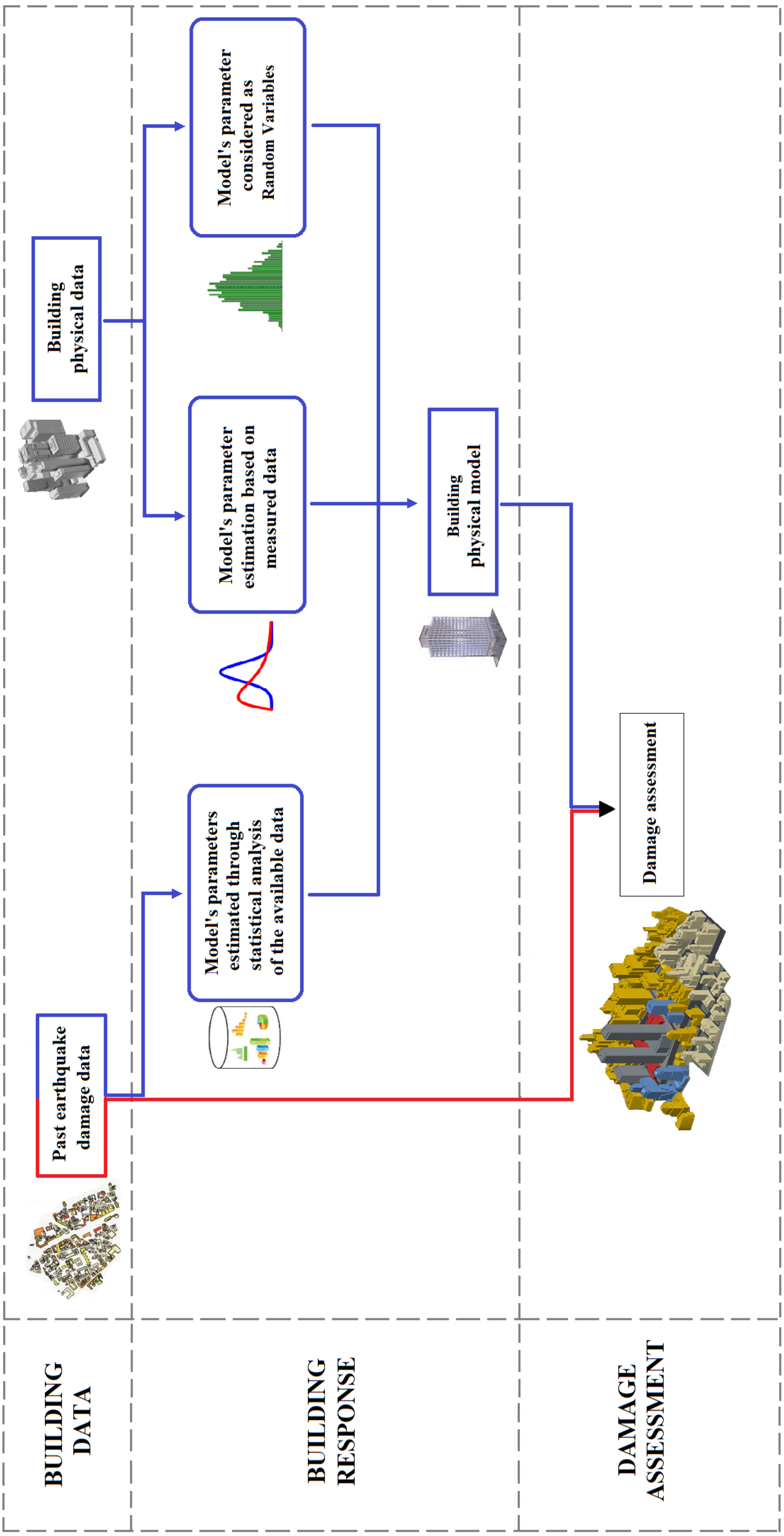

Figure 13. Simulation methods for estimating the damage to the buildings.

3.6 Summary of the proposed simulation model

The available large-scale simulation models predict the structural seismic vulnerability classifying the buildings into groups. Usually, buildings are grouped based on building archetype, number of story, seismic design level, etc. Although these approaches provide a rapid and simplified estimate, their results might be inconsistent with the expected results. Indeed, response of individual building is significantly dependent on various parameters such as building geometry, structural characteristics, construction elements, etc. Therefore, definition of an exposure building database with a high level of granularity is a key point in increasing the accuracy of the result of the simulations.

3.6.1 Building exposure database

This research proposes a simulation model aimed to assess the level of damage of individual building considering its specific characteristics. A comprehensive exposure building database is created through an intensive data collection and manipulation procedure based on the seismic standard and regulations associated with different periods of construction.

Most of the building attributes are of random nature, and consequently, uncertainty exists in the behavior of the structural members. Therefore, a probabilistic approach for an appropriate treatment of uncertain building attributes is performed by considering the building input variables as Random Variables (RVs) that are normally distributed. The stochastic nature of the input variables leads to investigate different input dataset representative of the typical building portfolio and then providing a set of possible damage scenarios.

The entire data processing and collection adopted to create the building exposure database is detailed explained in *Chapter 4*.

3.6.2 Capacity model

The global capacity of each building is modeled by consider a significant amount of parameters. MCS is performed to take into account the input uncertainties by repeating random input sampling to obtain different numerical outputs. On the probabilistic point of view, each building is represented through a "window" of possible seismic behaviors, while the median backbone curve is assumed as representative of the seismic capacity of the building. Furthermore, due to the lack of available information, the dynamic degradation is modeled based on the Takeda model (Takeda et al., 1970). Detailed information on the capacity model of individual building (both RC and masonry) is provided in *Chapter 5*.

3.6.3 Damage assessment under given seismic scenario

Each building is modeled as an equivalent SDOF with a specific dynamic behavior identified by the median backbone curve. Therefore, the building performances are assessed through nonlinear time history analyses in terms of absolute maximum top displacements by setting a given seismic scenario. The maximum absolute top displacements (global demand) are then converted into maximum inter-story drifts (local demand) through a simplified seismic response model. Finally, the level of damage is estimated based on the inter-story drift threshold proposed by Ghobarah (2004).

Detailed information on the buildings damage assessment is provided in *Chapter 7*.

Chapter 4

Building exposure database of *IDEAL CITY*

4.1 Introduction

Modeling building stock requires a large amount of data which may not be available or accessible especially for medium or large scale urban areas. Furthermore, the risk-based methodologies applied at city level need to be tested and verified, therefore, the concept of virtual city is attracting the interest of researchers due to the benefit in testing algorithms and methodologies. Virtual cities are capable to model different types of infrastructures and hazards according to pre-determined design approaches which may be representative of a seismic prone area.

The Center of Excellence for Risk-Based Community Resilience Planning (McAllister, 2015) developed a measurements science and technology to understand what makes a community resilient. For this purpose, different physics-based models capable to consider single or cascading hazards and their effects on the built environment were developed. The proposed methodologies and models were tested at city level both for real and virtual built environments. Four real small size cities subjected to one or more natural hazards were assumed as testbed problems: Seaside, OR (Earthquake and Tsunami), Shelby County, TN (Riverine Flood, climate change), Joplin, MO tornado (event of May 22, 2011), and Galveston, TX Hurricane (event of Sept 1, 2008). Furthermore, a virtual city named Centerville was designed to have a maximum flexibility in designing, testing and stressing a multidisciplinary computational environment with fully integrated supporting databases (IN-CORE: Interdependent Networked Community Resilience Modeling Environment) developed by the Center. The virtual city was envisioned as being a typical middle-class city situated in a

Midwestern United State. Centerville development involved more than 90 individuals with different expertise (engineers, social scientists, computer scientists).

4.2 IDEAL city model

A virtual city consisting of different buildings categories and infrastructure is designed. Four building sectors that provide essential functions to a community including housing (residential building, hotel, shelter), education (school, university, library), business (shopping centers, retail stores, heavy industries), and public services (hospital, police station, churches, airport etc.) are considered. The virtual city is envisioned as being representative of the building stock of the city of Turin, Italy, and it is named as *IDEAL CITY*. Table 2 resumes all the considered building categories and the corresponding number of buildings.

The overall area of the city of Turin is around 120 km^2 with a population of more than 900.000 inhabitants. The building stock of the city is representative of the typical Italian building stock which has an old downtown zone mainly composed of masonry buildings. Additional uniform housing zones have been built after the Second World War (60^{th} -70^{th}) around the downtown. During those years the predominant building archetypes was represented by RC buildings. In the last decade, the residential zones have been expanded in the disused industrial zones located in the suburbs. The residential building stock of the city of Turin is mostly composed by five-story building with a high percentage of historical structures.

Table 2. Detailed information on physical and social infrastructure of *IDEAL CITY*.

Physical Infrastructure		
Building	Residential	23420
	Mobile home	62
Hospital		17
Fire Station		3
Police	Police Station	18
	Municipal Police	11
	Police Headquarters	31
Educational	Elementary School	157
	Middle School	105
	High School	97
	University	70
Social Infrastructure		
Hotel		31
Historical Building		951
Castel and Palace		18
Church		176
Sport Centre		265
Cinema		48
Museum		156
Theater		38
Library		15

The geospatial distribution of the buildings and the administrative division of *IDEAL CITY* is based on the data collected for the city of Turin. Five critical infrastructures supporting the community indispensable demands, i.e., water and waste water distribution system, gas networks, power grids, transportation and communication networks are identified. A plan view of *IDEAL CITY* is provided to illustrate the residential building framework (Figure 14.a) and the transportation framework (Figure 14.b).

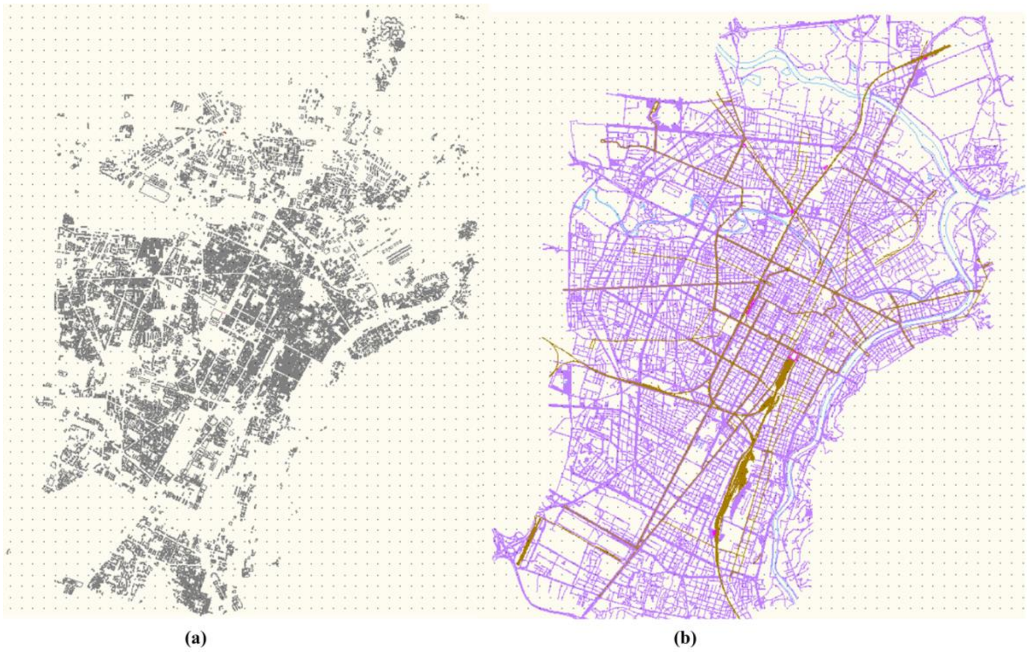

Figure 14. Residential buildings (a) and transportation framework (b) of *IDEAL CITY*.

The transportation network is represented through lines and joints (joint model) for different categories of road infrastructures (highway, principal, secondary, urban, sub-urban, railway, and bridges).

IDEAL CITY is developed as part of a European project "IDEal rescue (Integrated DEsign and control of Sustainable CommUnities during Emergencies)".

4.3 Buildings exposure database

A built environment made up of physical systems such as buildings and lifelines is considered as a complex system. Therefore, identifying all the entities and attributes of this system may result in large economic and management efforts, or, in most cases it could be not a reachable goal. Let's focus on residential buildings which are the largest and the most vulnerable physical system within an urban area.

A complete characterization of the entire building stock at urban scale is the most accurate and consistent process to be addressed. However, some problems exist such as lack of documentation (unknown or not-updated building information), inaccessibility of the data (e.g. customer records for marketing, public data recorded by a governmental institution, etc.), as well as limitation in data sharing (permission request to access to the data) lead to a time consuming and impractical data collection process. Mostly, the amount of data may be not sufficient to characterize the buildings with an adequate level of knowledge. For the reasons mentioned above, a typology-based approach is adopted to define the physical characteristics of the building stock (building archetype, year of construction, height, number of story, etc.). Furthermore, three main building entities are selected and classified into construction elements, mechanical properties, and geometrical properties, while each building attribute is identified through its mean characteristic value. Moreover, the year of construction is considered as main attribute affecting the seismic standard construction procedures used to design the buildings of *IDEAL CITY*.

The buildings' design process is affected by the uncertainties which are defined as the deficiency that may occur due to lack of knowledge (Oberkampf et al., 2002). The sources of uncertainty are different and mostly related to the lack of knowledge on the mechanical, geometrical and design parameters which characterize a structural model. Furthermore, uncertainties refer to the non-deterministic variables definition, numerical methods applied to assess the outputs, and the physical model used to predict the structural response.

Most of the structural parameters are of random nature, and consequently, uncertainty exists in the behavior of the structural members. Therefore, a realistic estimate of the behavior of structural systems requires a probabilistic approach for an appropriate treatment of uncertain structural properties, especially under seismic loading (Lee & Mosalam, 2006). In this research, the input variables are assumed as RVs that are normally distributed. These RVs are generated from uniform samples by setting the mean and standard deviation values. Where the random variables have a multivariate normal distribution, correlations provide a complete description of their dependence. Therefore, correlation between some RVs is considered by assuming the correlation coefficients between two or more variables according to the current literature (Vrouwenvelder, 1997, Mirza & Mac Gregor, 1979).

The stochastic nature of the input variables leads to investigate different input dataset representative of the typical building portfolio and then providing a set of possible damage scenarios. Indeed, the definition of a set of damage scenarios may help decision makers to better understand how to allocate resources considering a maximum and minimum level of alerts.

4.4 Data collection

A conceptualization of the city model is necessary to characterize the attributes of the system under consideration. Data collection and manipulation (data processing) are the basic procedures required to capture the essential features of a complex system such as a building portfolio. Data processing may involve various processes based on the arranging, combining, sorting and dividing the collected information.

The most crucial stage of the data processing cycle is represented by the raw data collection which could have a heavy impact on the output. Furthermore, data collection process is characterized by a certain level of knowledge which refers to the amount of collected data and the methodologies used to collect these data. Some types of data collection include census (arranging into group or statistical population), sample survey (including part of the total population), and administrative.

In this thesis, the following categories of buildings' raw data are identified:

- *Geometry*: including coordinates of the footprint vertices, coordinates of the center of gravity, and story height and number of story;
- *Structural and nonstructural parameters*: which are crucial for the dynamic characterization of each building;
- *Population data*: consisting in number of inhabitant/building and administrative information;
- *Year of construction*: which represents an important parameters associated with the building design approaches;
- *Additional information:* which includes economical, statistical and administrative data. Additional information is often required to overcome some limitations in the data availability and to validate the existing ones.

4.4.1 Geometrical parameters

The buildings distribution within the virtual city is based on the real urban plan of the city of Turin, Italy. For this purpose, the Cad model of the city has been obtained through *CADMAPPER* (https://cadmapper.com/). This online tool is capable of transforming data from public sources (e.g. OpenStreetMap, NASA, and USGS) into organized CAD files containing the geometrical arrangement of the buildings and infrastructures. For each building located into the considered physical boundary, the coordinates of the footprint vertices and the coordinates of the center of gravity have been collected.

Additional buildings' geometrical data (story height and number of story) have been collected through the Web GIS tool provided by the municipality of Turin. This tool allows the free visualization of the geographical information for the whole administrative territory of the city and it is available at the link: http://www.comune.torino.it/geoportale/. All the data are organized in shape-file format (readable by ARCGIG and QGIS) that contain the following building geometrical information:

- *Census building code*: it is composed by the character "EDF" and a numerical code (e.g. EDF06);
- *Soil elevation* which provides information about the elevation of the ground level where the building is located;
- *Building eaves height*: which considers the distance between the ground level and the eaves of the building;
- *Number of story*: the definition of number of story building refers to the inhabitable building volumes;
- *Building footprint perimeter*;
- *Building footprint area*.

An illustrative example of the shape-file readable by QGIS is shown in Figure 15.

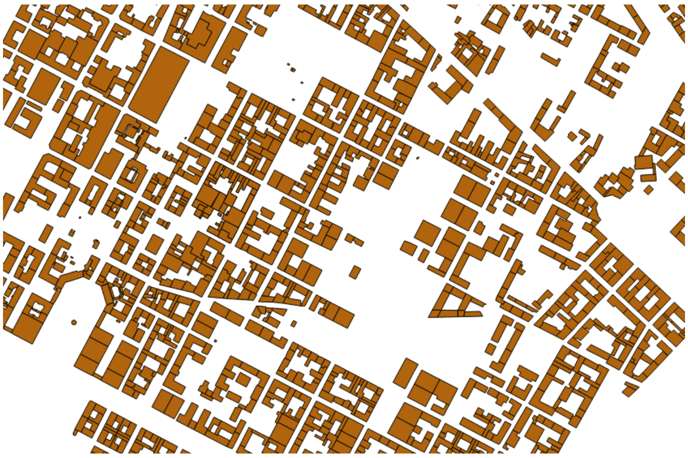

Figure 15. Illustrative example of the QGIS shape-file.

The soil elevation, building eaves height, and number of story data are unknown or unavailable for some buildings. In these cases, additional information and methodologies have to be used to overcome the lack of data (see "*Data processing*").

4.4.2 Structural and nonstructural parameters

The structural characterization of all the buildings at the urban scale may result complicated in terms of costs and time. Furthermore, the availability of the data is not sufficient to meet the expected requirements. In addition, a complete characterization of the structural parameters (such as structural components arrangements and sizes) may be impossible at urban scale.

Building archetypes

In the early stage of data collection, the structural properties of a building are represented by the lateral load-resisting system and the building archetype. To gather the building archetypes, the GIS shape-file provided by the municipality of Turin has been used. However, many building archetypes information are unknown or imprecise and this in turn leads to use complementary data sources. In this regard, the Italian census Institute (ISTAT) provides useful data concerning the number of buildings located into the urban area of Turin and their archetypes (http://dati-censimentopopolazione.istat.it/Index.aspx?DataSetCode=DICA_EDIFICIRES). Based on the ISTAT data, the following percentage has been derived (Table 3).

Table 3. Percentage of the residential building archetypes of Turin (ISTAT).

RC [%]	Masonry [%]	Other [%]
55.16	42.70	2.14

The census data clearly shows how the main two residential building archetypes are represented by the RC frames and the masonry structures. For sake of simplicity, the two aforementioned building archetypes have been assumed as representative of the housing portfolio of *IDEAL CITY*.

Construction elements

The dynamic characterization of individual building is also dependent on its construction elements that affect the definition of the mass and stiffness properties. As previously mentioned, the incomplete knowledge of the building elements at urban scale does not lead to an accurate building conceptualization. Therefore, different strategies need to be investigated to predict the main dynamic properties of the analyzed building portfolio. In this regard, the concept of *building typology* has become commonly accepted in many European countries at national and regional level which is based on the classification of the building stock according to certain common properties. This classification approach leads to easily characterize the buildings at big scale (such as City, Region or Nation scale). In the context of European researches, the TABULA project (Typology Approach for Building Stock Energy Assessment) was aimed to assess the energy consumption of national building stock (Cyx and Verbeke, 2011) through the definition of the building typologies. Each building typology represents a set of building models (building-type) that is characterized by a certain construction period and building size. The Italian contribution to the TABULA project was based on the improvement of the existing residential building typologies which was supported by large statistical data obtained from census (Corrado et al., 2012). Technical standards, expert supports, and statistical data were used as basis for characterizing the residential Italian building stock through the definition of the types of building construction elements (e.g. roofs, ceilings, walls, floors, doors, windows) associated with a given construction period. In the context of dynamic characterization of the Italian building stock, the typical vertical (walls) and horizontal (floors) construction elements have been considered. More specifically, seven Floor types (Figure 16), three External Wall types (Figure 17), and five Masonry Wall types (Figure 18) are assumed according to Corrado et al. (2012). In order to consider a wider range of masonry buildings, historical researches and surveys have been conducted with the aim of identify additional masonry wall types representative of the Italian residential building stock. As results of the survey, the masonry wall types *MW 3*, *MW 4*, *MW 5* and *MW 6* have been identified (Figure 18).

Type ID	Description		Year
F 1	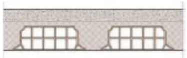	Floor with reinforced brick-concrete slab	> 1930
F 2		Concrete floor on soil, low insulation	> 1976
F 3		Floor with reinforced concrete	1901 - 1930
F 4		Vault floor with solid bricks	< 1900
F 5		Floor with hollow bricks and steel beams	1920 - 1945
F 6		Vault floor with bricks and steel beams	< 1900
F 7		Floor with wood beams and hollow bricks	< 1930

Figure 16. Floor types representative of the residential building stock of *IDEAL CITY* (Corrado et al., 2012).

Type ID	Description		Year
EW 1	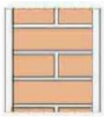	Solid brick masonry (25 cm)	1900 - 1950
EW 2	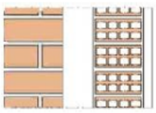	Hollow wall brick masonry with solid and hollow bricks (40 cm)	1930 - 1975
EW 3	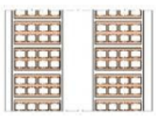	Hollow wall brick masonry (40 cm)	> 1930

Figure 17. External wall types representative of the residential building stock of IDEAL CITY (Corrado et al., 2012).

Type ID	Description		Year
MW 1	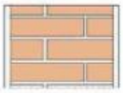	Solid brick masonry	1900 - 1950
MW 2		Masonry with lists of stones and bricks	< 1930
MW 3		Squared block masonry	< 1930
MW 4	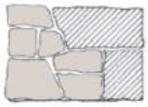	Freestone wall with external layer of regular blocks	< 1920
MW 5		Rubble masonry	< 1930
MW 6		Hollow brick masonry	> 1974

Figure 18. Masonry wall types representative of the residential building stock of *IDEAL CITY* (Corrado et al., 2012).

4.4.3 Population data

Population data have been gathered through the public information provided by the municipality of the city of Turin. Population data refers to the resident and nonresident population within the urban area in terms of inhabitant per unit area (inhabitant/km^2) and average value of persons per building. The population data refers to the administrative districts in which the urban area is divided.

4.4.4 Year of construction

The year of construction is an important property of each building. It affects the definition of certain structural, nonstructural, and geometrical parameters. The GIS shape-file provided by the municipality of Turin has been used as the basis for collecting the year of construction data. Some of this information is unknown or provided for large time periods, so that additional information is required to overcome this problem (see "*Additional information*").

4.4.4 Additional information

Additional sources need to be exploited to gather complementary information aimed to fully characterize the building portfolio of IDEAL CITY. Additional information has been gathered with the aim of estimate the missing year of construction of the analyzed building stock. To reach this goal, the economic depreciation theory of real estate has been adopted (see "*Data processing*"). The property values of the residential segment of 40 cadastral micro-zones in the city of Turin have been provided by the "Turin Real Estate Market Observatory" (http://www.oict.polito.it/microzone_e_valori). These values are expressed in terms of listing prices per unit (€/m2) using statistical indicators (e.g. mean, median, minimum, maximum, and standard deviation).

Moreover, the national institute of statistic (ISTAT) provides the global percentage of residential buildings built in established time ranges (≤ 1918, 1919-1945, 1946-1960, 1961-1970, 1971-1980, 1981-1990, 1991-2000,2001-2005, ≥ 2006). These data have been collected with respect to the residential building stock within the urban area of the city of Turin. This information has been manipulated to extract useful data associated with the brackets of years that are related to building code changes.

Figure 19 resumes all the collected raw data and the associated sources.

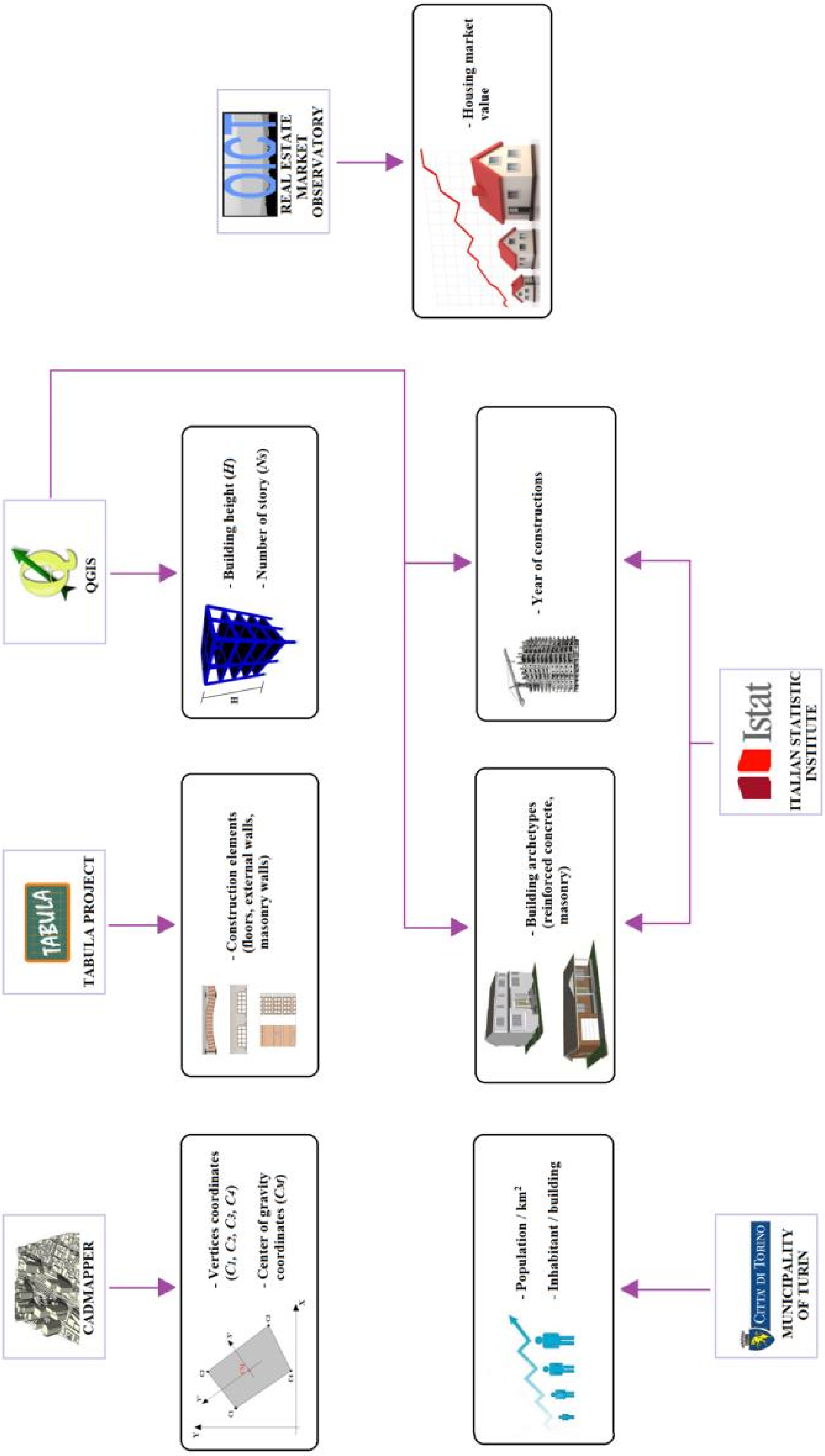

Figure 19. Data collection flow: data sources and associated information.

4.5 Data preparation and data input

The collected raw data need to be manipulated in order to be suitable for further analyses (data preparation). Data preparation can be carried out through arranging and sorting the raw data. The accuracy of the data has to be carefully checked into this stage. Inaccuracy or inconsistent data will affect the further stage of the cycle. The manipulated data are then converted into machine readable form to be processed by a computer (data input).

The considered urban area has been divided into 10 administrative districts (http://www.comune.torino.it/geoportale/ser_professionali_3.htm#tabs-4). Each administrative district is divided in neighborhoods on a total of 34. Figure 20 illustrates the administrative division of the city of Turin which has been used as basis for *IDEAL CITY*.

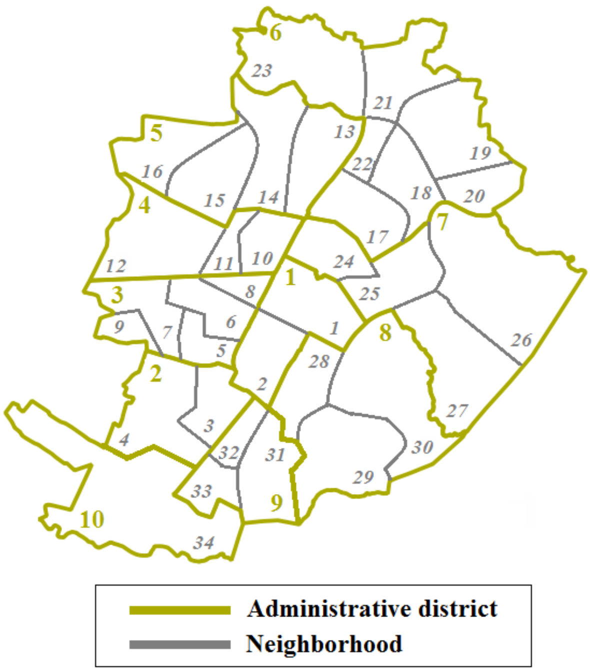

Figure 20. Administrative districts and neighborhoods of *IDEAL CITY* (based on the city of Turin).

The administrative, economic, and population data have been collected for each district, therefore, their arrangement per neighborhood has been performed.

A classification approach has been also applied to arrange the year of construction into certain specific periods. In this regard, six different categories of year of construction have been selected consistently to the main changes of the Italian seismic standards for RC and masonry buildings (Table 4).

Table 4. Year of construction categories.

I	II	III	IV	V	VI
< 1916	1916-1937	1938-1974	1975-1996	1996-2008	> 2008

The Italian seismic standards referring to the six identified categories are below listed:

- *II*: Decreto Legge n. 1526 del 1916;
- *III*: Regio Decreto n. 2105 del 22 Novembre 1937 (G.U. n.298 del 27/12/1937);
- *IV*: Legge n. 64 del 2 Febbraio 1974 (G.U. n. 76 del 21/03/1974);
- *V*: Decreto Ministeriale LL.PP. del 24 Gennaio 1996 (G.U. n. 108 del 12/05/1996);
- *VI*: Decreto Ministeriale del 14 Gennaio 2008 (G.U. n. 29 del 4/02/2008).

Furthermore, the collected data provided by ISTAT have been arranged to meet the new year of construction periods (Table 5).

Table 5. Residential buildings percentage per year of construction.

Buildings type	**I**	**II**	**III**	**IV**	**V**	**VI**
Masonry [%]	100	67.78	31.16	0	0	0
RC [%]	0	32.22	68.84	100	100	100

4.6 Data processing

The data processing is the core of the cycle and it consists in the application of specific methodologies aimed to estimate and assign the missing data. The procedures and methodologies used in the data processing stage are below explained in detail.

4.6.1 Assessment of the unknown years of construction

The missing information associated with the year of construction has been derived through the economic approach of the depreciation theory of real estate. The mean (μ_{cu}) and standard deviation (σ_{cu}) values of the listing prices per unit have been collected for 40 micro-zones of the urban area of the city of Turin. Assuming a perfect competition market structure, the listing prices can be assimilated to the cost of the real estate. According to this hypothesis, the *cost approach* can be used to estimate the depreciation of each building within the urban area. The cost approach is a valuation technique intended to estimate the market value of a real estate considering its depreciation. In the case of residential buildings, the age life ratio model is commonly employed to define the depreciation of a structure. Mean depreciation (μ_{du}) is assessed by multiplying the ratio between the effective age (t_u) and the economic life (n_u) by the mean cost (Equation (6)).

$$\mu_{du} = \mu_{cu} \cdot \left(1 - \frac{t_u}{n_u}\right) \tag{6}$$

In order to take into account the quality of the residential building, three different quality types are assumed (historical buildings, residential buildings, and public housing). For each quality type, the minimum ($D_{c,min}$) and maximum ($D_{c,max}$) distances from the downtown have been fixed. Therefore, the depreciation has been reasonably fixed for each building's quality type as being proportional to the mean cost (Table 6).

Table 6. Mean depreciation, maximum and minimum distance from the downtown based on the building's quality type.

Distance	**Historical buildings**	**Residential buildings**	**Public housing**
$D_{c,min}$ [km]	0	2	4
$D_{c,max}$ [km]	3	7	10
μ_{du} [€/m^2]	0.35 μ_{cu}	0.20 μ_{cu}	0.10 μ_{cu}

The mean depreciation is uniform for each building's quality type, while the associated standard deviation is arranged for each of the 34 neighborhoods. Given the aforementioned hypothesis, the mean value of the building's year of construction may be derived from Equation (6) by setting an economic life of 50 years. Furthermore, the minimum and maximum fluctuations of the year of construction per each neighborhood have been estimated by assuming the minimum ($\mu_{cu} \cdot (1-\sigma_{cu})$) and maximum ($\mu_{cu} \cdot (1+\sigma_{cu})$) building cost. Therefore, Equation (7) resumes the process that has been carried out to estimate the mean (t_u), maximum ($t_{u,MAX}$), and minimum ($t_{u,MIN}$) year of construction for each neighborhood.

$$\begin{cases} t_u = n_u \cdot \left(1 - \dfrac{\mu_{du}}{\mu_{cu}}\right) \\ t_{u,MAX} = n_u \cdot \left(1 - \dfrac{\mu_{du}}{\mu_{cu} \cdot (1+\sigma_{cu})}\right) \\ t_{u,MIN} = n_u \cdot \left(1 - \dfrac{\mu_{du}}{\mu_{cu} \cdot (1-\sigma_{cu})}\right) \end{cases} \tag{7}$$

The whole procedure is resumed in Figure 21.

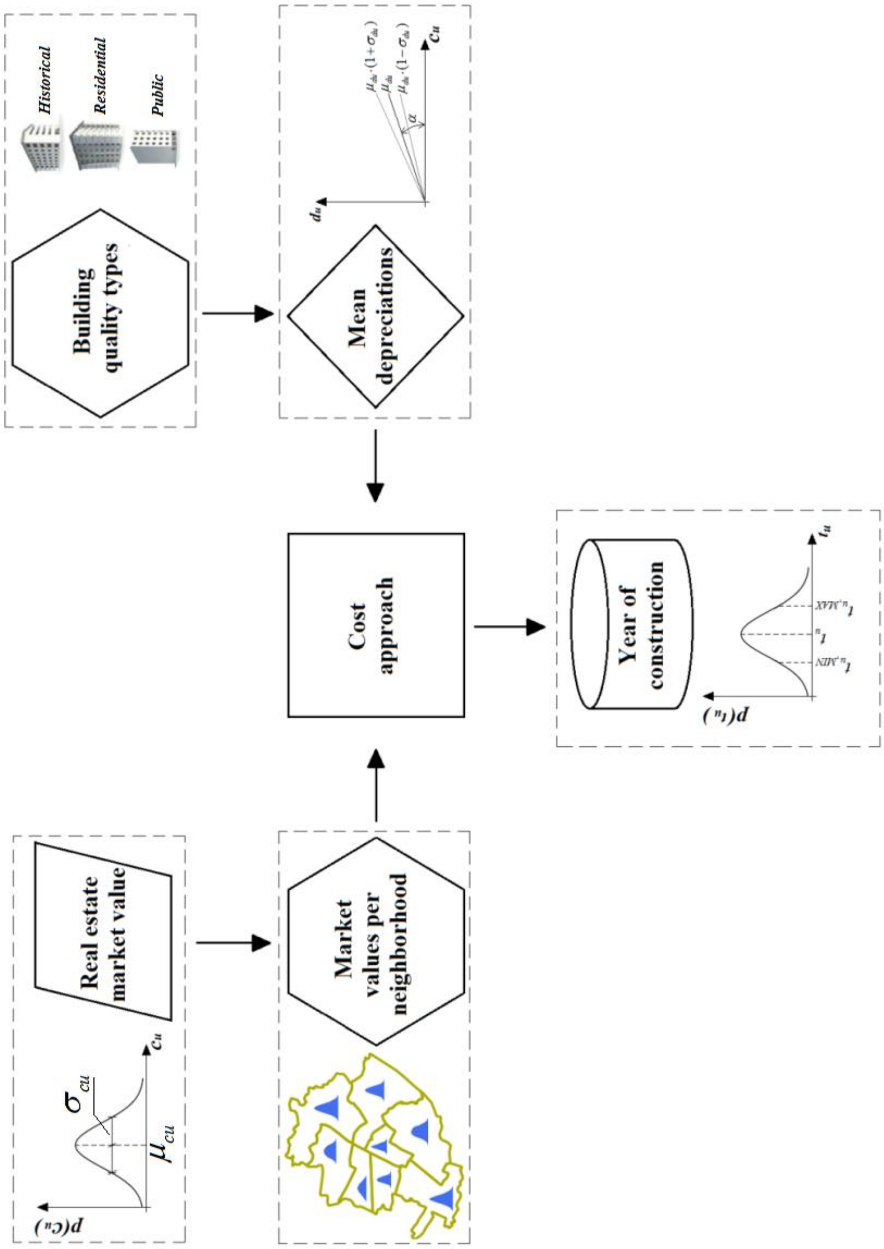

Figure 21. Data flow used to estimate the year of construction based on the cost approach.

4.6.2 Assignment of the year of construction properties to the unprovided buildings

The assignment of the year of construction to the unprovided building has been performed as below resumed:

- The year of construction (Y_C) must satisfy the following condition (Equation (8)).

$$t_{u,MIN} \leq Y_C \leq t_{u,MAX} \tag{8}$$

- The global percentages of residential buildings for each category of year of construction have to meet the requirements derived from ISTAT and listed in Table 5.

4.6.3 Assessment and assignment of the unknown number of story and building archetypes

Some of the geometrical parameters may affect the assignment of the structural and nonstructural properties of a building. To clarify this statement, let's suppose to identify the building archetype of a ten-story building. The geometrical parameter is identified by the number of story, while the structural property is represented by the building archetype. Since the maximum number of story for a masonry building may be limited to 5, it is suitable to assume RC as building archetype. This example highlights how certain "reasonable" considerations and/or well-known design rules can be adopted to assess the missing geometrical and structural parameters. Therefore, the unknown number of story and building archetypes have been evaluated through a simple procedure following resumed:

- *Step 1*: masonry buildings have been mainly located near to the historical center of the city while RC buildings have been uniformly distributed within the urban area.
- *Step 2*: the global percentage of masonry and RC buildings need to verify the requirements provided in the Table 5.
- *Step 3*: the number of stories have been assigned based on the following simple rules:
  - *I)* the maximum number of stories for masonry buildings has been set to 5.
  - *II)* the absolute maximum number of stories for residential building stock has been set to 15.
  - *III)* the maximum building height and story height have been derived according to the minimum seismic requirements associated with the considered year of construction.

4.6.4 Assessment and assignment of the construction elements (external walls and floors)

Seven floor types (Figure 16) and three external wall (Figure 17) types have been assumed to characterize the construction elements of the building portfolio of *IDEAL CITY*. The construction elements have been assessed and assigned to meet the requirements on the provided year of construction ranges (Corrado et al., 2012).

4.6.5 Assessment and assignment of the structural configuration and reinforcement

Seven Structural Configuration types (*SC*) and four Reinforced Element types (*RE*) have been assumed to characterize the residential buildings stock. The first classification refers to the mean span length both for RC and masonry building archetypes (Table 7). In the first case, the span length is defined as distance between two adjacent columns, whereas the distance between two adjacent masonry panels is intended for masonry buildings.

Table 7. Structural configuration types and related mean span lengths.

Structural Configuration type	SC 1	SC 2	SC 3	SC 4	SC 5	SC 6	SC 7
Mean span Length [m]	4.00	4.50	5.00	5.50	6.00	6.50	7.00

The maximum limit of the span length depends on the building's flooring system. Therefore, the SC types have been assigned to meet the requirements resumed in Table 8.

Table 8. Floor types and related maximum span length.

Floor type	F 1	F 2	F 3	F 4	F 5	F 6	F 7
Max Span Length [m]	7.00	6.00	6.00	5.50	6.00	6.50	5.00

The RE types deal with the percentage of reinforcement on the columns or on the masonry panels. Then, three level of reinforcement have been assumed (Table 9).

Table 9. Reinforced element types and related percentage of reinforcement.

Reinforced Element type	RE 1	RE 2	RE 3	RE 4
Percentage of Reinforcement [%]	0	< 1.50	1.50 - 3.00	> 3.00

Mostly, the percentage of reinforcement in the structural members is unknown. Therefore, different sources of information need to be exploited to estimate the percentage of reinforcement with certain accuracy. For this reason, the maximum and minimum values of percentage of reinforcement provided by the seismic guidelines have been used (Table 10).

Table 10. Ranges of the percentage of reinforcement based on the year of construction.

Year of Construction	I	II	III	IV	V	VI
Max percentage of reinforcement (ρ_{max})	–	0.60	0.80	0.60	1.00	1.00
Min percentage of reinforcement (ρ_{min})	–	–	–	5.00	4.00	4.00

When the maximum and minimum values the value of 6.00 % and 0.50 % are set, respectively. In addition, the percentage of reinforcement is considered as normally distributed, while the assessment and assignment of the RE types have been executed through a random process based on the normal PDF.

4.6.6 Assessment of the minimum design requirements (RC buildings)

The design requirements (e.g. mechanical and strength characteristics, load combinations, etc.) have been collected for the different building archetypes based on the seismic standards associated with the year of construction. In case of RC buildings, the mechanical characteristics are resumed in Table 11.

Table 11. Mean mechanical characteristics for RC based on the year of construction.

	Concrete strength class **f_{ck} [MPa]**	**E_{cm} [MPa]**	**Reinforcement bars strength class** **f_{yk} [MPa]**	**E_{sm} [MPa]**
I	15 17	18000	353 391	10 E_{cm}
II	15 17 20	19620	353 391 440	10 E_{cm}
III	12 15 17 20 25	19620	216 353 391 440	10 E_{cm}
IV	15 20 25 30 40	$6066\sqrt{f_{ck}}$	216 313 333 373 402 430	$f_{yk}/0.002$
V	12 16 20 25 30 35 40 45	$6257\sqrt{f_{ck}}$	215 315 375 430	200000
VI	12 16 20 25 30 35 40 45	$6257\sqrt{f_{ck}}$	391 400	200000

where f_{ck} refers to the characteristic compression strength of the concrete, while f_{yk} is the characteristic yielding stress of the reinforcement bars. Furthermore, the elastic Young modulus for concrete (E_{cm}) and steel bars (E_{sm}) have been provided.

In addition, the seismic load combinations have been also itemized for each category of year of construction (Figure 22).

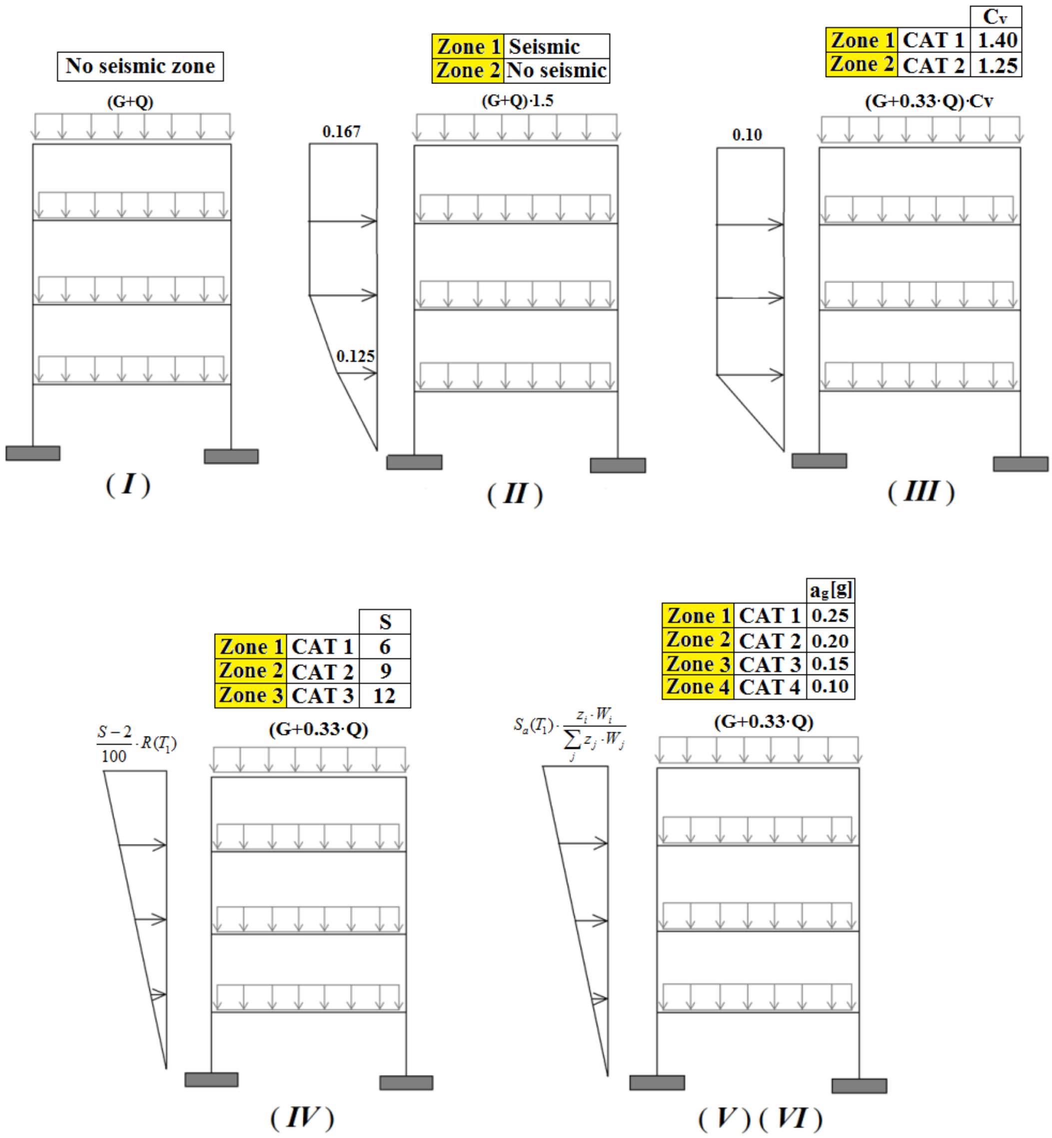

Figure 22. Seismic load combinations based on the year of construction for RC buildings.

Figure 22 illustrates the different horizontal and vertical loads for a generic multi-story building. The permanent vertical loads (structural and nonstructural) are represented by G, whereas Q refers to the vertical live loads. The seismic action is assimilated through specific patterns where each force is applied in the center of the mass of the related floor system. The intensity of the seismic action depends on the hazard level of the site in which the building is located.

The typology-based approach is emphasized through the classification of the geometrical, mechanical, and structural parameters into different “types” as shown in Figure 23.

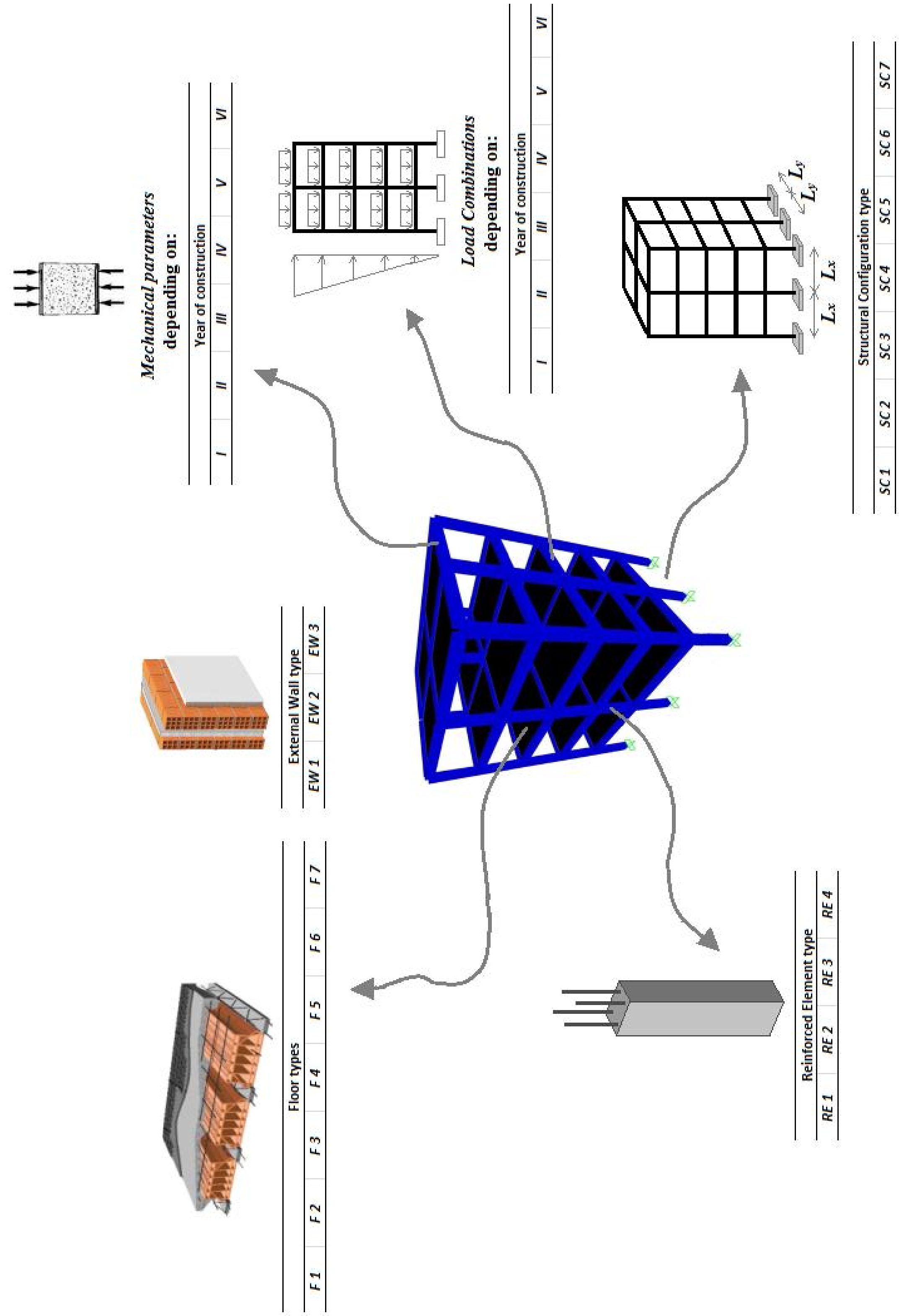

Figure 23. Data collection and processing flow adopted in the typological characterization of RC buildings.

4.6.7 Assessment of the minimum design requirements (masonry buildings)

Mechanical characteristics of masonry buildings depend on the elements of the masonry panels, the quality of the elements, the construction techniques, and the percentage of openings on the panel. The current Italian seismic standards (NTC08, 2008) provide supplementary guidelines on the definition of the mechanical characteristics for different type of masonry panels (maximum and minimum values). These parameters are considered for poor quality masonry panels (poor quality mortar, masonry panel unconsolidated, no toothing among the wythes, and no listatum masonry panel). Table 12 resumes the maximum and minimum values of the mechanical characteristics of the five different MW types in terms of mean compression strength (f_m), mean tangential strength (τ_0), mean elastic Young modulus (E_m), and mean elastic shear modulus (G_0).

Table 12. Maximum and minimum values of the mechanical parameter of masonry buildings (NTC08, 2008).

	f_m [MPa]		τ_0 [MPa]		E_m [MPa]		G_0 [MPa]	
	Min	Max	Min	Max	Min	Max	Min	Max
MW 1	240	400	6	9.2	1200	1800	400	600
MW 2	600	800	9	12	2400	3200	780	940
MW 3	200	300	3.5	5.1	1020	1440	340	480
MW 4	200	300	3.5	5.1	1020	1440	340	480
MW 5	260	380	5.6	7.4	1500	1980	500	660
MW 6	500	800	24	32	3500	5600	875	1400

The NTC (2008) provides also some corrective coefficients to be applied to the mechanical characteristics in order to consider the real conditions of the masonry panel. Due to the unavailability of detailed information related to the quality of the masonry buildings, a typology-based approach has been used to assign the geometrical and mechanical characteristics. Then, the following masonry quality types have been assumed:

- Mortar Quality types (*MQ*): *Low, Medium, and High.*
- Transversal Confinement type (*TC*): *Low, Medium, High.*
- Consolidation Action type (*CA*): *Unconsolidated, Consolidated.*

For each of these masonry quality types, the mechanical corrective coefficients have been defined according to the NTC 2008 (Table 13).

Table 13. Mechanical corrective coefficients for each masonry wall type (NTC08, 2008).

	MQ			***TC***			***CA***	
	Low	***Medium***	***High***	***Low***	***Medium***	***High***	***No***	***Yes***
MW 1	1.10	1.30	1.50	1.10	1.20	1.30	1.00	1.50
MW 2	1.07	1.15	1.20	1.10	1.15	1.20	1.00	1.20
MW 3	1.07	1.25	1.40	1.15	1.25	1.50	1.00	1.70
MW 4	1.07	1.25	1.40	1.15	1.25	1.50	1.00	1.70
MW 5	1.10	1.20	1.40	1.10	1.20	1.30	1.00	1.55
MW 6	1.00	1.00	1.00	1.00	1.00	1.00	1.00	1.00

The mortar quality has been considered as inversely proportional to the time. According to this criterion, the following classification has been performed (Table 14).

Table 14. Mortar quality based on the year of construction.

	Year of construction					
	I	**II**	**III**	**IV**	**V**	**VI**
MQ	Low	Low	Medium	Medium	High	High

Moreover, the transversal confinement is dependent on the construction techniques, while the consolidation actions are required in some cases. Both aspects are unpredictable due to the limited data and sources. Then, the TC type and the CA type have been assigned using a random process.

Lastly, the geometrical configuration of the panel is affected by the dimension and arrangement of the openings on the masonry panel. Also in this case, detailed analyses are necessary to fully characterize the geometrical configuration of the masonry buildings. To overcome this limit, historical analyses have been performed to identify the typical opening standard sizes adopted in the national territory (Figure 24).

Opening	Type ID	Dimensions	Year
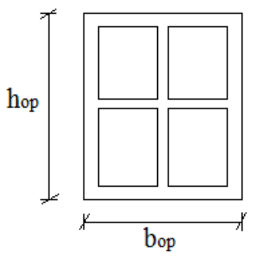	**O 1**	$b_{op} = 1.20m \quad h_{op} = 1.40m$	> 1940
	O 2	$b_{op} = 0.90m \quad h_{op} = 1.20m$	1900 - 1960
	O 3	$b_{op} = 1.10m \quad h_{op} = 1.50m$	< 1950
	O 4	$b_{op} = 0.80m \quad h_{op} = 1.60m$	< 1930

Figure 24. Opening (O) typologies for masonry buildings.

Furthermore, three Opening Ratios (*ORs*) have been defined (Table 15). They represent the ratio between the area of the openings distributed on a single panel and the area of the masonry panel.

Table 15. Opening ratio associated with the Opening Ratio types.

	Opening Ratio type		
	Low	Medium	High
OR [%]	10	15	20

The OR type has been assigned to the masonry building within the urban area using a random process.

Finally, the seismic load combinations have been also collected for each category of year of construction (Figure 25).

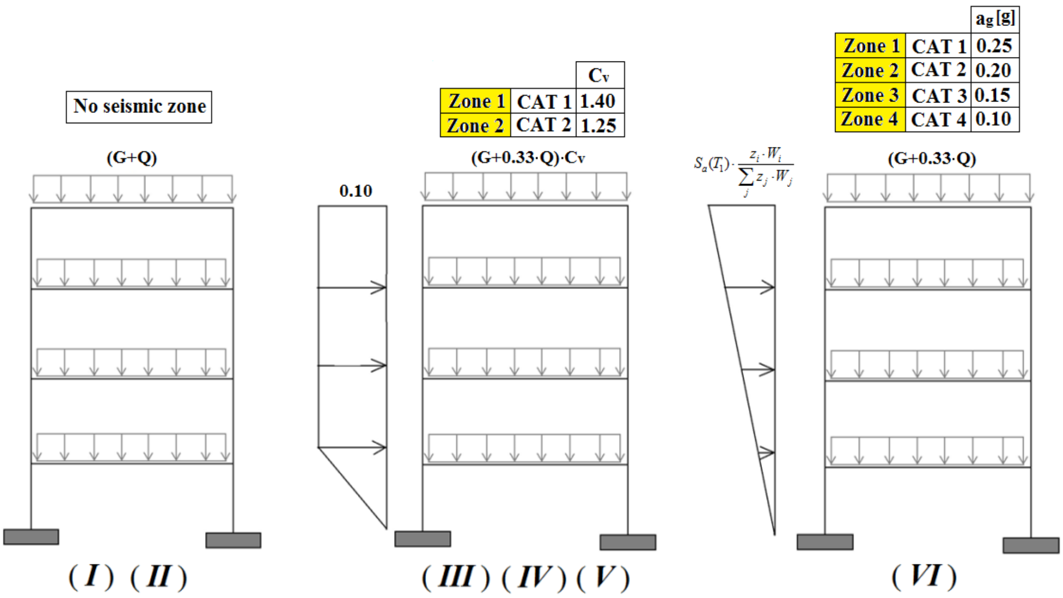

Figure 25. Seismic load combinations based on the year of construction for masonry buildings.

A sketch that resumes all the "types" used in the definition of the geometrical, mechanical, and structural parameters of the masonry buildings is illustrated in Figure 26.

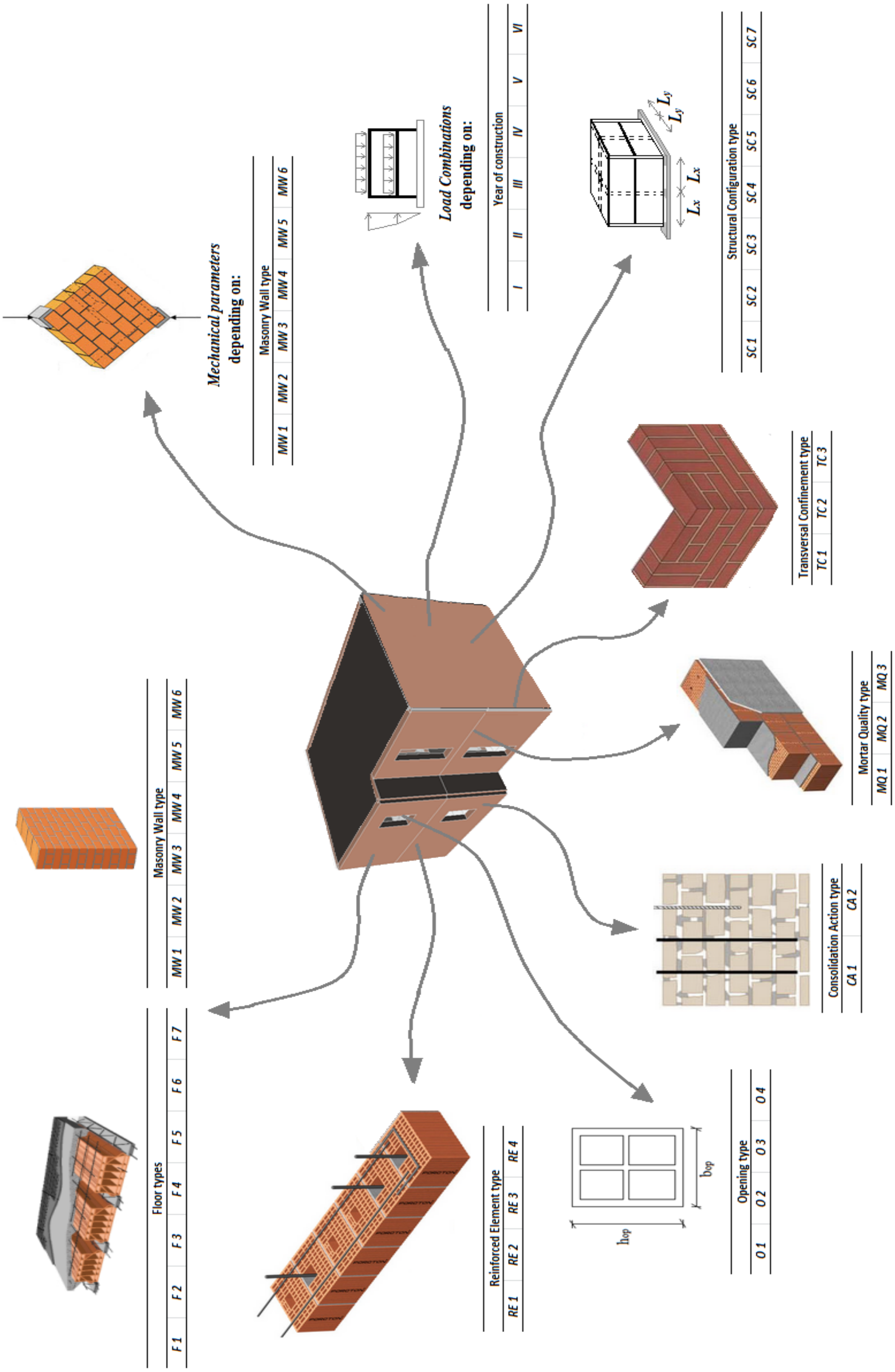

Figure 26. Data collection and processing flow adopted in the typological characterization of masonry buildings.

4.6.8 Assessment of the lateral resisting frame dimensions

A MATLAB (MATLAB, 2018) algorithm has been developed with the aim of assessing and assigning the design structural properties. The algorithm collects all the minimum design requirements associated with the considered year of constructions. Then, the structural properties are evaluated in order to verify the minimum design requirements established by the assumed Italian seismic standards. Therefore, the lateral resisting frame dimensions of each building of the structural members are evaluated. To accomplish this goal, a typological-based approach has been adopted to identify all the input variables necessary to characterize the structural members of each building.

The seismic design minimum requirements are based on the hazard parameters of a certain site. Given the virtual characteristic of the city, different seismic scenarios have been considered with the aim of analyze different exposure databases representative of the entire national territory. For this purpose, three seismic hazard levels have been envisioned as being representative of the national hazard (Table 16).

Table 16. Hazard levels representative of the Italian seismic hazard and related PGA values.

	Hazard Level		
	Low	Medium	High
PGA [g]	0.10	0.20	0.30

Therefore, the geometrical information (structural configuration and percentage of reinforcement), construction elements, and load combinations have been assessed for the three aforementioned Hazard Levels (HLs). Then, the proposed algorithm is implemented through the following steps:

- *Step 1*: vertical and horizontal loads are assessed for a predetermined seismic hazard scenario and the internal stress is defined for each structural element.
- *Step 2*: the minimum dimensions of the structural elements (cross section's width and depth for the columns and beams, and thickness for the masonry panels) is determined.
- *Step 3*: the minimum design requirements for the considered year of construction category are verified and the final structural elements' dimensions are assessed.

4.7 Input variables description, stochastic dependence and uncertainties

The accuracy of the gathered information is affected by the uncertainties introduced into the data collection, preparation and processing stages. The main sources of uncertainties are represented by the physical and statistics uncertainties. Therefore, statistical inference processes have been used to deduce some of the missing or inadequate properties describing the system. All the mechanical and geometrical parameters have been assumed as RVs normally distributed and a set of mean and standard deviation values have been set. In other words, each generic value of a certain building's attribute B_p is expressed as given in Equation (9).

$$B_p = \mu \cdot \left(1 + \Delta B_p \cdot \eta\right) \tag{9}$$

where μ represents the mean observed attribute value while ΔB_p refers to its maximum absolute dispersion, and η is a uniform random variable defined in the interval [-1; +1]. The mean value corresponds to the value assessed in the data collection and processing stages, while the dispersion parameters have been theoretically fixed to get a Confidence Interval (*CI*) of 95.4% (Figure 27).

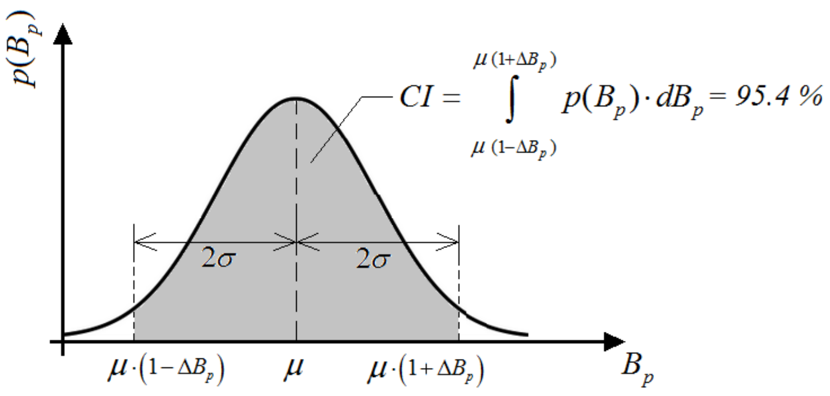

Figure 27. Building's property normally distributed and related confidence interval.

Then, the Equation (10) is given

$$\Delta B_p = 2 \cdot \sigma \tag{10}$$

where σ represents the standard deviation of the normal probability density function.

In this research, three types of statistical and physical uncertainties have been assumed:

- uncertainty associated with the mechanical parameters (σ_M);
- uncertainty associated with the geometrical parameters (σ_G);
- uncertainty associated with the construction elements parameters (σ_{CE}).

The quantification of the uncertainties is a complicated process which requires a deepen analysis of the data. Herein, a standardized procedure has been performed in order to assess the set of the dispersion parameters. First, the standard deviation associated with the mechanical parameters has been assumed according to the standard requirements provided by the ATC-58-1 (ATC, 2011) (Table 17).

Table 17. Dispersion coefficients associated with the mechanical parameters of RC and masonry buildings.

RC	**Masonry**
0.2 μ_M	0.25 μ_M

where μ_M represents the mean value of the observed mechanical parameter. Furthermore, the uncertainties associated with the geometrical and construction elements properties have been defined using a standard procedure based on the following assumptions:

- lack of knowledge is proportional to the building's age;
- physical uncertainty is greater in masonry buildings than in RC buildings.

According to these hypotheses, the dispersion values provided in Table 18 have been selected. μ_G and μ_{CE} represent the mean value of the observed geometrical and construction element entities, respectively.

Table 18. Standard deviations associated with the geometrical parameters and construction elements of RC and masonry buildings based on the year of construction.

		Year of construction					
		I	**II**	**III**	**IV**	**V**	**VI**
RC	σ_G/μ_G	0.20	0.18	0.16	0.13	0.10	0.08
	σ_{CE}/μ_{CE}	0.25	0.22	0.20	0.18	0.15	0.10
Masonry	σ_G/μ_G	0.25	0.22	0.20	0.17	0.13	0.10
	σ_{CE}/μ_{CE}	0.28	0.26	0.24	0.22	0.20	0.18

In the context of seismic damage assessment of buildings, part of the inputs variables are correlated. The incorporation of such correlations in the computational process becomes important. In fact, ignoring correlation between RVs may leads to unrealistic simulation results. According to the current literature, the dependence among the area of the reinforcing bars (A_s), the characteristic concrete compressive strength and (f_{ck}), the reinforcing bar yield strength (f_{yk}), and the elastic modulus of the concrete (E_c) have been considered. According to the Probabilistic Model Code (Vrouwenvelder, 2001) the correlation coefficient of A_s and f_{yk} has been set to 0.50, while the dependence between f_{ck} and E_c has been considered through a correlation coefficient of 0.80 (Mirza & Mac Gregor, 1979).

Since the construction element entities are used to define the mass of the building, a correlation coefficient equal to 0.90 (strong correlation) has been assumed between the variables associated with the construction element and the span length. All the other input variables have been assumed uncorrelated.

In Table 19 a complete description of the input variables and the related mean and standard deviation values is provided.

Table 19. Complete description of the input variables.

Building entity	**Building attribute**	**Symbol**	**Unit measure**	**Distribution type**	**Mean [μ]**	**Standard deviation [σ]**
CONSTRUCTION ELEMENT PARAMETERS	Concrete density	ρ_c	kg/m^3	Normal	2450	f(YC, BA) **
	Light concrete density	ρ_{lc}	kg/m^3	Normal	1750	f(YC, BA)
	Flooring density	ρ_f	kg/m^3	Normal	420	f(YC, BA)
	Reinforcing bars density	ρ_r	kg/m	Normal	2.50	f(YC, BA)
	Hollow blocks density	ρ_b	kg/m^3	Normal	1050	f(YC, BA)
	Brick density	ρ_{sb}	kg/m^3	Normal	1550	f(YC, BA)
	Steel density	ρ_s	kg/m^3	Normal	7850	f(YC, BA)
	Wood density	ρ_w	kg/m^3	Normal	600	f(YC, BA)
	Insulation density	ρ_i	kg/m^3	Normal	80	f(YC, BA)
	Stone density	ρ_{sw}	kg/m^3	Normal	2200	f(YC, BA)
	Concrete slab depth	t_c	kg/m^3	Normal	0.12	f(YC, BA)
	Light concrete slab depth	t_{lc}	m	Normal	0.03	f(YC, BA)
	Flooring depth	t_f	m	Normal	0.02	f(YC, BA)
	Hollow brick width	B_b	m	Normal	0.45	f(YC, BA)
	Hollow brick depth	t_b	m	Normal	0.22	f(YC, BA)
	Brick depth	t_{sb}	m	Normal	0.17	f(YC, BA)
	Distance concrete joists	i_c	m	Normal	0.60	f(YC, BA)
	Distance steel joists	i_s	m	Normal	1.10	f(YC, BA)
	Distance wood joists	i_w	m	Normal	0.75	f(YC, BA)
	Live loads	Q	kN/m^2	Normal	f(YC) *	f(YC, BA)
GEOMETRIC PARAMETERS	Span length in x_p direction	l_x	m	Normal	f(SC) [Table 7]	f(YC, BA)
	Span length in y_p direction	l_y	m	Normal	f(SC) [Table 7]	f(YC, BA)
	Story height	h	m	Deterministic	3.00	–
	Column depth of i^{th} story in x_p direction	$b_{c,x}$	m	Deterministic	f(YC, SC, HL) [Designed]	–
	Column width of i^{th} story in y_p direction	$b_{c,y}$	m	Deterministic	f(YC, SC, HL) [Designed]	–
	Beam depth	h_b	m	Deterministic	f(YC, SC, HL) [Designed]	–
	Masonry wall thickness in x_p direction	t_x	m	Deterministic	f(YC, SC, HL) [Designed]	–

	Masonry wall thickness in y_p direction	t_y	*m*	Deterministic	f(YC, SC, HL) [Designed]	–
	Percentage of reinforcement	ρ	%	Normal	f(YC, RE)	f(YC, BA)
	Bar diameter	φ	mm	Deterministic	f(ρ, $b_{c,x}$, $b_{c,y}$)	–
	Stirrup spacing	*s*	*m*	Normal	f(YC)	f(YC, BA)
	Concrete cover	*c*	*m*	Normal	$0.1 \cdot h_b$	f(YC, BA)
	Openings dimension	b_{op} x h_{op}	m^2	Deterministic	f(O)	–
MECHANICAL PARAMETERS	Concrete elastic modulus	E_c	*MPa*	Normal	f(YC) [Table 11]	0.20·μ
	Reinforcing bar elastic modulus	E_s	*MPa*	Normal	f(YC) [Table 11]	0.20·μ
	Concrete compressive strength	f_{ck}	*MPa*	Normal	f(YC) [Table 11]	0.20·μ
	Reinforcing bar yield strength	f_{yk}	*MPa*	Normal	f(YC) [Table 11]	0.20·μ
	Masonry Young elastic modulus	E_m	*MPa*	Normal	f(MW)[Table 12]	0.25·μ
	Masonry shear elastic modulus	G_0	*MPa*	Normal	f(MW) [Table 12]	0.25·μ
	Masonry compressive strength	f_m	*MPa*	Normal	f(MW) [Table 12]	0.25·μ
	Masonry shear strength	τ_0	*MPa*	Normal	f(MW) [Table 12]	0.25·μ
	Mechanical masonry corrective coefficient	c_m	–	Deterministic	f(MW, MQ, TC, CA) [Table 13]	–

* YC: Year of Construction

** BA: Building Archetype

4.8 Data output and storage

The goal of the data processing cycle is to create an output suitable for all the users. The output format is chosen accordingly to the needs of the users and to guide future actions and decisions. Furthermore, all the processed data must be held for future purposes and uses, and then they need to be stored into database which allows quick access and retrieval of the information (data storage).

In this research, all the generic building information has been structured into a text file which allows a faster importing process (*Building_Database.txt*). The file is organized in different columns such that each of them refers to a specific building attribute. The first column identifies the *building ID* which ranges from 1 to 23420, whereas the global geometrical properties of each building are listed below:

- footprint perimeter;
- footprint area;

- coordinates of the center of gravity in x direction;
- coordinates of the center of gravity in y direction;
- inertia with respect to the x-axis based on the footprint section;
- inertia with respect to the y-axis based on the footprint section;
- angle between the principal inertia direction and the global direction;
- number of story.

In order to better understand the abovementioned properties, Figure 28 is provided.

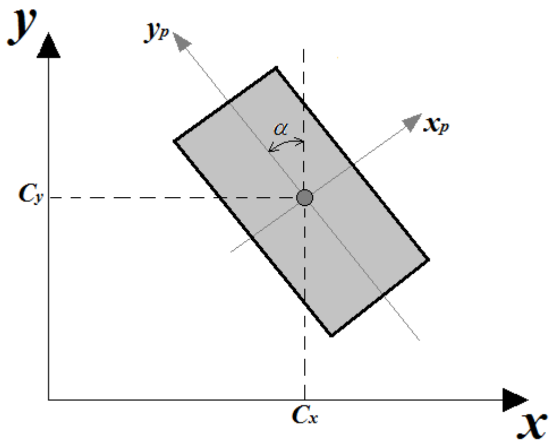

Figure 28. Schematic representation of the global geometrical parameters of a building.

Figure 28 illustrates the main global geometrical properties of a building. The coordinates of the center of gravity are represented by C_x and C_y, while α is the angle between the global reference system (*x-y*) and the local reference system of the building (x_p-y_p), which refers to the principal inertia directions.

The year of construction, the building archetypes, the construction elements, and all the other building's attributes have been classified into the database as listed in Table 20.

Table 20. Numerical classification of the buildings data.

Year of construction	**1 (I)**	**2 (II)**	**3 (III)**	**4 (IV)**	**5 (V)**	**6 (VI)**	–
Building archetype	1 (Masonry)	2 (RC)	–	–	–	–	–
Floor type	1 (F 1)	2 (F 2)	3 (F 3)	4 (F 4)	5 (F 5)	6(F6)	7 (F 7)
External wall type	1 (EW 1)	2 (EW 2)	3 (EW 3)	–	–	–	–
Masonry wall type	1 (MW 1)	2 (MW 2)	3 (MW 3)	4 (MW 4)	5 (MW 5)	–	–
Structural Configuration type	1 (SC 1)	2 (SC 2)	3 (SC 3)	4 (SC 4)	5 (SC 5)	6 (SC 6)	7 (SC 7)
Reinforced Element type	1 (RE 1)	2 (RE 2)	3 (RE 3)	4 (RE 4)	–	–	–
Opening type	1 (O 1)	2 (O 2)	3 (O 3)	4 (O 4)	–	–	–
Opening Ratio type	1 (Low)	2 (Medium)	3 (High)	–	–	–	–
Mortar Quality type	1 (Low)	2 (Medium)	3 (High)	–	–	–	–
Transversal Confinement type	1 (Low)	2 (Medium)	3 (High)	–	–	–	–
Consolidation Action type	1 (No)	2 (Yes)	–	–	–	–	–

In the last part of the building database the values of the dispersion parameters (mechanical, geometrical, and mass properties) are resumed.

The design parameters (such as cross section dimensions or wall thickness) have been arranged into different text files. Each file refers to a fixed principal direction of the building (x_p and y_p) and a given hazard level (Low (*L*), Medium (*M*), and High (*H*)). The design parameters of the RC buildings are represented by the columns and beams cross section dimensions, whereas the masonry buildings design parameters are identified through the panel thickness in both horizontal directions (Figure 29).

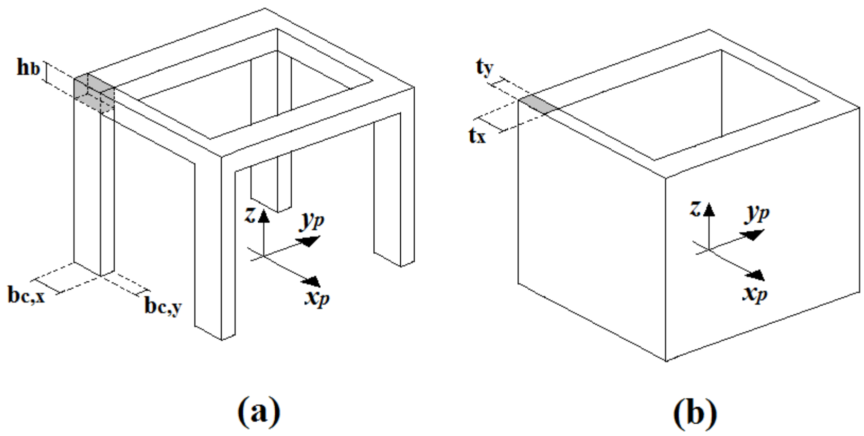

Figure 29. Design parameters for RC (a) and masonry (b) buildings.

The following filenames have been defined (Table 21).

Table 21. Building design parameters per each hazard level collected into different file.

Hazard level	**Structural elements**					
	Columns (dimensions)		Beams (depth)		Masonry panels (thickness)	
	x_p direction	**y_p direction**	**z-x_p plane**	**z-y_p plane**	**x_p direction**	**y_p direction**
Low	Column_L_X	Column_L_Y	Beam_L_X	Beam_L_Y	tchick_L_X	tchick_L_Y
Medium	Column_M_X	Column_M_Y	Beam_M_X	Beam_M_Y	tchick_M_X	tchick_M_Y
High	Column_H_X	Column_H_Y	Beam_H_X	Beam_H_Y	tchick_H_X	tchick_H_Y

The first part of the filename refers to the structural elements, the second character identifies the hazard level (e.g. L: Low, M: Medium, and H: High) and the third character represents the principal building direction (X: x_p and Y: y_p). Each of those files is composed by a number of rows equal to the number of residential buildings within *IDEAL CITY* and a number of columns equal to the absolute maximum number of stories (set to 15). In other words, the i^{th} column refers to the i^{th} story of the considered building while the j^{th} row is associated with the building ID. An illustrative example of design parameters format is shown in Figure 30.

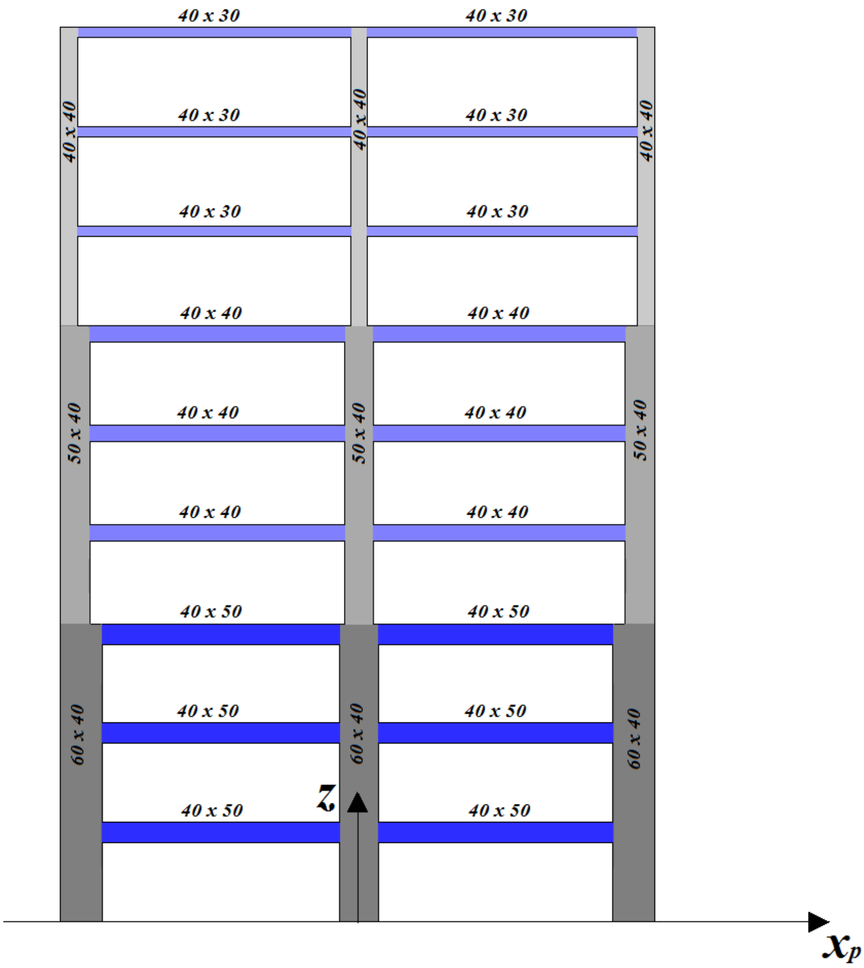

Column dimensions in x_p direction

0.60	0.60	0.60	0.50	0.50	0.50	0.40	0.40	0.40	–	–	–	–	–	–

Column dimensions in y_p direction

0.40	0.40	0.40	0.40	0.40	0.40	0.40	0.40	0.40	–	–	–	–	–	–

Beam depth in the plane z-x_p

0.50	0.50	0.50	0.40	0.40	0.40	0.30	0.30	0.30	–	–	–	–	–	–

Beam depth in the plane z-y_p

0.40	0.40	0.40	0.40	0.40	0.40	0.40	0.40	0.40	–	–	–	–	–	–

Figure 30. Illustrative example of design parameters file format.

All the generated text files containing the building information and their design properties have been stored into the *IDEAL_SERVER* database which is the main server of the Disaster Simulation Resilience Center (DSRC) located in the Structural and Geotechnical Department (DISEG) of the Polytechnique University of Turin.

Chapter 5

A new physical model for assessing the seismic capacity of the building portfolio

5.1 Introduction

To improve the predictability of structural damage for a given hazard scenario, it is essential to identify factors that influence the structural response and evaluate their contributions. Several studies have been focused on the assessment of parameters that influence the inelastic response of structures under seismic action (Kumar, 2013). Many existing researches aim to the definition of standardized force-displacement relationships simulating the structural behavior of certain building category (Steelman et al., 2009, Ellingwood et al., 2008). These researches have in most cases been limited to SDOF systems with controlled mass and stiffness distribution characteristics.

Terán-Gilmore et al. (2009) proposed a practical-based evaluation procedure to estimate the capacity curve of confined masonry buildings. The inelastic roof displacement was estimated through the application of the Coefficient Method, while nonlinear simplified model is used to perform pushover analysis.

Other studies have been instead dealt with the definition of the generalized inter-story backbone curves and hysteretic parameters. Lu et al., (2017) proposed a method to estimate the inter-story backbone curve of RC and masonry buildings with regular planar layout. The characteristic force-displacements parameters were determined based on the simulated design procedure and statistical analyses for RC and masonry building categories.

.

Given the large number of buildings in urban areas, the building simulation model has to accurately capture the main nonlinear properties of typical Multi Degree Of Freedom (MDOF) and reduce the computational time required to assess the damage. A new nonlinear physical model is proposed to assess the global seismic capacity of individual building that is simulated through a four-linear backbone curve and tri-linear backbone curve for RC and masonry (unreinforced and reinforced) buildings, respectively. Therefore, each capacity curve is able to reflect the seismic behavior of the equivalent SDOF system associated with the building under consideration. This approach leads to reduce the computational effort required to assess the structural response. Furthermore, the proposed methodology focuses on identifying a capacity curve that is characteristic of each individual building (*individual approach*) rather than assess the capacity of certain groups of buildings (*typological approach*).

Detailed information on the definition of the buildings' capacity is provided in the following sections, both for RC and masonry buildings.

5.2 Reinforced concrete buildings

The RC buildings are modeled as 3D MDOF system involving the following physical assumptions:

- *Uniform frame distributions in both horizontal directions*;
- *inextensible frame elements*;
- *bending type system*;
- *lumped mass*;
- *regular planar layout*;
- *seismic global capacity simulated through a four-linear backbone curve*.

The equivalent global seismic behavior is assessed by considering an equivalent 2D frame in both principal horizontal directions (Figure 31).

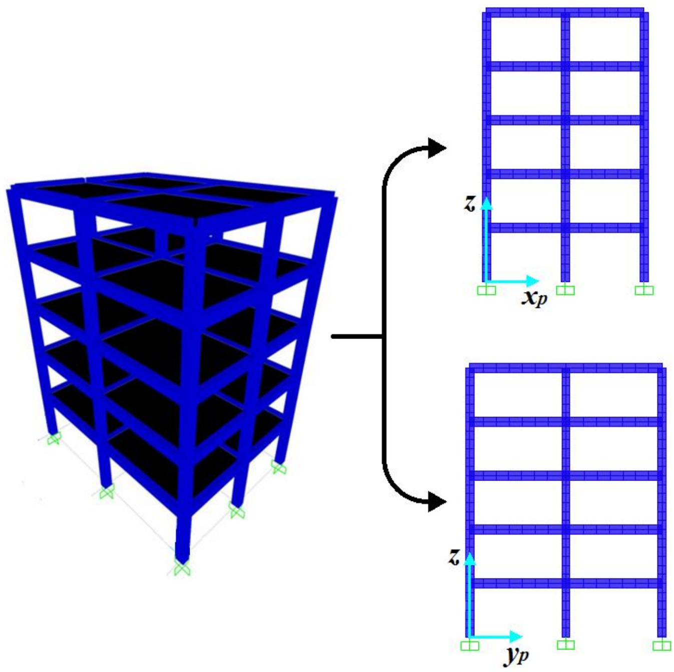

Figure 31. 2D building models in both principal horizontal directions.

The global capacity is expressed as the function between the base shear (V_b) and the top displacement (u_{top}) for a given horizontal direction.

Commonly used tri-linear backbone curve is a suitable simplification of the building's capacity. However, ductile frames (such as RC buildings designed according to the seismic rules) may require additional points to accurately describe the post-elastic response. To better focus on this aspect, HAZUS (FEMA, 2011) provides a standardized relationship between the building's performance for a given seismic intensity and the associated Damage State (DS) (Figure 32).

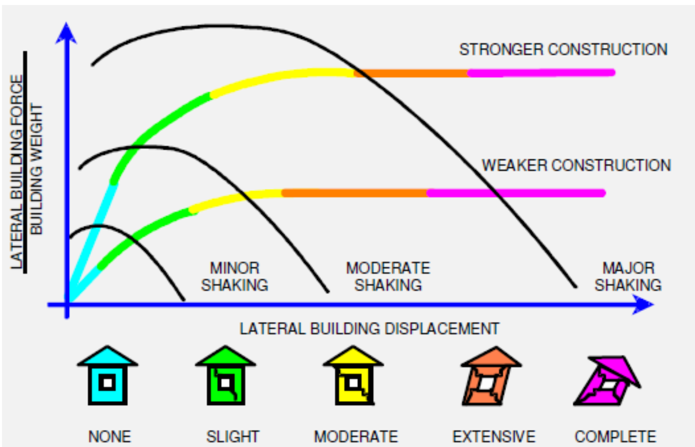

Figure 32. Building capacities vs. seismic demands (FEMA, 2011).

The capacity curve on the top refers to ductile and resistant constructions *(stronger construction*) which are representative of medium or high-code structures. In these cases, the approximation of the capacity curve with a tri-linear function does not represent an accurate model for Moderate DSs caused by moderate and higher shaking. Thus, a four-linear backbone curve is a suitable approximation of the seismic capacity of a RC building (Figure 33).

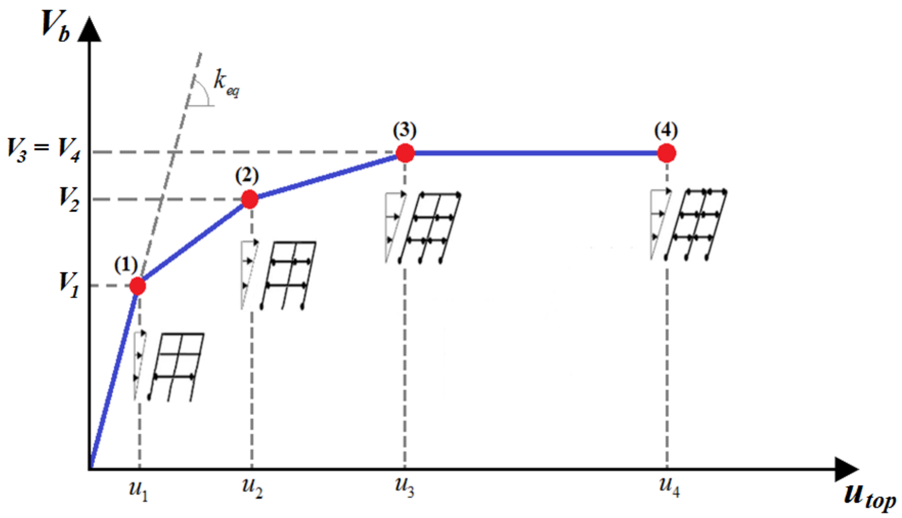

Figure 33. Proposed four-linear backbone curve, representative of the global capacity of RC buildings.

The first point of the backbone curve (*1*) refers to the yield condition associated with the formation of the first plastic hinge in the weakest column. After the yield point, the global stiffness decrease until the next point (*2*). This point is representative of moderate damage level in which the weakest column reaches its maximum capacity. The structure is subjected to a massive distribution of the internal actions while the stiffness decreases. When all the columns of the weakest story are plasticized, the maximum capacity is reached (point (*3*)). The structure is then subjected to a plastic mechanism until the collapse (point *4*). Collapse occurs when the number and disposition of the generated plastic hinges are such that an unstable scheme is identified (collapse mechanism). The generic scheme of the four-linear backbone curves is illustrated in Figure 33. It highlights the evolution of the plastic hinges formation into a generic multi-story frame subjected to a monotonically increasing horizontal forces distribution.

The following sections deal with the definition of the characteristic points of the proposed backbone curve model.

5.2.1 Elastic parameters

The elastic parameters are identified by the base shear and top displacement associated with the point (*1*) of the backbone curve. Modal analysis is performed to assess the elastic properties of a building in both horizontal principal directions.

Stiffness properties

A bending type model is assumed to determine the stiffness matrix. As illustrative example, the DOFs of a five story buildings composed by two spans is depicted in Figure 34. Each vertical and horizontal element is considered as inextensible, whereas the flooring systems are assumed as rigid bodies. The rotations in each beam-column joint and the horizontal displacements of the center of the mass are the DOFs of the system under consideration.

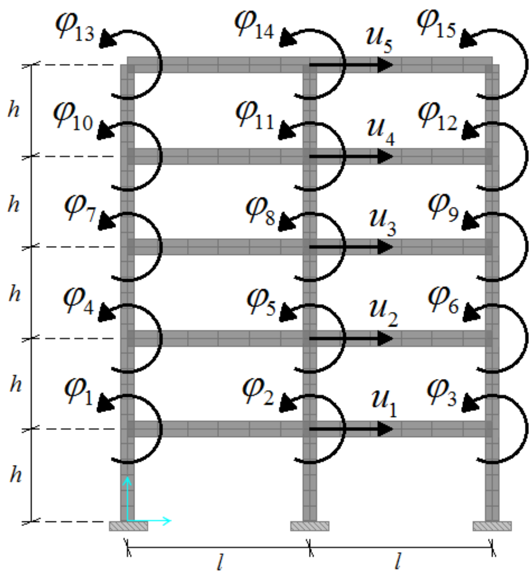

Figure 34. Rotational and translational DOFs for a 2D frame.

The bending type model is capable to take into account the flexibility of the flooring systems, or in other words, the flexibility of the beams is considered to assess the stiffness of the structure. However, the computational effort required by a bending type frame is greater than a shear type frame. Furthermore, the predominant DOFs of a multi-story building are the lateral displacements (roof displacements). Therefore, the total DOFs of the system can be reduced by applying the condensation method. One of the most commonly used approaches is the Guyan reduction which is based on the division of the DOFs into master and slave DOFs. The first ones are the lateral roof displacements, whereas the second ones include the nodal rotations. The matrix form of the equation of motion has to be arranged in order to divide the master DOFs (m) from the slave DOFs (s) (Equation (11)).

$$\begin{bmatrix} [M_{mm}] & [M_{ms}] \\ [M_{sm}] & [M_{ss}] \end{bmatrix} \begin{Bmatrix} \{\ddot{\delta}_m\} \\ \{\ddot{\delta}_s\} \end{Bmatrix} + \begin{bmatrix} [K_{mm}] & [K_{ms}] \\ [K_{sm}] & [K_{ss}] \end{bmatrix} \begin{Bmatrix} \{\delta_m\} \\ \{\delta_s\} \end{Bmatrix} = \begin{Bmatrix} \{F(t)_m\} \\ \{F(t)_s\} \end{Bmatrix} \tag{11}$$

This equation can be simplified by assuming that the inertial contributions associated with the slave DOFs are equal to zero ($[M_{ms}]=[M_{sm}]=[M_{ss}]=[0]$). In addition, the external forces applied to the slave DOFs can be neglected ($\{F(t)_s\}=\{0\}$). The system of the equations of motion can be rewritten in matrix format (Equation (12)).

$$\begin{bmatrix} [M_{mm}] & [0] \\ [0] & [0] \end{bmatrix} \begin{Bmatrix} \{\ddot{\delta}_m\} \\ \{\ddot{\delta}_s\} \end{Bmatrix} + \begin{bmatrix} [K_{mm}] & [K_{ms}] \\ [K_{sm}] & [K_{ss}] \end{bmatrix} \begin{Bmatrix} \{\delta_m\} \\ \{\delta_s\} \end{Bmatrix} = \begin{Bmatrix} \{F(t)_m\} \\ \{0\} \end{Bmatrix} \tag{12}$$

The vector of the slave DOFs δ_S can be obtained from the second row of the matrix given in previous equation.

$$[K_{sm}]\{\delta_m\} + [K_{ss}]\{\delta_s\} = \{0\} \rightarrow \{\delta_s\} = -[K_{ss}]^{-1}[K_{sm}]\{\delta_m\} \tag{13}$$

Substituting the expression found in the first equation of motion, Equation (14) is given.

$$[M_{mm}]\{\ddot{\delta}_m\} + \left([K_{mm}] - [K_{ms}][K_{ss}]^{-1}[K_{sm}]\right)\{\delta_m\} = \{F(t)_m\} \tag{14}$$

The reduced or condensed stiffness matrix ($[K_R]$) is then determined (Equation (15)).

$$[K_R] = \left([K_{mm}] - [K_{ms}][K_{ss}]^{-1}[K_{sm}]\right) \tag{15}$$

The dimension of this matrix is equal to the master DOFs. The reduced stiffness matrix of a bending type frame is a full matrix as reported in the Equation (16).

$$\left[K_{BT_R}\right] = \begin{bmatrix} k_{11} & k_{12} & \cdots & \cdots & k_{1n} \\ k_{21} & k_{22} & \vdots & \vdots & \vdots \\ \vdots & \vdots & \ddots & \vdots & \vdots \\ \vdots & \vdots & \vdots & \ddots & k_{n-1\ n} \\ k_{n1} & \cdots & \cdots & k_{n\ n-1} & k_{nn} \end{bmatrix} \tag{16}$$

The stiffness matrix components are calculated based on the mean mechanical and geometrical properties collected into the database. Figure 35 depicts the geometrical parameters which describe the cross sections of the columns and the beams with reference to the i^{th} story building.

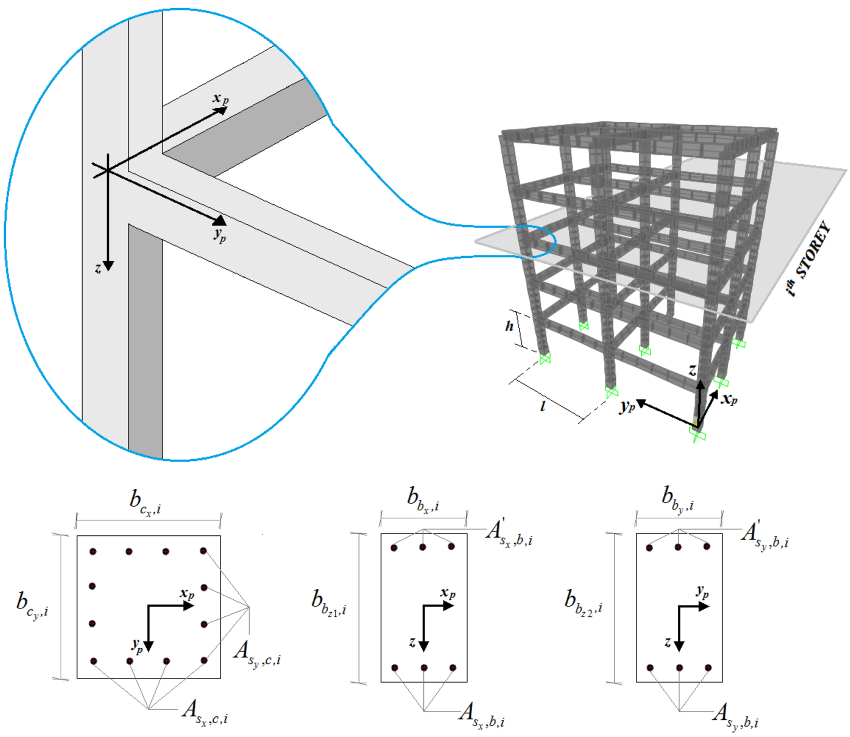

Figure 35. Geometrical parameters associated with the cross section of the columns and the beams.

According to the geometrical parameters shown in Figure 35, the moment of inertia of the columns and beams with respect to the x_p and y_p axes are defined for the i^{th} story (Equation (17) and (18)).

$$I_{c,x_p-x_p,i} = \frac{b_{c_y,i} \cdot b_{c_x,i}^3}{12} + n_{om} \cdot \sum_{j=1}^{n_{st,x}} n_{sx,j} A_{sx,c,j} \cdot x_{sx,j}^2$$
$$I_{c,y_p-y_p,i} = \frac{b_{c_x,i} \cdot b_{c_y,i}^3}{12} + n_{om} \cdot \sum_{j=1}^{n_{st,y}} n_{sy,j} A_{sy,c,j} \cdot y_{sy,j}^2 \qquad (17)$$

$$I_{b,x_p-x_p,i} = \frac{b_{b_x,i} \cdot b_{b_{z1},i}^3}{12} + n_{om} \cdot A_{s_x,b,i} \cdot \left(\frac{b_{b_{z1},i}}{2} - c\right)^2$$
$$I_{b,y_p-y_p,i} = \frac{b_{b_y,i} \cdot b_{b_{z2},i}^3}{12} + n_{om} \cdot A_{s_y,b,i} \cdot \left(\frac{b_{b_{z2},i}}{2} - c\right)^2 \qquad (18)$$

where n_{om} represents the homogenization coefficient that is evaluated as ratio between the elastic modulus of the steel bars (E_{sm}) and the elastic modulus of the concrete (E_{cm}). The concrete cover c is assumed constant and equal to 10 % of the cross section depth. The arrangement of the bars into the section is assessed through a simplified iterative procedure below resumed:

- *Step 1*: the minimum distance between two adjacent bars ($d_{b,min}$) is fixed according to Euro Code 2 (EC2, 2005) which is expressed in Equation (19).

$$d_{b,\min} = \max\left(\phi;\ \mathrm{d_g} + 0.05;\ 0.02\right)\ [m] \qquad (19)$$

where ϕ is the diameter of the bar, while d_b represents the dimension of the aggregate (d_b = 0.025 m). A first tentative diameter of the bar (ϕ_t) is fixed in order to respect the following range (Equation (20)).

$$0.018 \leq \phi_t \leq 0.026 \;\; [m] \tag{20}$$

The minimum value of the provided range is consider as first tentative value for the bar diameter.

- *Step 2*: the maximum number of bars in both horizontal directions for a considered cross section level is calculated (Equation (21)).

$$\begin{aligned} n_{b_{c,x},\max} &= \frac{\left(b_{c_x} - 2c\right)}{d_{b,\max}}; \;\; n_{b_{b,x},\max} = \frac{\left(b_{b_x} - 2c\right)}{d_{b,\max}} \\ n_{b_{c,y},\max} &= \frac{\left(b_{c_y} - 2c\right)}{d_{b,\max}}; \;\; n_{b_{b,y},\max} = \frac{\left(b_{b_y} - 2c\right)}{d_{b,\max}} \end{aligned} \tag{21}$$

- *Step 3*: The percentage of reinforcement is then calculated ($\rho = A_s / A_c$). The total area of the reinforcement is represented by A_s, whereas the concrete cross section area is identified by A_c. The total area of the reinforcement is given by Equation (22).

$$A_s = n_{b,tot} \cdot \frac{\pi \cdot \phi^2}{4} \tag{22}$$

where $n_{b,tot}$ represents the total number of bars into the cross section. Assuming a constant value of the diameter of the bar, the percentage of reinforcement is calculated (Equation (23)).

$$\rho_{cal} = \frac{\pi \cdot \phi_t^2}{4} \cdot A_c \tag{23}$$

- *Step 4*: the calculated percentage of reinforcement has to be equal to the percentage of reinforcement provided into the database (ρ). If the two aforementioned values are not equivalent, a second tentative value of percentage of reinforcement is fixed and the procedure shown from *Step 1* to *Step 4* is implemented. The fixed values of ϕ are selected in order to be coherent with the commercial sizes.

- *Step 5*: if the condition stated in the *Step 4* is respected, the iterative process ends.

Figure 36 summarizes the iterative procedure used to assess the diameter of the bars and their arrangement into the cross sections.

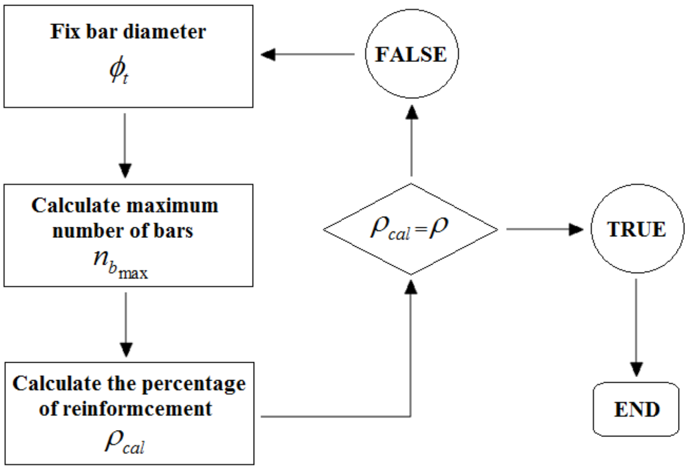

Figure 36. Iterative process for calculating the diameter of the bars and their arrangement into the cross sections.

The buildings' story height *h* is considered as constant parameter ranging from 2.70 m to 3.50 m for typical RC residential buildings, while the span length *l* is defined based on the SC type (*SC1*, *SC2, SC3, SC4, SC5, SC6, SC7*).

Mass properties

The calculation of mass matrix components is based on the vertical load combination associated with the year of construction of the building. The permanent structural and nonstructural loads are estimated by considering the seven floor types (*F1*, *F2*, *F3*, *F4*, *F5*, *F6*, *F7*) and the three external walls types (*EW1, EW2, EW3*). Each of those construction elements are characterized by the mean values of density and thickness of each structural and nonstructural components. Figure 37 shows the horizontal construction elements and the definition of their attributes.

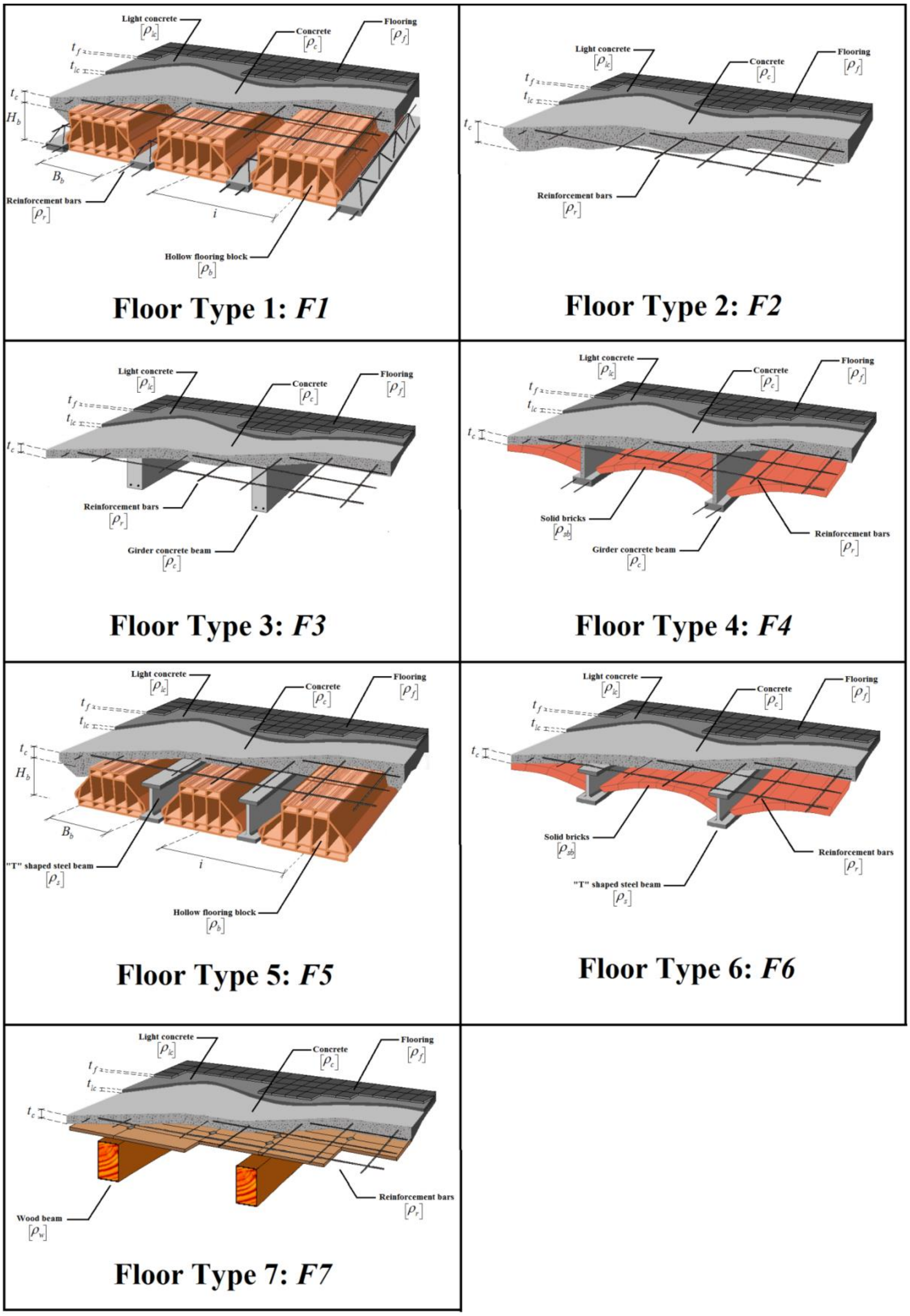

Figure 37. Horizontal construction elements and definition of their attributes.

The vertical nonstructural components and their mean characteristic attributes are depicted in Figure 38.

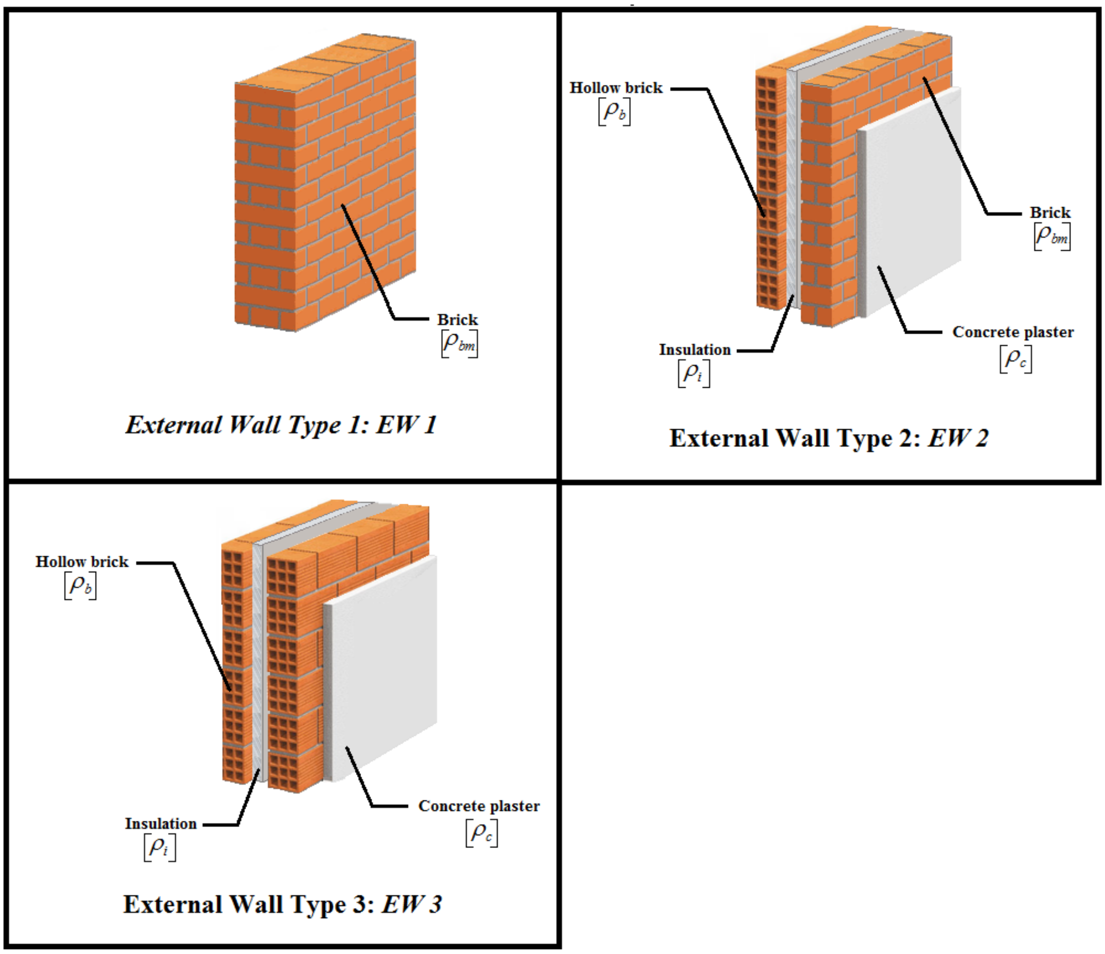

Figure 38. Vertical construction elements and definition of their attributes.

Moreover, the live loads and their combination coefficients are deduced from the design prescriptions in terms of vertical load combination for residential buildings (Equation (24)).

$$\left(G_{k1}+G_{k2}\right)\cdot\gamma_G+\psi_Q\cdot Q_k\cdot\gamma_Q \tag{24}$$

where G_{k1}, G_{k2} and Q_k are the characteristic permanent structural and nonstructural loads, and the live loads, respectively. The safety combination coefficients are represented by γ_G, and γ_Q, while the combination coefficient associated with the live load is ψ_Q. The general form of the mass matrix of a building is expressed in Equation (25).

$$[M]=\frac{1}{g}\cdot\begin{bmatrix} (G_{k1}+G_{k2})\cdot\gamma_G+\psi_Q\cdot\gamma_Q\cdot Q_{k,\mathrm{int}} & 0 & \cdots & \cdots & 0 \\ 0 & (G_{k1}+G_{k2})\cdot\gamma_G+\psi_Q\cdot\gamma_Q\cdot Q_{k,\mathrm{int}} & \vdots & \vdots & \vdots \\ \vdots & \vdots & \ddots & \vdots & \vdots \\ \vdots & \vdots & \vdots & \ddots & 0 \\ 0 & \cdots & \cdots & 0 & (G_{k1}+G_{k2})\cdot\gamma_G+\psi_Q\cdot\gamma_Q\cdot Q_{k,top} \end{bmatrix} \tag{25}$$

The permanent structural and nonstructural loads are assumed equal for each floor, while the live load values are distinguished for internal and top flooring systems ($Q_{k,\text{int}}$, $Q_{k,top}$). The term g refers to the gravity acceleration.

Multimodal pushover analysis

It is widely accepted practice to assimilate the building seismic demand to a lateral invariant force distribution proportional to the predominant modal shape of the structure (Modal Pushover Analysis, MPA). In the proposed methodology, the modal analysis is performed in order to evaluate the modes of vibration in both horizontal directions of the buildings (Equation (26)).

$$\det\left(\left[K_{BT_R}\right]-\omega^2\left[M\right]\right)=0 \tag{26}$$

A set of modes equal to the number of story of the building is obtained. Each column of the modal shape matrix $[\Phi]$ refers to the i^{th} mode of vibration. Furthermore, the modal participation factors are calculated (g_i). A multi-modal approach is carried out to consider all the modal shape contributions (Equation (27)).

$$\Phi_{eq}=\sum_{i=1}^{dof}\left\{\Phi_i\right\}\cdot g_i \tag{27}$$

where Φ_{eq} is the equivalent modal shape considering all the modal contributions (Φ_i). The seismic demand is assumed as a lateral invariant force distribution proportional to the calculated equivalent modal shape (Equation (28)).

$$\left\{F\right\}=\alpha\left[K_{BT_R}\right]\left\{\Phi_{eq}\right\} \tag{28}$$

where α represents the linear monotonic coefficient and $\left\{F\right\}$ indicates the lateral horizontal force distribution applied to the center of the mass at each story level. Figure 39 illustrates a generic horizontal force distribution proportional to the equivalent modal shape.

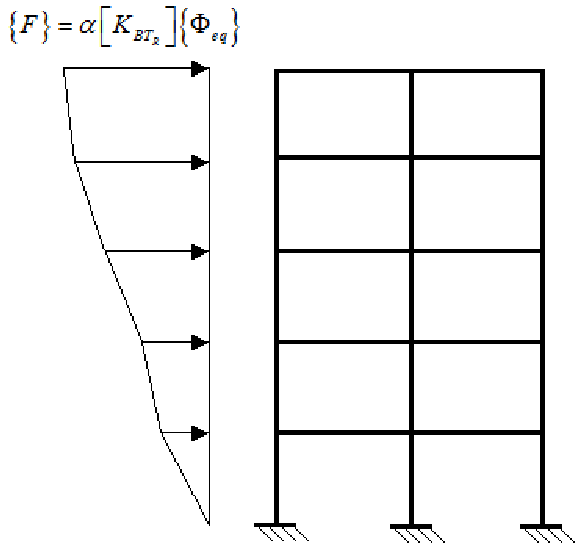

Figure 39. Horizontal force distribution proportional to the equivalent modal shape.

Pushover analysis is performed by increasing α coefficient at each step of the analysis.

The seismic resistance of a building is mainly provided by the columns which are subjected to a shear stress induced by the earthquake excitation. The global capacity of a building is then strictly dependent on the columns resistance. Herein, the internal stress in the columns is assessed by assuming a uniform distribution of the shear action into the columns located at the same story level. Figure 40 depicts the internal stress in the beam-column joint of the i^{th} story of the building.

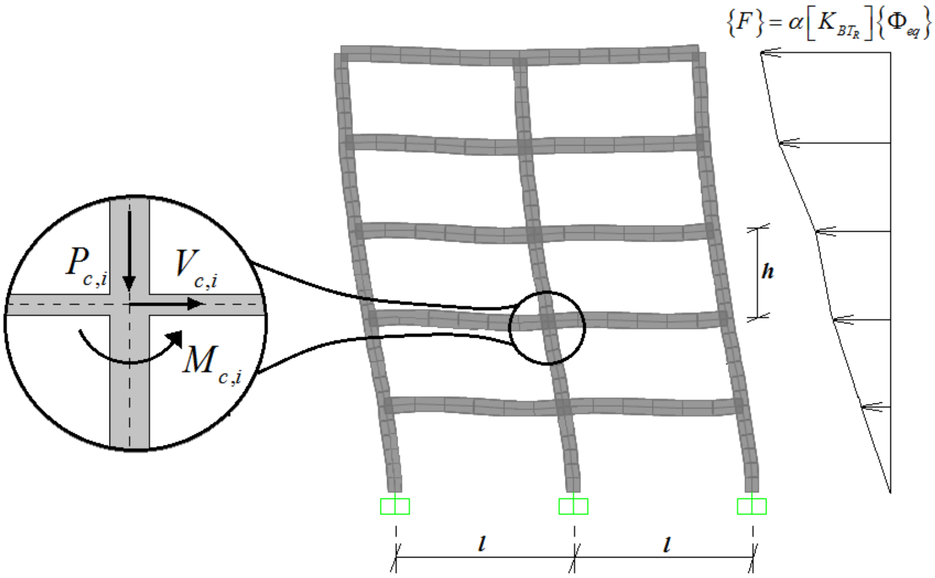

Figure 40. Beam-column joint internal stress.

Considering a generic beam-column joint located at the i^{th} story, the axial load is represented by $P_{c,i}$, while $M_{c.i}$ and $V_{c,i}$ identify the bending moment and shear, respectively. The internal stress in the columns is assessed (Equation (29)).

$$\begin{cases} P_{c_{int},i} = \sum_{i=1}^{dof} \frac{g \cdot m_i}{\sum_{j=1}^{n_{span}} l_j} \cdot l_i ; \quad P_{c_{ext},i} = \sum_{i=1}^{dof} \frac{g \cdot m_i}{\sum_{j=1}^{n_{span}} l_j} \cdot \frac{l_i}{2} \\ V_{c_{int},i} = V_{c_{ext},i} = c_{f,i} \cdot 12 \cdot \frac{E_i \cdot I_i}{h_i^3} \cdot \Delta u_i \\ M_{c_{ext},i} = c_{f,i} \cdot 6 \cdot \frac{E_i \cdot I_i}{h_i^3} \cdot \Delta u_i + \frac{\frac{g \cdot m_i}{\sum_{j=1}^{n_{span}} l_j} \cdot l_i^2}{12} ; \quad M_{c_{int},i} = c_{f,i} \cdot 6 \cdot \frac{E_i \cdot I_i}{h_i^3} \cdot \Delta u_i \end{cases} \tag{29}$$

where $P_{c,int,i}$ and $P_{c,ext,i}$ are the axial loads acting on the internal and external columns of the i^{th} storey, respectively. $V_{c,int,i}$ and $V_{c,ext,i}$ are the shear loads acting on the internal and external columns of the i^{th} storey, respectively, whereas $M_{c,int,i}$ and $M_{c,ext,i}$ are the axial loads acting on the internal and external columns of the i^{th} storey, respectively. The parameters $c_{f,i}$ is the stiffness ratio controls the degree of participation of flexural and shear deformations multistory buildings (Equation (30)).

$$c_{f,i} = \frac{k_{BT_R,ii}}{k_{ST,ii}} \leq 1 \tag{30}$$

where $k_{ST,ii}$ represents the stiffness component obtained through a shear type model of multistory building. The uniform vertical distributed load is considered through the coefficient $g \cdot m_i / \sum_{j=1}^{n_{span}} l_j$, where g represents the gravity acceleration, m_i is the total mass of the i^{th} floor, and $\sum_{j=1}^{n_{span}} l_j$ refers to the total length of the building in the considered direction.

Internal stress on the most stressed column is calculated through the Navier formulation (Equation (31)).

$$\sigma_{c_x} = \frac{P_{c,i}}{A_{om,i}} \pm \frac{M_{c_x,i}}{I_{y_p-y_p,i}} \cdot \frac{b_{c_y,i}}{2}$$

$$\sigma_{s_x} = n_{om} \cdot \left[\frac{P_{c,i}}{A_{om,i}} \pm \frac{M_{c_x,i}}{I_{y_p-y_p,i}} \cdot \left(\frac{b_{c_y,i}}{2} - c \right) \right]$$

$$\sigma_{c_y} = \frac{P_{c,i}}{A_{om,i}} \pm \frac{M_{c_y,i}}{I_{x_p-x_p,i}} \cdot \frac{b_{c_x,i}}{2} \tag{31}$$

$$\sigma_{s_y} = n_{om} \cdot \left[\frac{P_{c,i}}{A_{om,i}} \pm \frac{M_{c_y,i}}{I_{x_p-x_p,i}} \cdot \left(\frac{b_{c_x,i}}{2} - c \right) \right]$$

Figure 41 illustrates the internal stress distribution of a generic column.

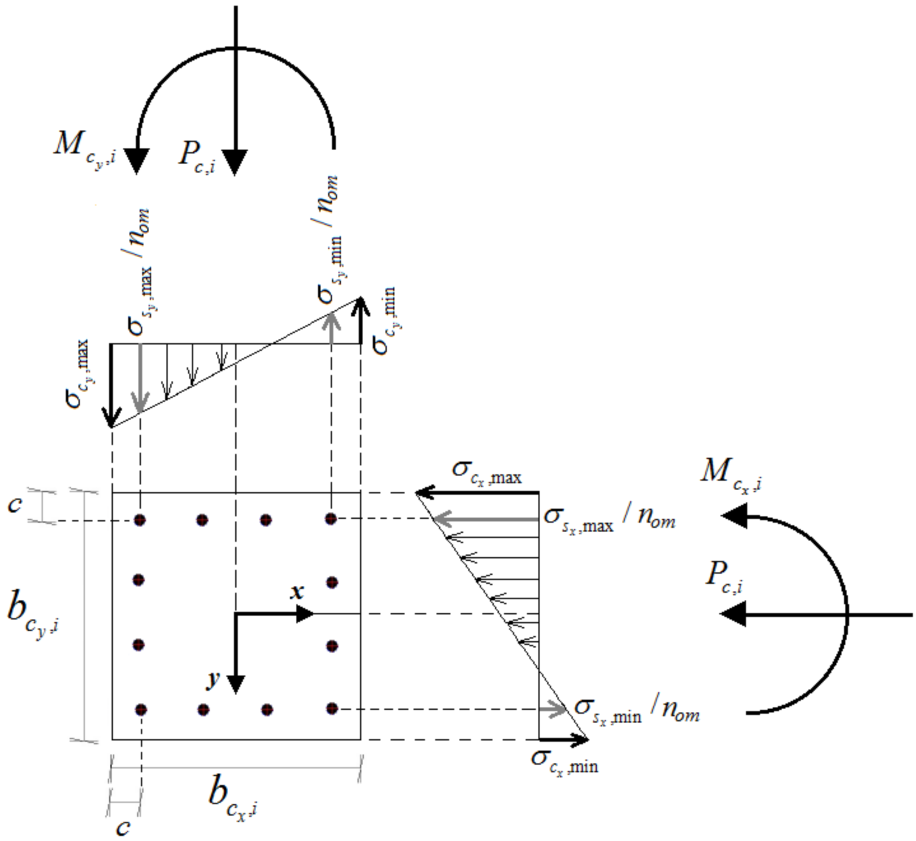

Figure 41. Internal stress distribution of a generic RC cross section.

where σ_{cx} and σ_{cy} represent the maximum internal normal stress in the concrete in x_p and y_p directions, respectively. Similarly, σ_{sx} and σ_{sy} identify the maximum internal normal stress in the steel bars in x_p and y_p directions, respectively. $A_{om,i}$ identifies the homogeneous cross section area of the generic column located at the i^{th} story (Equation (32)).

$$A_{om,i} = b_{c_x,i} \cdot b_{c_y,i} + n_{om} \cdot n_b A_b \tag{32}$$

The yielding moment of the generic column in the considered direction is evaluated both for x_p (Equation (33)) and y_p (Equation (34)) directions.

$$\begin{cases} M_{y_{cx},i} = 2 \cdot \dfrac{I_{y_p - y_p,i}}{b_{c_y,i}} \cdot \left(f_{cd} - \dfrac{P_{c,i}}{A_{om,i}} \right) \\ M_{y_{sx},i} = 2 \cdot \dfrac{I_{y_p - y_p,i}}{\left(b_{c_y,i} - 2 \cdot c \right)} \cdot \left(\dfrac{f_{yd}}{n_{om}} - \dfrac{P_{c,i}}{A_{om,i}} \right) \end{cases} \rightarrow M_{c,y_x,i} = \min\left(M_{y_{cx},i}; M_{y_{sx},i} \right) \tag{33}$$

$$\begin{cases} M_{y_{cy},i} = 2 \cdot \dfrac{I_{x_p - x_p,i}}{b_{c_x,i}} \cdot \left(f_{cd} - \dfrac{P_{c,i}}{A_{om,i}} \right) \\ M_{y_{sy},i} = 2 \cdot \dfrac{I_{x_p - x_p,i}}{\left(b_{c_x,i} - 2 \cdot c \right)} \cdot \left(\dfrac{f_{yd}}{n_{om}} - \dfrac{P_{c,i}}{A_{om,i}} \right) \end{cases} \rightarrow M_{c,y_y,i} = \min\left(M_{y_{cy},i}; M_{y_{sy},i} \right) \tag{34}$$

The global yielding of the building (point (*1*)) occurs when the most stressed column reaches the maximum allowable internal stress for the concrete or for the reinforcement in the considered direction. The pushover analysis is stopped at the step corresponding to the conditions aforementioned and the yield base shear force ($V_{b1}=V_{b,y}$) and the associated top displacement ($u_1=u_y$) are identified.

5.2.2 Post-elastic parameters

The post elastic parameters are associated with the base shear-top displacement corresponding to the point (*2*), (*3*), and (*4*) of the backbone curve. Nonlinear pushover analysis requires the determination of the nonlinear properties of each structural component quantified by strength and deformation capacities (Inel et al., 2006). When a member of the structure reaches its maximum elastic capacity in the most stresses section, a plastic hinge occurs (concentrated plasticity model). Performing a pushover analysis for each building within the virtual city require a large computational effort and time. A simplified procedure is proposed to assess the post-elastic behavior of RC buildings.

Maximum shear capacity

The maximum shear capacity ($V_{b3}=V_{b4}$) is estimated based on the kinematic theorem of the limit analysis. The kinematic theorem claims that "*the exact collapse load multiplier λ is the smallest one among all possible kinematic solutions corresponding to the set of all kinematically and plastically admissible mechanisms*".

After the global yield condition, the building is subjected to an invariant horizontal forces distribution with monotonically increasing intensity. When the total number of generated plastic hinges makes the structure unstable, collapse occurs. The value of the multiplier which identifies the collapse condition is named *collapse multiplier* (λ).

Different in-plane collapse mechanisms of RC buildings may be identified. Generally, the collapse mechanism depends on the resistance of the structural elements of the frame and on their nonlinear characteristics. Herein, two different collapse mechanisms can be considered as representative of RC frames (Figure 42).

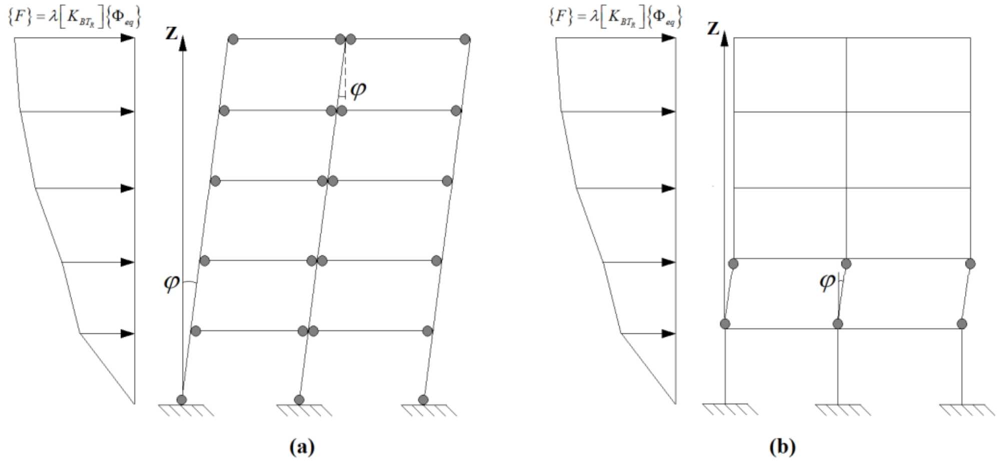

Figure 42. Global (a) and local (b) collapse mechanism of a RC building.

Figure 42.a depicts a *global collapse mechanism* which is typical of the RC frames designed according to the capacity design rules. In this case all the beams (or most part of the beams) are plasticized while the columns have a greater resistance. The collapse of the building occurs for the formation of certain number of plastic hinge into the weakest level, typically associated with the base. In case of *local collapse mechanism* (Figure 42.b), the columns of a given story level are plasticized in both extreme cross sections. This phenomenon is also called soft-story mechanism.

Therefore, the collapse multiplier is calculated both considering a global collapse mechanism (Equation (35)) and local collapse mechanism (Equation (36)).

$$\lambda = \frac{n_c \cdot M_{c,y,j} + \sum_{i=1}^{dof} 2 \cdot n_{b,pl,i} \cdot M_{b,y,i}}{\sum_{i=1}^{dof} \{F_i\} \cdot \{z_i\}} \tag{35}$$

$$\lambda = \frac{2 \cdot n_c \cdot M_{c,y,j}}{\sum_{i=1}^{dof} \{F_i\} \cdot \{z_i\}} \tag{36}$$

where i represents the i^{th} story level and j identifies the j^{th} weakest story in which the plastic hinge forms. $M_{c,y,i}$ and $M_{b,y,i}$ are the yield bending moment of the i^{th} columns and beams, respectively. The denominators refer to the external work due to the horizontal forces distributions, while n_c and $n_{b,pl,i}$ represent the number of plasticized columns and the number of plasticized beams for the i^{th} story level. The internal stress into the beams and columns are checked in order to recognize if a global or local collapse mechanism occurs and then the maximum shear capacity is assessed (Equation (37)).

$$V_3 = V_4 = \lambda \cdot V_{b,y} \tag{37}$$

One of the limitations of this procedure consists on the load pattern's shape. In fact, the monotonic horizontal force distribution does not change its shape due to the progressive formation of the plastic hinges in the columns (non-adaptive approach).

Ultimate top displacement

The global displacement capacity (u_4) associated with the building collapse condition is identified according to the experimental expression given by Equation (38).

$$u_4 = \theta_u \cdot h_j + H_e \cdot \left(\theta_u - \frac{F_j \cdot h_j^2}{3 \cdot E_j \cdot I_j} \right) \tag{38}$$

The above mentioned formulation is derived from the simplified model depicted in Figure 43.

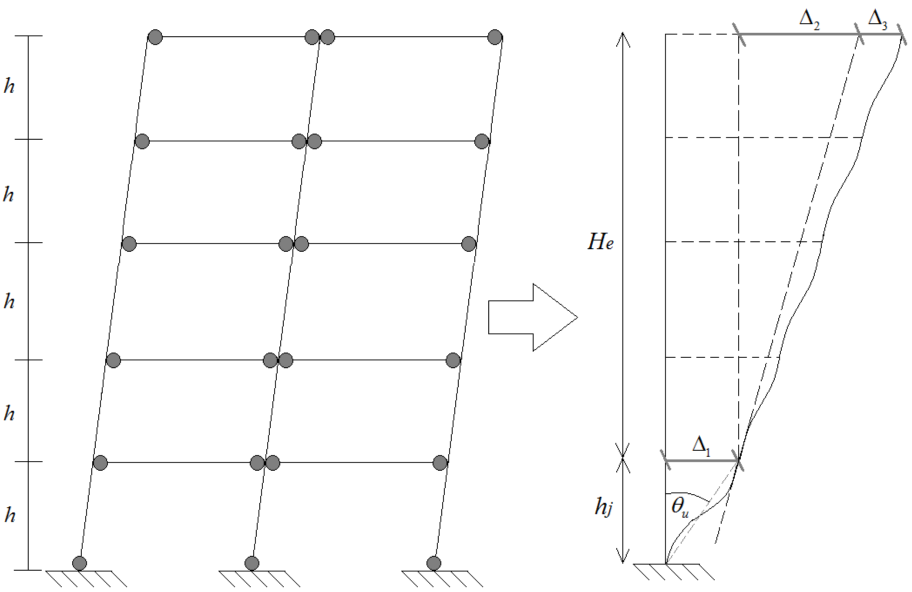

Figure 43. Simplified geometrical model used to estimate the collapse top displacement of RC building.

The global displacement capacity is derived as sum of three displacement different contributions (Δ_1, Δ_2, Δ_3). The first contribution Δ_1 represents the top column displacement due to the formation of the plastic hinge at the base of the weakest column. The contribution Δ_2 is the horizontal displacement at the top of the building due to the rotation on the top of the weakest column. The sum of the elastic deformation at each story level is given by Δ_3. Equation (39) provides the mathematical expressions used to define the three displacement contributions.

$$\Delta_1 = \theta_u \cdot h_j$$
$$\Delta_2 = \left(\theta_u - \frac{F_j \cdot h_j^2}{3 \cdot E_j \cdot I_j}\right) \cdot H_e \tag{39}$$
$$\Delta_3 \simeq 0$$

The index *j* refers to the weakest story level, whereas H_e is the effective building height measured from the weakest level to the top. The elastic contribution is neglected while the contribution Δ_2 is evaluated by considering an elastic nodal rotation at the j^{th} node equal to $(F_j \cdot h_j^2 / 3 \cdot E_j \cdot I_j)$, where F_j is the horizontal force applied at j^{th} story for the collapse condition. In the case of local collapse mechanism, the displacements Δ_2 and Δ_3 are neglected. The rotation θ_u is the ultimate chord rotation which is estimated according to NTC08 (C 8.7.2.5, NTC08, 2008) as given in Equation (40).

$$\theta_u = \theta_y + (\chi_u - \chi_y) \cdot L_{pl} \cdot \left(1 - \frac{0.5 \cdot L_{pl}}{L_v}\right) \tag{40}$$

where θ_y is the yield chord rotation of the column and it is estimated by considering a flexural behavior of the column (Equation (41), NTC08, 2008).

$$\theta_y = \varphi_y \cdot \frac{L_v}{3} \tag{41}$$

L_v is the shear length of the column which is assumed to be equal to half column length. The length of the plastic hinge (L_{pl}) is considered as 10 % of the shear length. In addition, χ_u and χ_y identify the ultimate curvature and yield curvature of the weakest column. According to Figure 41, the yield curvature is obtained as given in Equation (42) for each generic horizontal direction.

$$\chi_y = \frac{f_{cd} / E_{cm}}{\Delta_{c,y}} \quad for: M_{c_y,i} = M_{y_{cy},i}$$
$$\chi_y = \frac{f_{yd} / E_{sm}}{(b_c / 2 - c) - \Delta_{c,y}} \quad for: M_{c_y,i} = M_{y_{sy},i} \tag{42}$$

Where b_c represents the generic section depth and $\Delta_{c,y}$ is the neutral axis depth.

Furthermore, the ultimate capacity of each columns of the building is assessed and the ultimate bending moment and the related curvature are calculated in both horizontal directions (Figure 42).

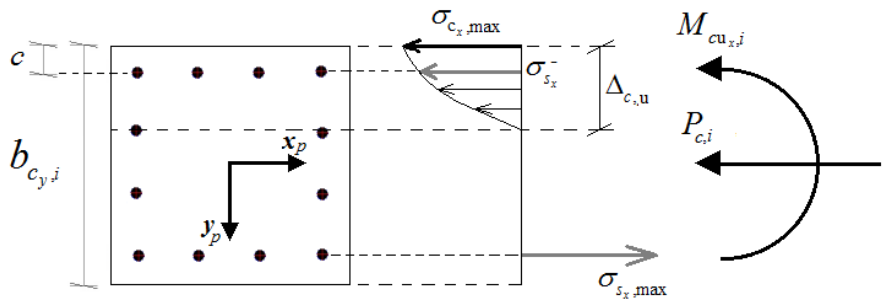

Figure 44. Ultimate stress capacity of a generic RC cross section.

where $M_{cux,i}$ is the ultimate bending moment of the column located at the i^{th} story level in x_p direction. Similar considerations may be made for the ultimate bending moment in y_p direction. The depth of the neutral axis at the collapse state is represented by the term Δ_{cu}. The hypotheses used to assess the ultimate bending moment are below resumed:

- the tensile resistance of the concrete is neglected;
- a parabolic stress-strain relationship is considered for the concrete;
- an elastic perfectly plastic stress-strain relationship is adopted for the steel bars

Shear capacity corresponding to moderate building damage

The base shear associated with the point (*2*) of the backbone curve is identified through the procedure illustrated in Figure 45.

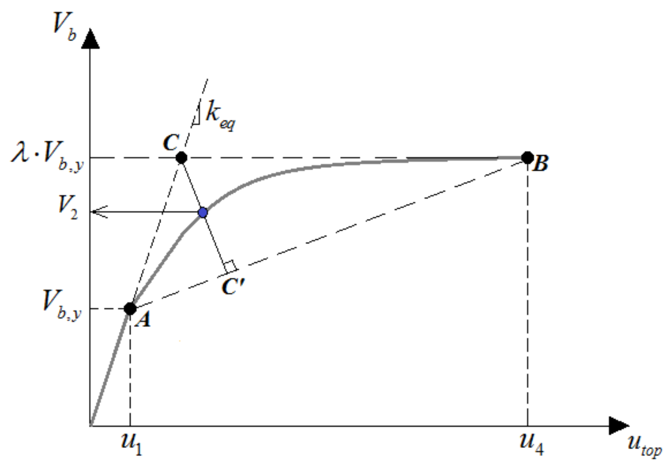

Figure 45. Geometrical scheme used for calculating the base shear associated with the point (2) of the proposed backbone curve.

AB is the straight line passing through the yield point and the ultimate capacity point. The point C is identified by the intersection between the horizontal line identifying the maximum shear capacity and the line associated with the elastic trend. The line CC is perpendicular to the line AB and passes from point C. The base shear V_2 is identified by the intersection between the line CC' and the capacity curve and it can be expressed as given in Equation (43)**.**

$$V_2 = c_2 \cdot \lambda \cdot V_{b,y} \tag{43}$$

The parameter c_2 represents the rate of ultimate shear capacity which provides the base shear V_2 and it assumes values lower than 1. The coefficient c_2 is derived by performing a sensitivity analysis. Therefore, five RC frame buildings with two, four, six, eight, and ten stories have been investigated. The span length has been fixed to 5.50 m while the story height has been assumed equal to 3.00 m. Four models having two, four, six, and eight spans have been analyzed. Uniform mass distribution over its height and a non-uniform lateral stiffness have been assumed. The building design has been conducted according to the general capacity design rules specified in the NTC08 (NTC08, 2008). For each RC frame a percentage of reinforcement less than 2% and greater than 2% have been considered in order to investigate the influence of the percentage of reinforcement on the global shear capacity.

Numerical models have been developed in SAP2000 (CSI, 2018). Figure 46 depicts the 2D frames representative of the 2 story, 4 story, 6 story, 8 story, and 10 story models for a given number of span equal to four.

A 5% Rayleigh damping has been considered for the building, while a concentrated plasticity model (FEMA 356 type P-M2-M3 for columns and M2-M3 for beams) has been chosen to account for the nonlinearity in the structural components. The analysis has been performed taking into consideration the P–Δ effects and applying a monotonically increasing lateral force distribution proportional to the predominant mode of the structure.

Sensitivity analysis has been performed and the Equation (44) has been obtained.

$$c_2 = 0.928 - \left(1 - 0.968^{\rho_d}\right) - 0.0155 \cdot n_{st} - 0.0037 \cdot n_{sp} \tag{44}$$

where n_{st} and n_{sp} are the number of story and the number of span of the building, respectively. ρ_d is a dummy variable which assumes the value of 0 for low reinforced building ($\rho<2\%$) and 1 for medium and high reinforced building ($\rho>2\%$).

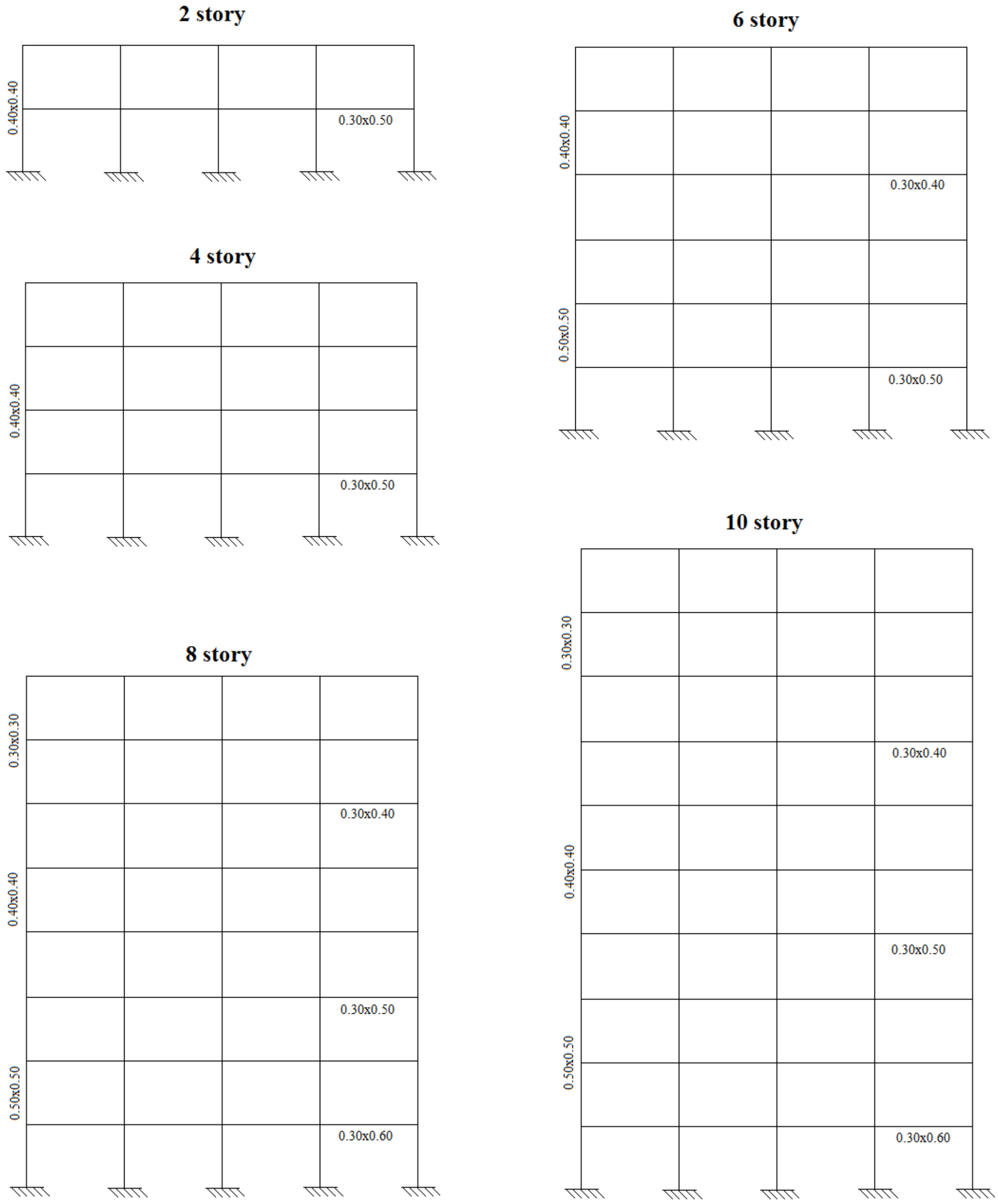

Figure 46. Representative 2D frames considered in the sensitivity analysis.

Displacements associated with point (*2*) and (*3*)

The displacements associated with the point (*2*) and (*3*) of the backbone curve are estimated based on two physical assumptions:

a) the equal energy rule is verified;
b) the line of the capacity curve passing through the point (2) and (3) is parallel to the line passing through the yield point (point (*1*)) and the collapse point (point (*4*)).

Figure 47 resumes the physical assumptions above listed.

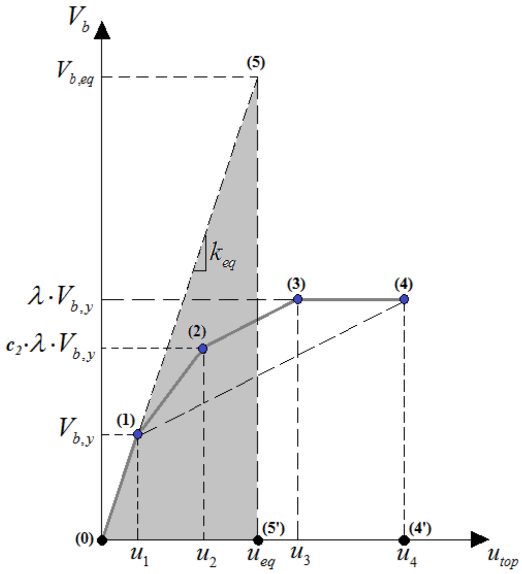

Figure 47. Illustrative scheme of the physical assumptions.

According to the equal energy rule, the equivalent elastic energy ($A_{055'}$) is equal to the deformation energy ($A_{012344'}$). Furthermore, the line *1-2* is assumed as parallel to the line *2-3*. According to the second assumption, the displacement u_3 is defined as below (Equation(45)).

$$u_3 = u_2 + \frac{u_4 - u_1}{V_{b,y} \cdot (\lambda - 1)} \cdot \lambda \cdot V_{b,y} \cdot (1 - c_2) \tag{45}$$

According to the Figure 47, the equal energy rule is expressed by Equation (46).

$$A_{055'} = A_{012344'} \rightarrow \frac{V_{b,eq} \cdot u_{eq}}{2} = V_{b,y} \cdot \left[\lambda \cdot u_4 + \lambda \cdot u_3 \cdot \left(\frac{c_2 - 1}{2} \right) + u_2 \cdot \left(\frac{1 - 3 \cdot c_2 \cdot \lambda}{2} \right) - u_1 \cdot \frac{c_2 \cdot \lambda}{2} \right] \tag{46}$$

where $V_{b,eq}$ and u_{eq} represent the equivalent base shear and elastic displacement associated with the point (*5*), respectively. According to the definition of the reduction factor (R_μ), the equivalent elastic force may be derived (Equation (47)).

$$R_\mu = \frac{V_{b,eq}}{V_{b,y}} \rightarrow V_{b,eq} = R_\mu \cdot V_{b,y} \tag{47}$$

If the reduction factor is fixed, the equivalent elastic energy can be assessed. The following procedure is proposed to assess all the possible values of the displacement u_2 and u_3:

- *Step 1*: A value of reduction factor is fixed;
- *Step 2*: The displacement u_2 is assessed based on the Equations (46) and (47);
- *Step 3*: The displacement u_3 is evaluated according to the Equation (45)
- *Step 4*: The following conditions are verified (Equation (48));

$$u_3 < u_4 \quad \text{and} \quad u_2 > \frac{c_2 \cdot \lambda \cdot V_{b,y}}{k_{eq}} \tag{48}$$

- *Step 5*: If the conditions expressed in Equation (48) are verified, the two calculated displacements are saved.
- *Step 6*: The procedure illustrated from *Step 1* to *Step 5* is then repeated.
- *Step 7*: Among all the values of the reduction factor which respected the condition reported in Equation(48), the mean value is considered as representative reduction factor ($R_{\mu,mean}$).
- *Step 8*: The displacements u_2 and u_3 associated with $R_{\mu,mean}$ are selected.

Figure 48 resumes the procedure above explained to assess the displacements u_2 and $u3$ of the proposed backbone curve.

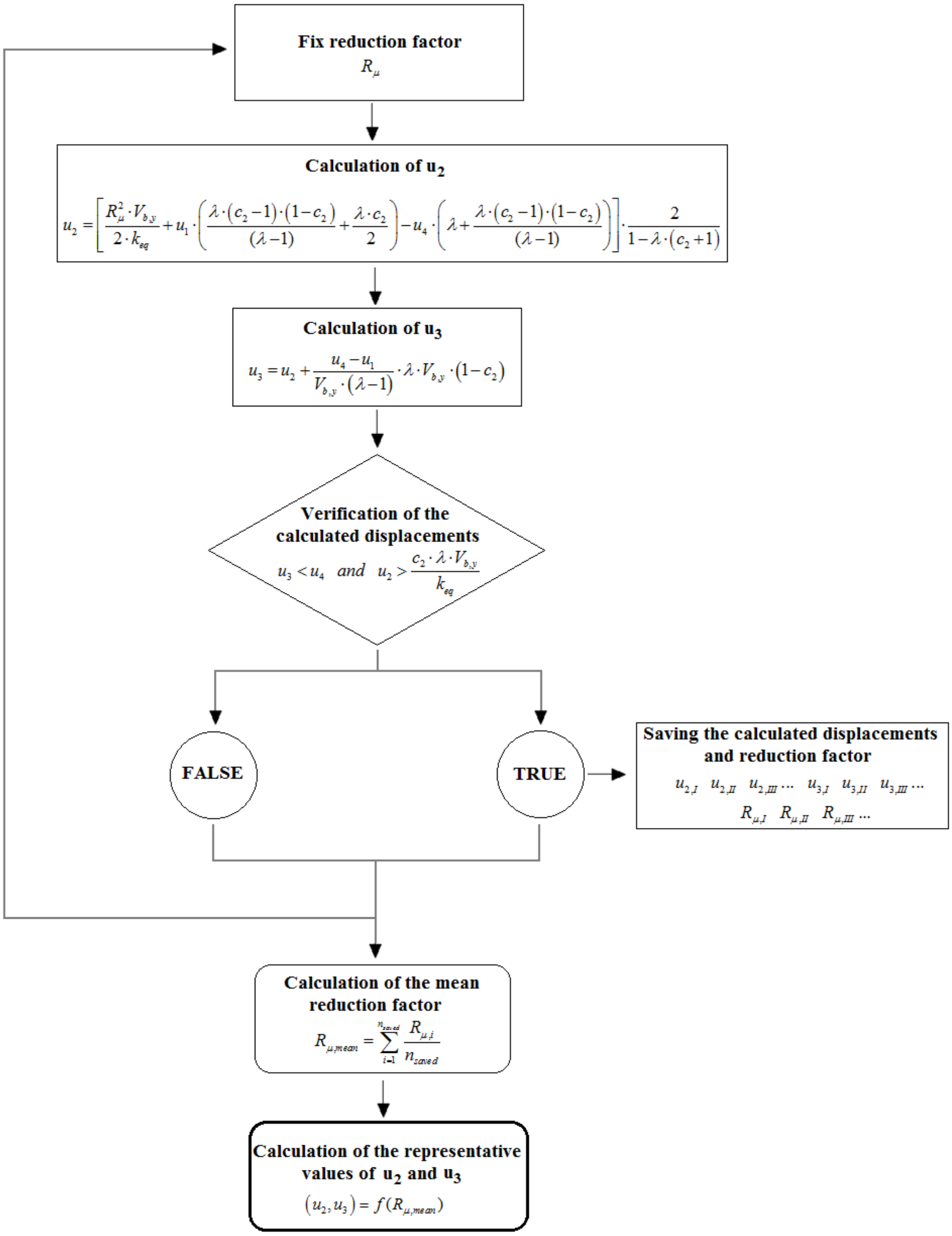

Figure 48. Iterative procedure used to assess the displacements u_2 and $u3$ of the proposed backbone curve.

5.2.3 Validation

The degree of accuracy associated with the proposed capacity model has verified by comparison with a case study building. The case study is a five-story RC building shown in Figure 49.

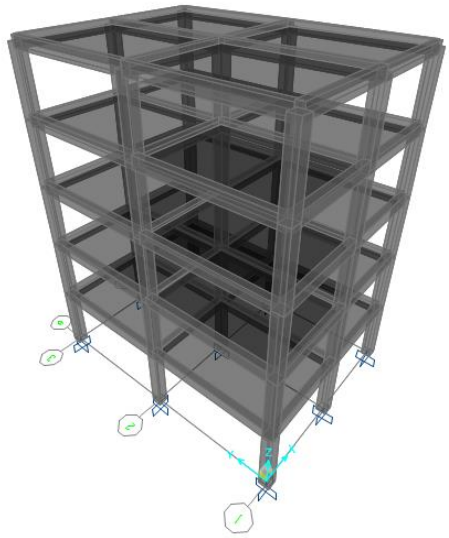

Figure 49. Case study RC building.

The structural members have been designed according to the Italian seismic regulations (NTC08, 2008). The seismic hazard has been selected to be representative of a high seismic hazard level of the national territory. For this purpose, the city of Soveria Mannelli, Italy (Lat: 39.0833, Long: 16.3667) has been selected as reference site. The columns have a square section (0.45x0.45 m) while the beam have been designed with a rectangular shape (0.30x0.50 m). Figure 50 illustrates the designed cross sections adopted for columns (Figure 50.a) and beams (Figure 50.b).

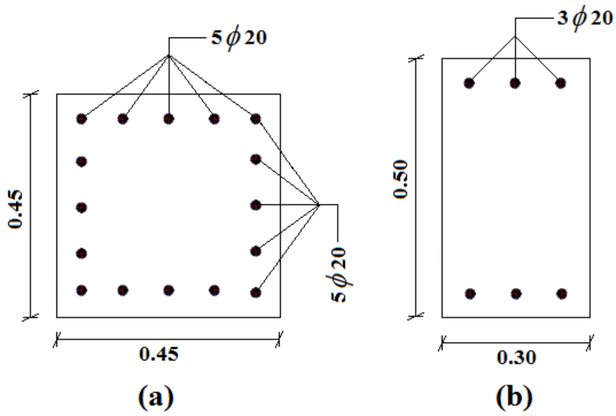

Figure 50. Cross section adopted for columns (a) and beams (b).

A symmetric reinforcement arrangement has been designed for the beams and the columns. A strength class C 30/37 has been chosen for the concrete, whereas the B450C strength class has been considered for the steel bars. The software Sap2000 (CSI, 2018) has been used to build the Finite Element Model (FEM) of the studied structure. Concentrated plasticity model (FEMA 356 type P-M2-M3 for columns and M2-M3 for beams) has been chosen to account for the nonlinearity in the structural components. A 5% damping ratio has been assigned to the frames according to Rayleigh formulation. Nonlinear pushover analysis has been performed in both horizontal directions by considering to different lateral force distributions:

- *Distribution 1*: proportional to the fundamental mode in the considered direction.
- *Distribution 2*: proportional to the equivalent mode of vibration obtained through the Equation (27). All the modes of vibration with a modal participation ratio greater than 5% in the considered horizontal direction have been considered.

The capacity curves associated with the two different distributions have been derived in both horizontal directions. For the same case study, the proposed methodology has been applied and the backbone curve has been assessed. A comparison between the capacity curves in a given horizontal direction considering the two assumed forces distribution is illustrated in Figure 51.

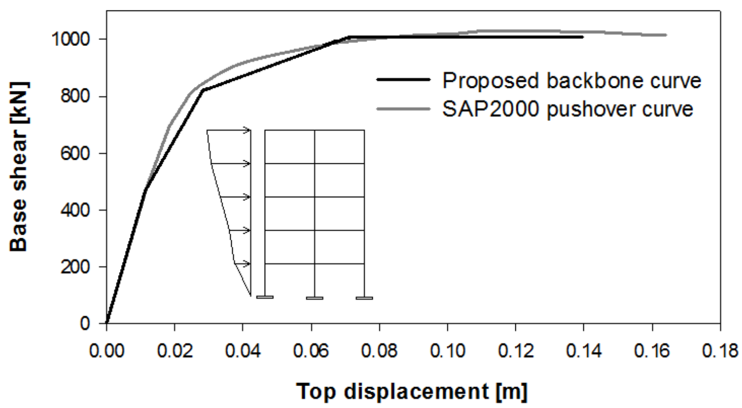

(a)

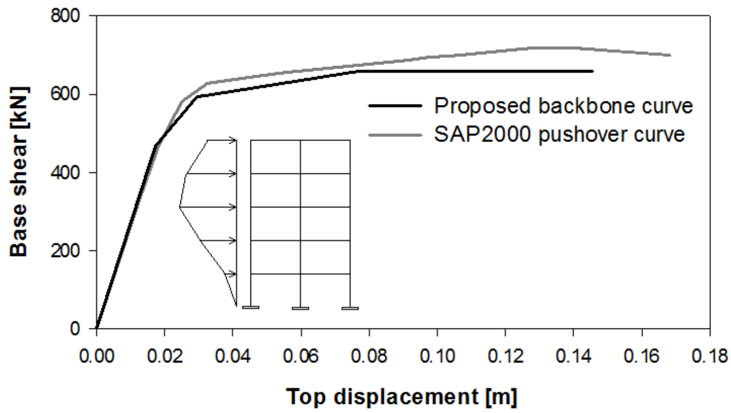

(b)

Figure 51. Comparison between the capacity curves in a given horizontal direction considering a lateral force distribution proportional to the first mode of vibration (a) and the equivalent modal shape (b).

The comparisons of the capacity curves show that the proposed physical model accurately simulates the global capacity of the building. A perfect correspondence between the elastic trends of the curves is shown. The post-elastic seismic behavior of the building obtained through the proposed model is similar to the plastic trend of the capacity curve resulted by the FEM analysis. Furthermore, the estimated ultimate top displacement is underestimated with respect to the ultimate top displacement obtained through the pushover analysis performed through SAP2000. Furthermore, the over-strength factor of the four-linear backbone curve is capable of describing the expected maximum base shear capacity with an acceptable degree of accuracy. The aforementioned observations are valid for both lateral force distribution models.

5.3 Masonry buildings

Seismic analysis of masonry buildings results in a complicated modeling process capable of overlooking several particularities and engineering aspects. Detailed structural modeling may be adopted to investigate the capacity of a masonry building subjected to a seismic excitation. Simplified analysis needs instead to be explored to simulate the seismic behavior of masonry buildings within a large scale area.

Based on the amount of reinforcement within the structural members, the masonry buildings are classified into UnReinforced Masonry (URM) and Reinforced Masonry (RM) buildings. The first category is the frequently encountered type of construction in existing or historical buildings. Horizontal reinforcement in mortar bed and vertical reinforcement into the cavities of the masonry vertical panel are used for RM buildings. Steel reinforcement in form of bars or truss systems is adopted in new building. The Italian heritage building stock is mainly composed by URM buildings which are vulnerable to the seismic action since they are mostly gravity load designed (Frumento et al., 2006).

Under seismic actions a masonry panel is simultaneously subjected to in-plane shear and out-of-plane bending loadings (Maheri et al., 2012) that lead to different collapse mechanisms. The out-of-plane mechanism is also called I mode collapse mechanism and it is associated with part of the masonry panel. Out-of-plane mechanisms occur when the anchorage with the orthogonal masonry panels is poor (transversal confinement) or the considered panel is not connected to the diaphragms. On the other hand, the II mode collapse mechanism is caused by the in-plane loading (Bucchi et al., 2013). The collapse concerns the entire masonry panel which can lead to the global collapse of the building. According to the definition of the state level which defines the structural performance (FEMA 273, 1997), the collapse of an entire wall of a masonry building may be assimilated to the total loss of building's occupancy and functionality (global collapse). Furthermore, it is common practice to consider only the in-plane mechanisms as representative of the global analysis of masonry structures.

Different simplified models for assessing the in-plane seismic response of masonry structures are available in the literature. The first simplified approach named POR method was proposed by Tomazevic (1978). The masonry building was assimilated to an equivalent shear type frame composed by vertical members (piers) connected by rigid horizontal elements (spandrels). Magnes and Calvi (1996) proposed a Simplified Analysis Method (SAM) similar to the POR method. The horizontal members were considered as deformable elements and the overlapping zones between the piers and spandrels were assumed as rigid offsets. The structural elements of the equivalent frame have an elastic-plastic behavior. Three different failure criteria were assumed for the piers: diagonal shear, sliding shear, and flexural/rocking. A rocking and shear failure mechanisms were identified for the horizontal elements.

A simplified methodology based on the Equivalent Frame Model (EFM) is used to model the seismic response of the masonry building portfolio of *IDEAL CITY*. Furthermore, due to the presence of openings on the external masonry façades, their in-plane load capacity may be considerably reduced with respect to the internal masonry panels. Therefore, only the weakest masonry panels have analyzed.

According to the EFM, the masonry walls are idealized as frame made up on deformable vertical (piers) and horizontal elements (spandrels) connected through rigid nodes. The nonlinearity of the elements is concentrated in the most stressed section of the elements (Lagomarsino et al., 2013). Piers are main resistant elements that carry vertical and horizontal loads, while spandrels affect the boundary conditions of piers. *Strong spandrels-weak piers* model and *weak spandrels-strong piers* model can be adopted to idealize the seismic response. In the first case the piers reach their maximum capacity first, while the spandrels are assumed as infinitely rigid. The arising mechanism is similar to the local soft story. In case of second model, the spandrels strength is neglected then the piers are uncoupled. Dolce (1989) proposed an approach for determining the effective heights of the piers and the spandrels by considering the openings geometry (Figure 52).

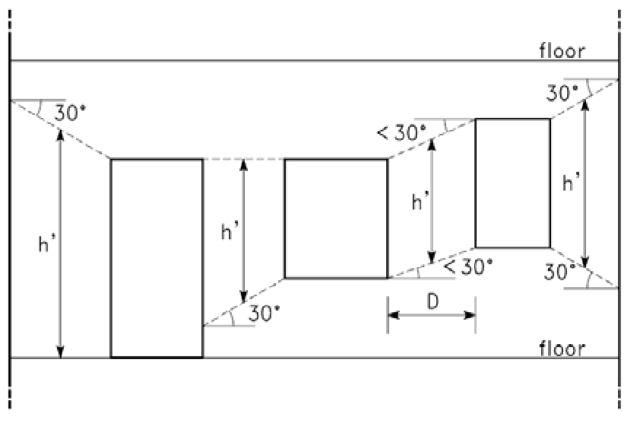

Figure 52. Definition of the effective height of the piers (Dolce, 1989).

The effective height of the pier (H_{eff}) is evaluated through the Equation (49).

$$H_{eff} = h' + \frac{1}{3} \cdot D \cdot \frac{\bar{H} - h'}{h'} \tag{49}$$

The width of each pier (D) is calculated based on the number and disposition of the openings on the masonry panel. The effective length of spandrels (l_s) is assumed equal to its deformable lengths. Figure 53 depicts an example of EFM of a two story masonry building and the effective height of a pier and a spandrel are also illustrated. The rigid offsets are identified by the black bold lines.

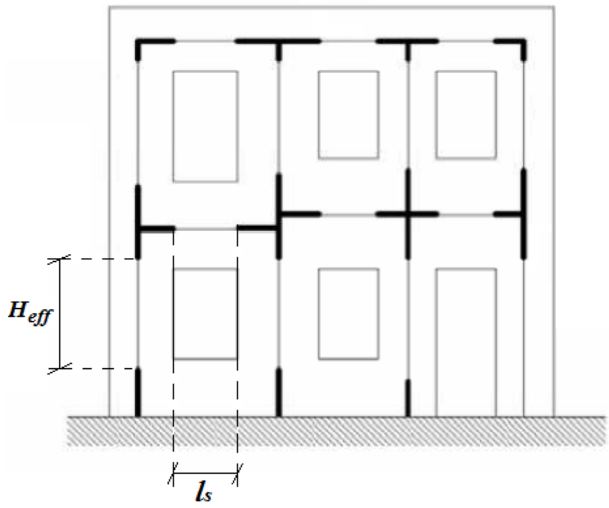

Figure 53. Equivalent Frame Model (EFM) for masonry building.

The following assumptions are considered for modeling the frame members:

- *EQM*: the in-plane resistance of masonry wall is assessed by idealized the wall as equivalent frame.
- *inextensible frame elements*;
- *rigid joints*: the overlapping zones between the piers and spandrels are assumed as rigid links.
- *lumped mass*;
- *regular planar layout*;
- *seismic response simulated through a tri-linear backbone curve*.

Masonry buildings subjected to a lateral forces distribution show a global brittle behavior which is defined by a capacity curve with reduced over-strength factor and ductility. Thus, a tri-linear backbone curve is a suitable model for simulating the seismic response of a masonry frame. Figure 54 illustrates the proposed the tri-linear backbone curve model.

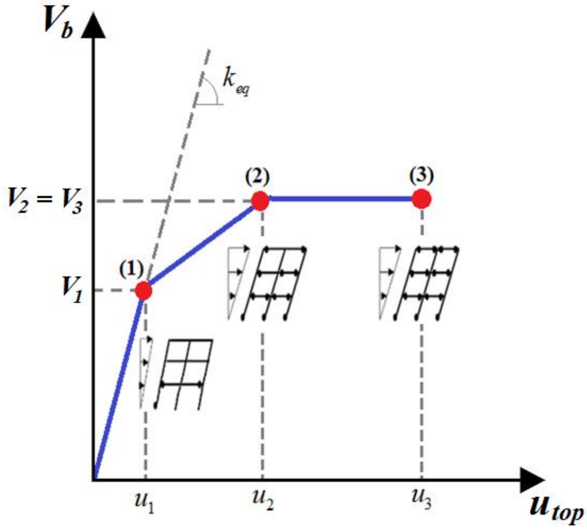

Figure 54. Proposed tri-linear backbone curve, representative of the global capacity of masonry buildings.

Similarly to the RC buildings, the global capacity is expressed as the function between the base shear (V_b) and top displacement (u_{top}) for a given horizontal direction. The first point of the backbone curve (*1*) indicates the yield point which refers to the formation of the first plastic hinge in the weakest pier. The maximum global capacity is reached in point (*2*) then the structure is subjected to a plastic mechanism until the collapse (point 3). Figure 54 highlights the evolution of the plastic hinges formation into a generic multi-story equivalent frame subjected to a monotonically increasing horizontal forces distribution.

5.3.1 Elastic parameters

The elastic parameters are identified by the base shear and top displacement associated with the point (*1*) of the backbone curve. Modal analysis is performed in both horizontal principal directions to assess the elastic properties of the equivalent frame model.

Stiffness properties

An equivalent bending type model is assumed to determine the stiffness matrix. A coupled shear-flexure behavior is considered for the piers and the related equivalent lateral stiffness ($k_{i,h}$) is derived (Equation (50)).

$$k_{ih} = \frac{1}{h_i^3 / E_i \cdot I_i + 1.2 \cdot h_i / G_i \cdot A_i} \tag{50}$$

where E_i and G_i represent the Young elastic modulus and shear elastic modulus, respectively. The principal moment of inertia is expressed by I_i, whereas A_i is the cross section area of the pier, and h_i refers to the effective height of the pier.

The reduced stiffness matrix is obtained by applying the Guyan reduction method and by considering the horizontal displacements at each story level as master DOFs. The stiffness matrix components are calculated based on the mechanical and geometrical properties collected into the database as mean characteristic values. Figure 55 resumes the main cross section properties of a masonry equivalent frame in both principal horizontal directions.

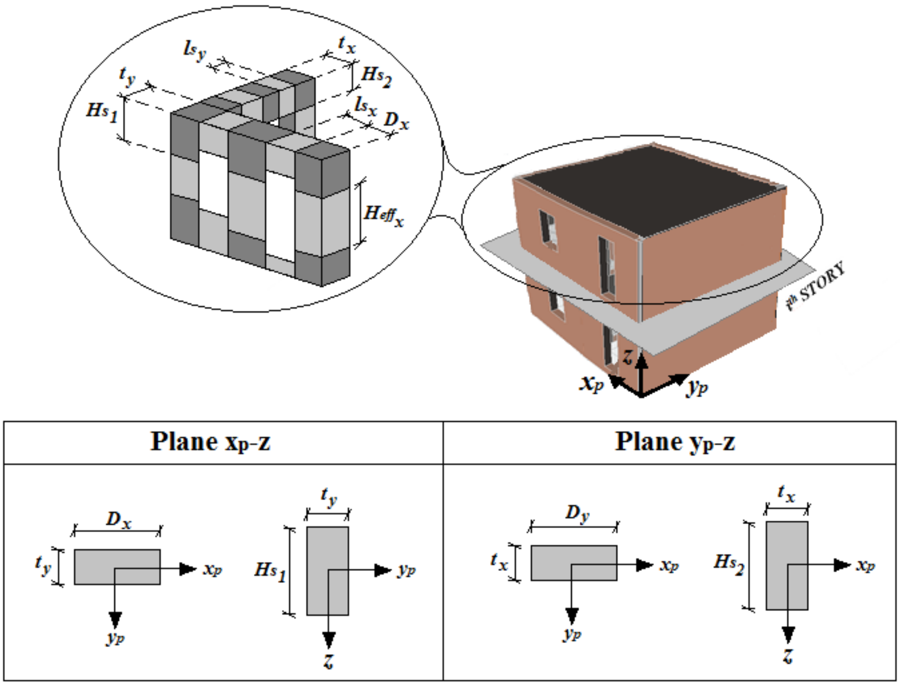

Figure 55. Cross section properties of a masonry equivalent frame in both principal horizontal directions.

A symmetric and uniform distribution of the openings on the masonry wall is assumed. This hypothesis leads to consider equal geometrical characteristics for each piers and spandrels (Figure 56).

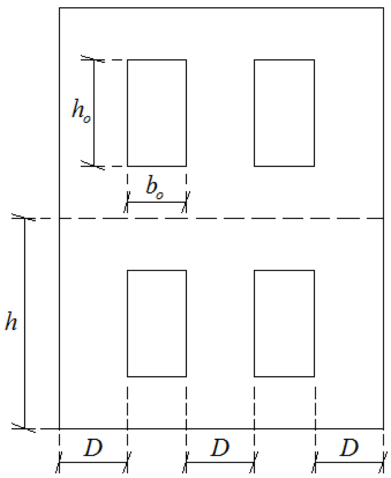

Figure 56. Schematic representation of external masonry façade.

The opening is identified by its depth (h_o) and width (b_o), while h represents the story height. The uniformly and symmetric distribution of the openings leads to have a given number of piers with the same width D. Assuming an uniform and symmetric openings distributions, the formulation proposed by Dolce (1989) to calculate the effective height of the piers is modified as given in Equation (51).

$$H_{eff} = h_o + \frac{0.33 \cdot D \cdot h}{h_o + 0.30 \cdot D} \tag{51}$$

The cracked moment of inertia is assessed to neglect the resistance contribution of the cracked portion of the masonry section. The cracked inertia is estimated as half of the moment of inertia of the un-cracked section. With reference to a URM building, Equation (52) expresses the cracked moment of inertia of the piers with respect to the principal horizontal axes x_p and y_p.

$$\begin{aligned} I_{p,y_p-y_p,i} &= 0.5 \cdot \frac{t_{y,i} \cdot D_{x,i}^3}{12} \\ I_{p,x_p-x_p,i} &= 0.5 \cdot \frac{t_{x,i} \cdot D_{y,i}^3}{12} \end{aligned} \tag{52}$$

Similarly, the moment of inertia of the spandrels are defined (Equation (53)).

$$\begin{aligned} I_{s,y_p-y_p,i} &= 0.5 \cdot \frac{D_{x,i} \cdot t_{y,i}^3}{12} \\ I_{s,x_p-x_p,i} &= 0.5 \cdot \frac{D_{y,i} \cdot t_{x,i}^3}{12} \end{aligned} \tag{53}$$

Mass properties

Similarly to the case of RC buildings, the permanent structural and nonstructural loads are estimated by considering the seven floor types (*F1*, *F2*, *F3*, *F4*, *F5*, *F6*, *F7*) and the three external walls types (*EW1, EW2, EW3*). Furthermore, the mass contribution due to the masonry walls is considered based on the six masonry wall types (*MW1*, *MW2*, *MW3*, *MW4*, *MW5*, *MW6*). Figure 18 depicts the six masonry wall types considered as representative of the vertical masonry construction elements.

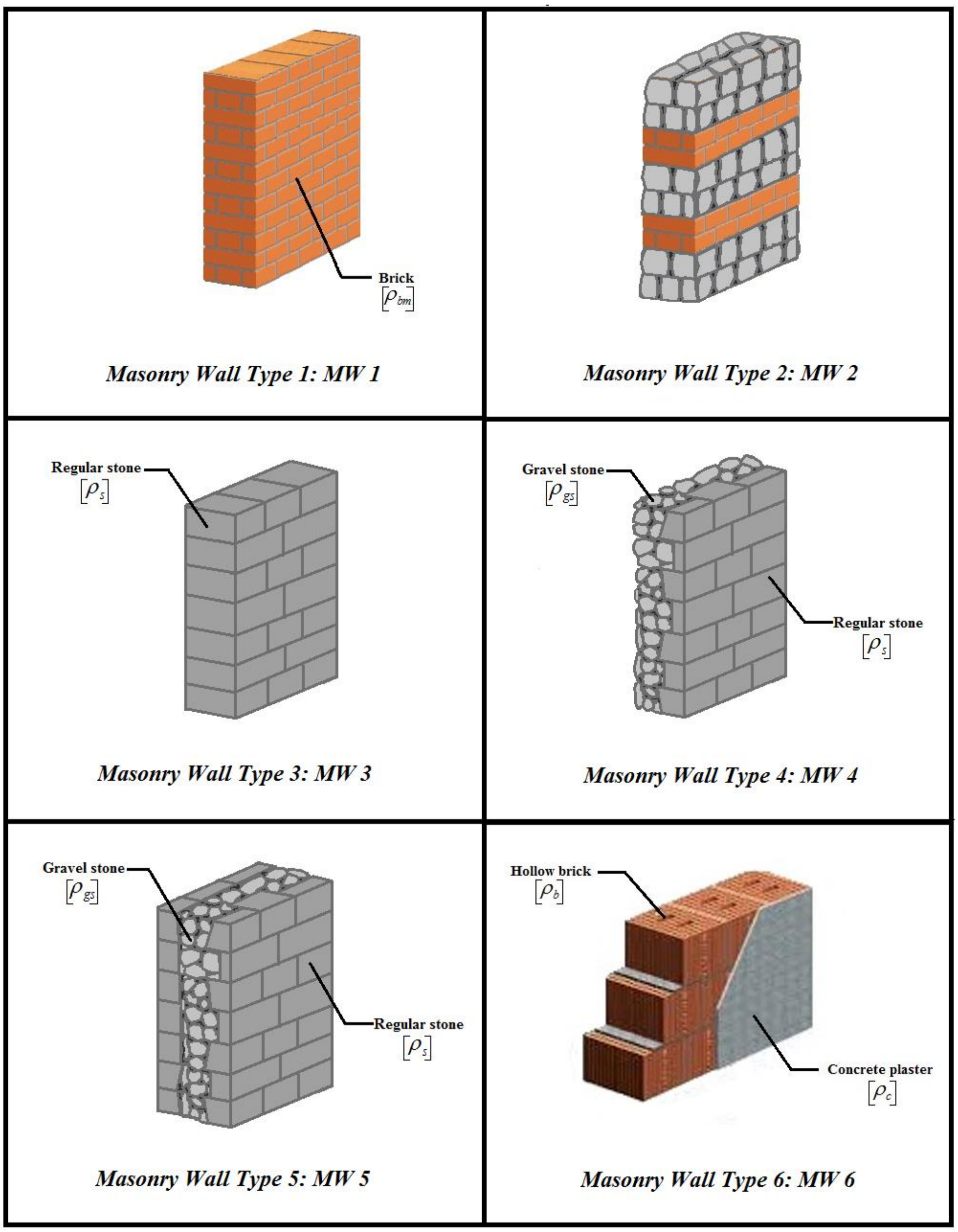

Figure 57. Masonry construction elements and definition of their parameters.

Moreover, the live loads and their combination coefficients are deduced from the design prescriptions in terms of vertical load combination for residential buildings (Equation (25)).

Multimodal pushover analysis

Similarly to the approach used for the RC buildings, an invariant lateral force distribution proportional to the equivalent modal shape Φ_{eq} is assumed. Pushover analysis is performed and the internal stress on the pier is monitored at each step of the analysis.

Different failure mechanisms are proposed in the literature to model the piers and spandrels behavior. Herein, collapse mechanisms shown in Figure 58 have been assumed for the piers. The axial load interaction is taken into account to assess the ultimate bending moment and shear.

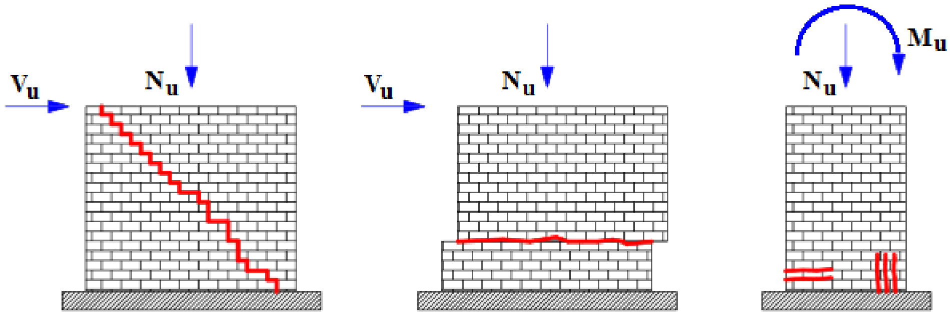

Figure 58. Failure mechanism of masonry piers.

The first two mechanisms refer to a shear failure mechanism while the third one represents the failure mechanism due to bending moment load. V_u, M_u, and N_u represent the ultimate shear, bending moment, and associated axial load, respectively.

Modeling the behavior of spandrels is a critical point. Experimental studies showed that diagonal shear and rocking typically occur as failure mechanisms. An elastic perfectly plastic behavior is assumed to simulate the shear (Figure 59.a) and bending moment (Figure 59.b) stress-strain relationships for piers and spandrels.

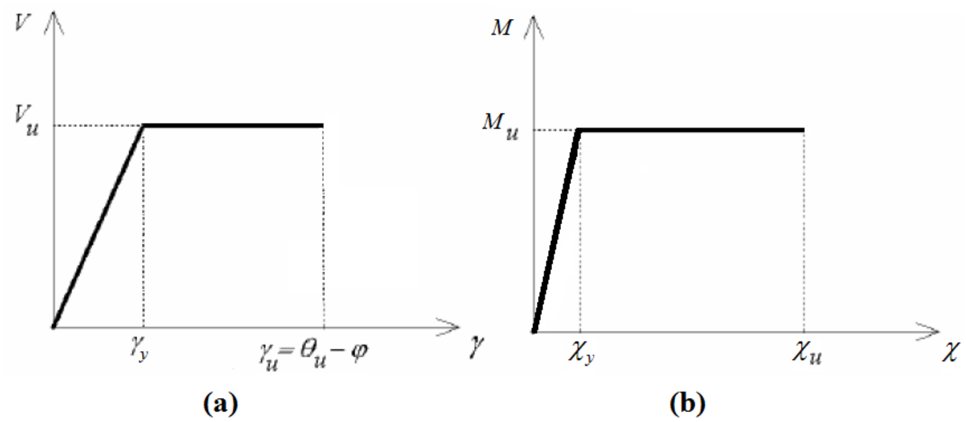

Figure 59. Shear (a) and flexural (b) behavior of masonry elements.

θ_u represents the ultimate chord rotation of the piers, whereas χ and γ refer to the curvature and shear deformation, respectively. According to the experimental results provided in literature, the values of the ultimate chord rotation are assumed to be equal to 0.6% in case of rocking failure and 0.4% in case of shear failure.

The ultimate capacity of the spandrels depends on the physical model used to simulate its seismic behavior (strong spandrels-weak piers or weak spandrels-strong piers model). Given the mean geometrical and mechanical properties of the masonry wall, the influence of the spandrels on the global seismic behavior is taken into account according to the model proposed by Rizzano et al. (2009). The cubic ratio between the slenderness of pier (λ_p) and spandrel (λ_s) was assumed as main parameter in the experimental analyses (Equation (54)).

$$\lambda_R = \left(\frac{\lambda_p}{\lambda_s}\right)^3 = \frac{12 \cdot E_i \cdot I_{p,i}}{H_{eff,i}^3} \cdot \frac{l_{s,i}^3}{12 \cdot E_i \cdot I_{s,i}} \tag{54}$$

Rizzano et al. (2009) conducted a parametric analysis in order to investigate the influence of the spandrels on the seismic response of the masonry walls. The over-strength factors of a case study masonry frame with different slenderness ratio values were investigated. The results showed that a strong spandrels-weak piers model can be assumed when λ_R is less than 1.50. On the contrary, a weak spandrels-strong pier model is considered if λ_R assumes values greater than 1.50. This observation is used to take into account the influence of the spandrels on the global seismic behavior.

Figure 60 resumes the mathematical expression adopted to assess the shear and bending moment resistance both for piers and "weak" spandrels.

	Ultimate bending moment	**Ultimate shear**	
		Diagonal shear	Sliding shear
Pier	$M_u = \left(\frac{\sigma_m \cdot t \cdot D^2}{2}\right) \cdot \left(1 - \frac{\sigma_m}{0.85 \cdot f_m}\right)$	$V_u = \frac{f_{td} \cdot t \cdot D}{\beta} \cdot \sqrt{1 + \frac{\sigma_m}{f_{td}}}$	$V_u = D_c \cdot t \cdot (\tau_k + 0.4 \cdot \sigma_{mc})$
Weak spandrel	$M_u = \left(\frac{f_{hd} \cdot t \cdot D^2}{2}\right) \cdot \left(1 - \frac{f_{hd}}{0.85 \cdot f_{hk}}\right)$	$V_u = 2 \cdot \frac{M_u}{l_s}$	—

Figure 60. Mathematical expression adopted to assess the shear and bending moment resistance both for piers and "weak" spandrels.

where σ_m is the ultimate axial load ratio which is given by the ratio between the ultimate compression load (N_u) and the cross section area of the pier. Similarly, f_{hd} represents the ratio between the ultimate horizontal compression load (N_{uh}) and the cross section area of the pier. f_m and f_{hk} represent the compression strength and the horizontal compression strength, respectively. The diagonal shear capacity is defined according to the model proposed by Turnsek and Cacovic (1971), where f_{td} is the diagonal shear strength. The coefficient β is equal to 1.5 for slender piers ($H_{eff} / D \geq 1.5$) and 1 for rigid piers ($H_{eff} / D < 1.5$). The sliding shear capacity of the pier is proportional to the equivalent compressed depth of the pier (D_c) and the sliding shear strength, which is given by the sum of the characteristic shear strength (τ_k) and 40% of the axial load ratio (σ_{mc}). The ultimate diagonal shear on the spandrels is calculated through the imposition of the local equilibrium.

The compressed depth of the cross section of the pier is calculated by imposing the equilibrium conditions reported in Equation (55).

$$D_c = D\left[1 + \frac{D}{6 \cdot M_u} \cdot \left(f_{td} \cdot t \cdot D - N_u\right)\right] \tag{55}$$

Therefore, the curvature χ_y is defined as given in Equation (56).

$$\chi_y = \frac{f_{td} / E}{(D - D_c)} \tag{56}$$

According to the elastic theory of an isotropic material, the yield shear angle γ_y is calculated as given in Equation (57).

$$\begin{aligned} \gamma_y &= \frac{V_u}{H_{eff} \cdot G \cdot A_{red}} \quad \text{for piers} \\ \gamma_y &= \frac{V_u}{l_s \cdot G \cdot A_{red}} \quad \text{for spandrels} \end{aligned} \tag{57}$$

where A_{red} represents the shear based reduced area of the considered cross section. When the maximum capacity is reached into the most stressed pier element, the pushover analysis is stopped and the corresponding global shear (V_1) and the related top displacements (u_1) are estimated. These parameters are representative of the global yield point of the proposed tri-linear backbone curve (V_1-u_1).

5.3.2 Post-elastic parameters

The point (2) and (3) of the tri-linear backbone curve describe the post elastic behavior of a masonry building. Also in case of masonry buildings, a simplified procedure is proposed to assess the post-elastic behavior.

Maximum shear capacity

As explained in detail for RC buildings, the maximum shear capacity (V_{b2}=V_{b3}) is estimated based on the kinematic theorem of the limit analysis. Therefore, different in-plane collapse mechanisms of EFM may be identified based on the pier-spandrel interaction model. Usually, the collapse mechanism depends on the resistance of the structural elements of the frame and on their nonlinear characteristics. A global and local collapse mechanism may be considered as representative of the behavior of a weak spandrel-strong pier model. On the other hand, a local mechanism may occur for a strong spandrel-weak pier model. Furthermore, the collapse condition of a masonry building is also dependent on the internal actions causing the maximum capacity on the spandrels and piers. Figure 61 depicts the possible collapse mechanisms for a generic two story masonry equivalents frame.

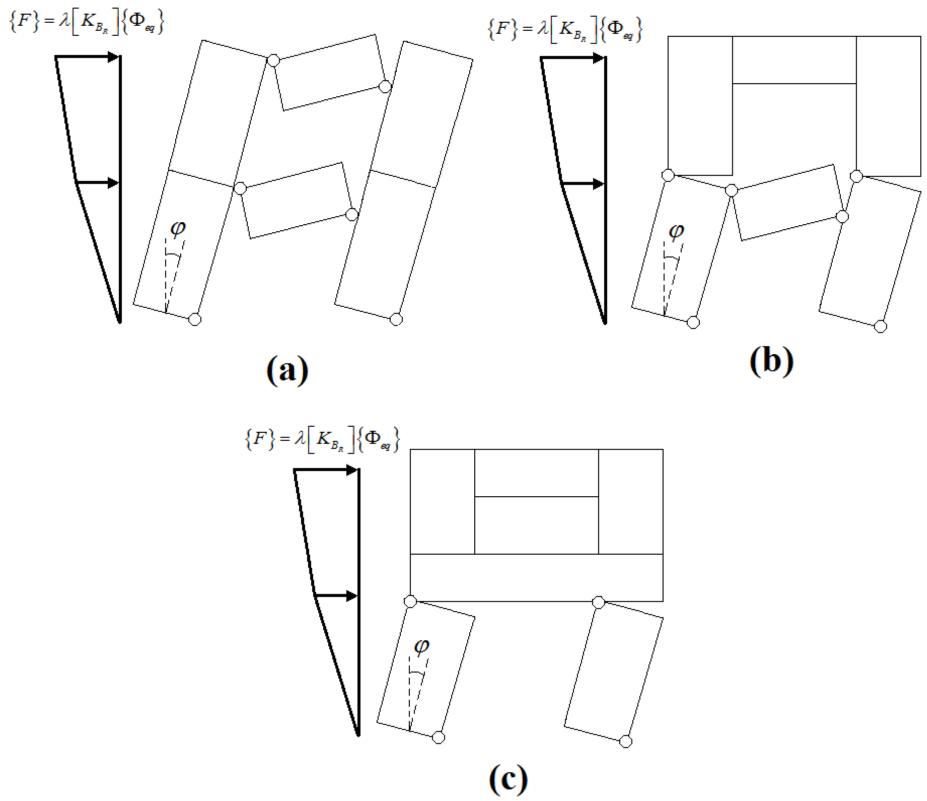

Figure 61. Collapse mechanism assumed for masonry walls.

Figure 61.a and Figure 61.b illustrate global and local collapse mechanisms for a weak spandrel-strong pier model, respectively. A local collapse mechanism associated with a strong spandrels-weak pier model is shown in Figure 61.c. Shear or flexural plastic hinges can be formed on the most stressed pier and spandrels sections. Figure 62 resumes the mathematical expressions used to estimate the collapse multipliers considering all the possible collapse mechanisms.

	Weak spandrel-Strong pier	**Strong spandrel-Weak pier**
Global collapse mechanism	$\lambda=\dfrac{n_p\cdot M_{p_u,j}+\sum_{i=1}^{dof}2\cdot n_{s,pl,i}\cdot M_{s_u,i}}{\sum_{i=1}^{dof}\{F_i\}\cdot\{z_i\}}$	——
Local collapse mechanism	$\lambda=\dfrac{2\cdot n_p\cdot M_{p_u,j}+2\cdot n_{s,pl,i}\cdot M_{s_u,i}}{\sum_{i=1}^{dof}\{F_i\}\cdot\{z_i\}}$	$\lambda=\dfrac{2\cdot n_p\cdot M_{p_u,j}}{\sum_{i=1}^{dof}\{F_i\}\cdot\{z_i\}}$

Figure 62. Mathematical expressions used to estimate the collapse multipliers considering all the possible collapse mechanisms.

where i represents the i^{th} story level and j identifies the j^{th} weakest story in which the plastic hinge forms. $M_{pu,i}$ and $M_{su,i}$ are the ultimate moment of the i^{th} pier and spandrel, respectively. The denominators refers to the external work due to the horizontal forces distributions, while n_p and $n_{s,pl,i}$ represent the number of plasticized piers and the number of plasticized spandrels for the i^{th} story level.

A flexural or shear plastic hinge may forms on the members of the equivalent frame (Equation (58)).

$$\begin{cases} M_{p_u}, M_{s_u} = M_u & for: flexural \quad hinge \\ M_{p_u} = 2\dfrac{M_u}{H_{eff}};\ M_{s_u} = 2\dfrac{M_u}{l_s} & for: shear \quad hinge \end{cases} \tag{58}$$

The internal stress of the structural members is checked in order to recognize if a global or local collapse mechanism occurs and then the maximum shear capacity is assessed (Equation (59)).

$$V_2 = V_3 = \lambda \cdot V_{b,y} \tag{59}$$

Ultimate top displacement

The global displacement capacity (u_3) associated with the building collapse condition is identified analogously to the RC case. As mentioned before, the ultimate chord rotation is set to 0.4% for shear failure and 0.6% for flexural failure (Equation (60)).

$$\begin{cases} \theta_u = 0.4\% & \text{for:shear} \quad \text{failure} \\ \theta_u = 0.6\% & \text{for:flexural} \quad \text{failure} \end{cases} \tag{60}$$

Displacement associated with point (*2*)

The displacement associated with the point (*2*) is estimated based on the equal energy rule. Figure 63 depicts the equivalent elastic energy identified by the area $A_{044'}$, while the total energy dissipated by the masonry frame is represented by the area $A_{01233'}$.

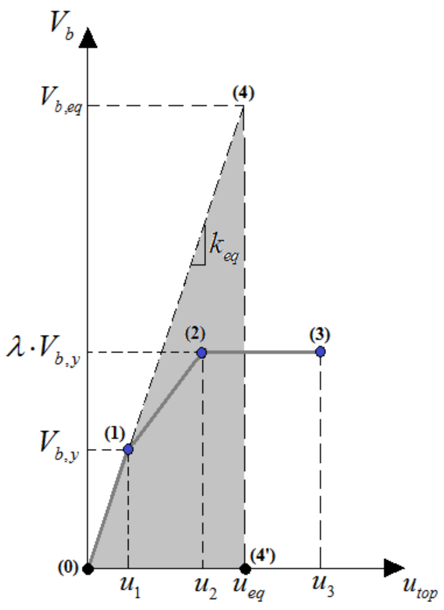

Figure 63. Model used for the equal energy rule.

Given the definition of reduction factor ($R_\mu = V_{b,eq} / V_{b,y}$), the displacement u_2 can be assessed based on the equal energy rule (Equation (61)).

$$u_2 = \frac{2 \cdot \lambda \cdot u_3 - \left(R_\mu^2 + \lambda\right) \cdot u_1}{(\lambda - 1)} \tag{61}$$

Fixing a value of reduction factor, the displacement u_2 is estimated based on the following procedure.

- *Step 1*: A value of reduction factor is fixed.
- *Step 2*: The displacement u_2 is assessed based on the Equation (61).
- *Step 3*: The following conditions are verified (Equation (62)).

$$u_2 < u_3 \quad and \quad u_2 > \frac{\lambda \cdot V_{b,y}}{k_{eq}} \tag{62}$$

- *Step 4*: If the conditions above reported are verified, the calculated displacement is saved.
- *Step 5*: The procedure illustrated from *Step 1* to *Step 4* is repeated.
- *Step 6*: Among all the values of the reduction factor which respect the condition reported in Equation (62), the mean value is considered as representative reduction factor ($R_{\mu,mean}$).
- *Step 7*: The displacement u_2 associated with $R_{\mu,mean}$ is selected.

5.3.3 Validation

The degree of accuracy associated with the model has been verified by comparison with a case study building. The case study is a four-story unreinforced brick masonry building with four spans having equal length in the considered horizontal direction. The derived EFM is illustrated in Figure 64.

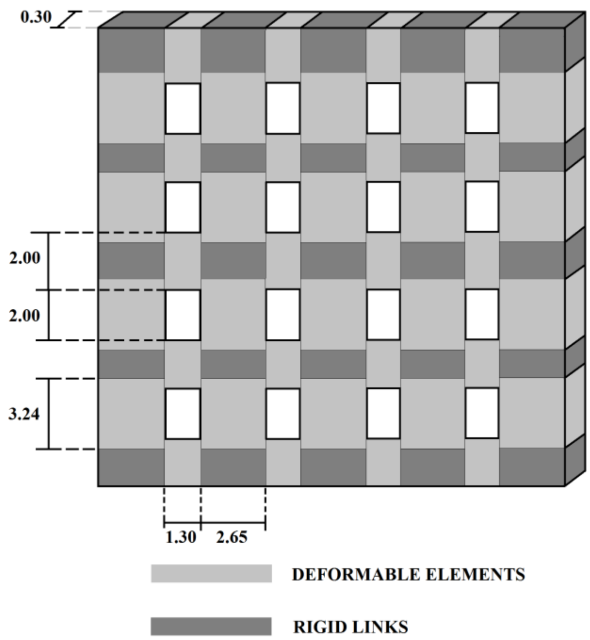

Figure 64. Case study equivalent frame model.

The material properties are resumed in .
Table 22.

Table 22. Material properties of the masonry wall.

f_m [MPa]	τ_0 [MPa]	E_m [MPa]	G_0 [MPa]
9.40	0.23	94000	37600

The seismic hazard has been selected to be representative of a high seismic hazard level of the national territory. For this purpose, the city of Soveria Mannelli, Italy (Lat: 39.0833, Long: 16.3667) has been selected as reference site. The wall thickness is equal to 0.30 m while the openings have dimension of 1.30x2.00 m. The masonry building has a story height of 4.00 m and the effective length of the piers have been assessed according to the mathematical expression proposed by Dolce (1989) and its value is 3.24 m. The deformable length of the beam is equal to 2.65 m.

The in-plane behavior of the masonry building has been investigated through SAP2000 (CSI, 2018). Shear and flexural plastic hinge have been set based on the procedure previously described. Nonlinear pushover analysis has been performed by considering a lateral force distribution proportional to the fundamental mode of the equivalent frame and the related capacity curve has been obtained. For the same case study, the proposed methodology has been applied and the backbone curves have been assessed. A comparison between the capacity curves describing the in-plane masonry wall behavior is depicted in Figure 65.

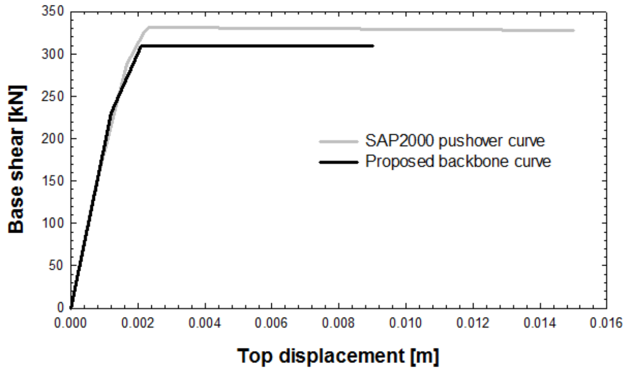

Figure 65. Comparison between the capacity curves in a given horizontal direction.

The comparisons of the capacity curves show that the proposed physical model accurately simulates the global capacity of masonry building. A perfect correspondence between the elastic trends of the curves is shown. The post-elastic seismic behavior of the building obtained through the proposed model is similar to the plastic trend of the capacity curve resulted by the FEM analysis. In addition, the ultimate top displacement is underestimated with respect to the ultimate top displacement obtained through the pushover analysis performed through SAP2000.

5.4. Uncertainties modeling

The proposed physical model provides a simplified tool for assessing the global capacity of the residential building stock within a built environment. The characteristic points of the backbone curve are estimated through a physic-driven approach based on the knowledge of the mean values of the geometrical and mechanical attributes. In spite of the used building collecting data process, considering a fixed set of parameters for estimating the seismic response of a building is not reliable. In fact, large scale simulations suffer of lack knowledge and data unavailability for accurately model the entire city building stock. Then, the building portfolio needs to be treated as an uncertain system and its inherent uncertainties must be taken into account.

Based on these observations, all the physical building's attributes are considered as RVs which varies between a fixed maximum and minimum thresholds on the basis of a normal PDF. The maximum and minimum thresholds are based on the standard deviation provided into the database and classified with respect to the mechanical, geometrical, and construction elements entities. Correlation among some of the assumed input variables have been considered as mentioned in *section 4.7*.

Monte Carlo Simulation (MCS) is performed to provide a probabilistic estimate of the uncertainties in the building capacity model. The backbone curve for each building of *IDEAL CITY* is derived assuming a set of input variables. The same procedure is repeated n_{STEP} times by assuming other set of values of the input variables. When the process is completed, a number n_{STEP} of backbone curves are identified for a given building. In other words, a set of samples of output variable are available for the statistical analysis (Figure 66).

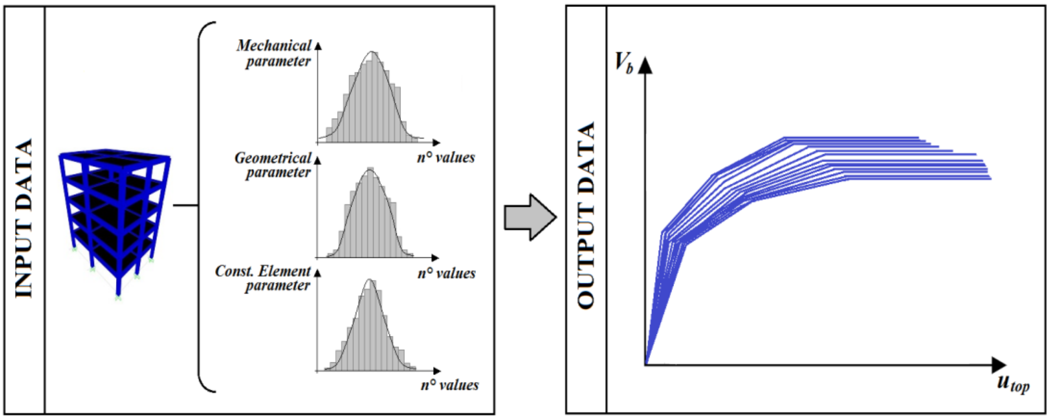

Figure 66. Input and output data flow.

Global capacity is assumed as RV lognormally distributed with median value θ_G and dispersion β_G.Thus, for each point of the backbone curve the median and dispersion values are identified as shown in Figure 67 for the four-linear backbone curve model.

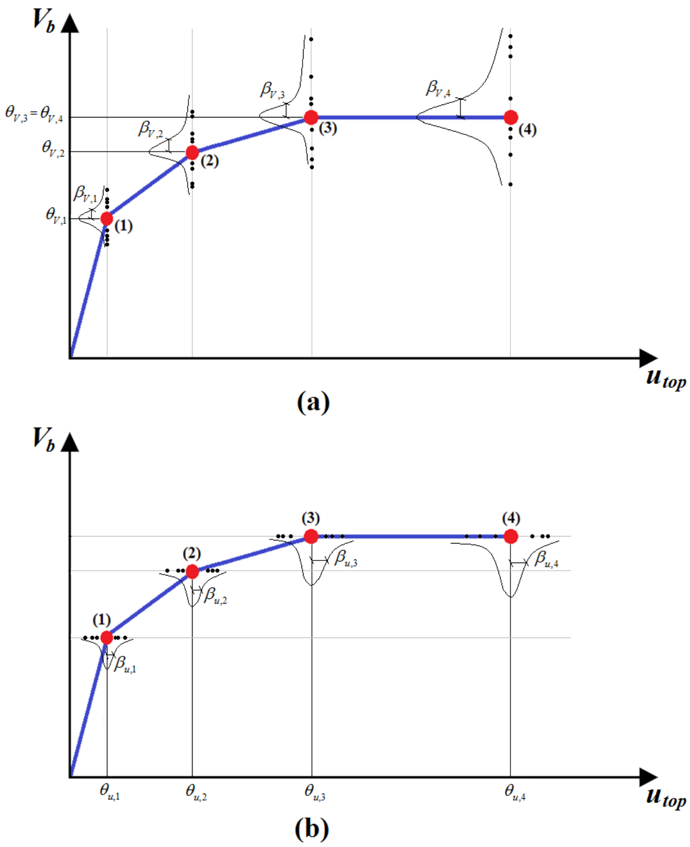

Figure 67. Base shear (a) and top displacements (b) dispersions associated with the characteristic points of the backbone curve.

The j^{th} point of the backbone curve is identified by the median values of the base shear ($\theta_{V,j}$) and top displacement ($\theta_{u,j}$). Moreover, the dispersion parameters associated with the base shear ($\beta_{V,j}$) and top displacement ($\beta_{u,j}$) are estimated.

The median capacity curve is represented by the envelope of the median pairs of base shear-top displacement and it is assumed as representative of the global seismic response of a building. The dispersion parameters represent the statistical variability of the seismic response of a building.

Figure 68 depicts the median backbone curve and the upper bound and lower bound curves which describe the maximum and minimum global seismic capacity variability.

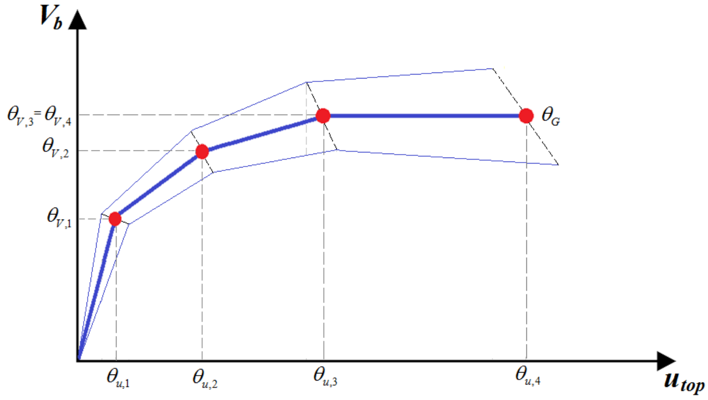

Figure 68. Median backbone curve and the upper bound and lower bound curves which describe the maximum and minimum global seismic capacity variability.

5.5. Physical modeling of the building portfolio

The proposed physical model is schematically shown in Figure 69. The median backbone curve is use to set the linear and nonlinear link elements which characterize the elastic and plastic behavior of the building.

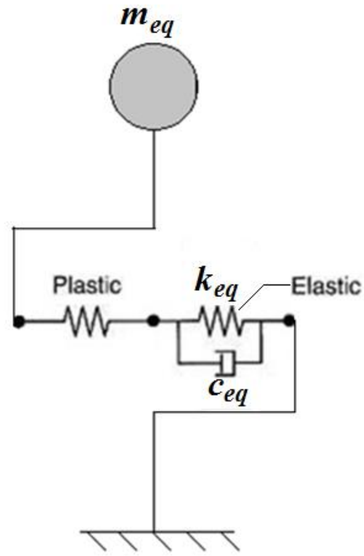

Figure 69. Proposed physical building model.

The equivalent elastic stiffness k_{eq} of the linear element is assessed as ratio between the base shear and top displacement corresponding to the point *(1)* of the median backbone curve (Equation (63)).

$$k_{eq} = \frac{V_{b,1}}{u_1} \tag{63}$$

The force–deformation relationship used to set the nonlinear properties is based on the post-elastic trend of the median backbone curve (from point *(1)* to point *(4)* for RC buildings, and from point *(1)* to point *(3)* for masonry buildings). The equivalent mass m_{eq} of the model corresponds to the total mass of the building associated to the modes of vibrations considered into the analysis.

Equivalent damping c_{eq} is evaluated according to the Rayleigh formulation (Equation (64)) by assuming the two predominant frequencies ($\omega_{\max}$, $\omega_{\min}$).

$$c_{eq} = \alpha \cdot m_{eq} + \beta \cdot k_{eq} \tag{64}$$

where the coefficient α and β are given in Equation (65).

$$\begin{cases} \alpha = 2 \cdot \xi \cdot \dfrac{\omega_{\max} \cdot \omega_{\min}}{\left(\omega_{\max} + \omega_{\min}\right)} \\ \beta = \dfrac{2 \cdot \xi}{\left(\omega_{\max} + \omega_{\min}\right)} \end{cases} \tag{65}$$

where ξ represents the damping ratio and is fixed to 5%. The dynamic strength degradation is modeled according to the Takeda model (Takeda et al., 1970). This model is based on experimental observations and considers the stiffness degradation at cracking and yielding point. Takeda model is widely used in nonlinear seismic response analysis of RC structures. Figure 70 resumes the adopted global physical model aimed to simulate the global dynamic buildings' behavior.

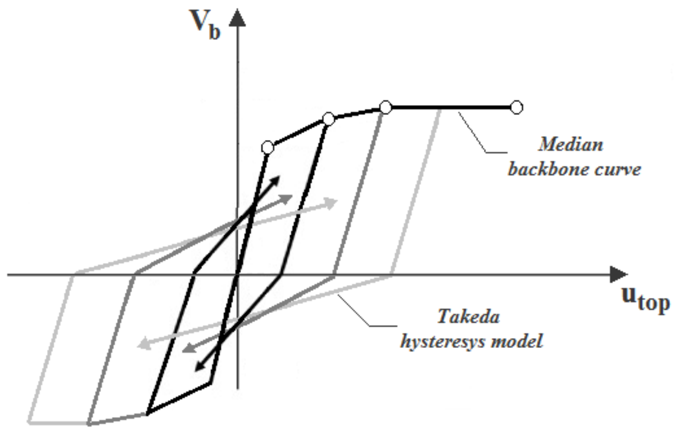

Figure 70. Global capacity model aimed to simulate the global dynamic buildings' behavior.

Chapter 6

Seismic scenario definition

6.1 Introduction

Estimation of the seismic ground motion in a given urban area requires detailed geotechnical data, knowledge on the subsurface geology profile, and probable location and properties of the seismic sources around the area.

Many earthquake prone zones are lacking in data needed for seismic response site. Furthermore, the computational effort and the related costs may be high and then simplified procedures may be adopted.

Sensitivity analysis of soil site response was performed to assess the seismic microzonation for Latipur, Nepal (Destegul, 2004). Given the limited amount of data required to perform site response analysis at urban level, numerical analyses may be used additionally to the existing data. Destegul (2004) adopted the available information of Kathmandu Valley in terms of borehole data, geotechnical, geological, and geophysical parameters to perform sensitivity analysis and estimate the rate of change in the ground motion parameters (Isukapelli, 1999). A generalized subsurface layer model was used (Piya, 2004) which is defined by four horizontal layers based on 185 boreholes data collected from the Kathmandu Valley. 1D site response analyses were performed using Shake2000 (Ordonez, 2000). Three real ground motions and artificial records, representative of different Kathmandu seismic hazard levels, were assumed. The sensitivity in terms of changes in shear wave velocity, input motion, soil unit weight, and soil thickness was analyzed.

Bazzurro et al. (2004) presented a statistical study on the effect of soil layers with uncertain properties subjected to multiple real records at the soil surface. Monte Carlo Simulation was used to generate the different characterizations of the soil column. The effects of the uncertainty in the soil parameters and the record-to-record variability on the estimation of the frequency-dependent amplification function were investigated.

Since a detailed seismic characterization of the site is beyond the scope of this research, a simplified scenario-based approach is used to estimate the seismic input to be applied on *IDEAL CITY*. For this purpose, the seismic scenario of *IDEAL CITY* is defined based on two different approaches. The first approach focuses on the definition of a given seismic source and seismic action which strike the virtual city. The second approach is based on the definition of a set of ground motions representative of different Hazard Levels (HLs). This set of motions is then used to estimate the seismic vulnerability of *IDEAL CITY*. For both approaches, given the virtual nature of the city and the nonlinearities that characterize the building models, the seismic hazard of the *IDEAL CITY* has been assumed at the highest level over the Italian territory. Therefore, the Italian site of Soveria Mannelli, (Lat: 39.0833, Long: 16.3667) has been selected as reference site to assess the hazard parameters.

6.2 Approach 1: definition of a simplified given seismic scenario

Seismic scenario is identified to test the proposed capacity model and then to evaluate the level of damage experienced by the entire building portfolio of *IDEAL CITY*.

6.2.1 Seismic source definition

The seismic scenario is assumed in terms of:

- seismic source;
- soil characteristics (geometrical attenuation);
- geometry of the fault rupture area;
- time history recorded in the epicenter (seismic action).

The seismic source is characterized by the fault type, expected moment magnitude of the seismic event, and localization of the hypocenter and epicenter. The fault rupture has been geometrically modeled through depth, strike, dip, and rake angles. Furthermore, the rupture area and its length has been calculated through the empirical relationship proposed by Wells et al. (1994), while the Joiner-Boore distance has been considered as source-to-site distance.

6.2.2 Geometrical attenuation

A simplified procedure is proposed to estimate the geometrical attenuation at any building location within the virtual city. The geometrical attenuation of the seismic excitation is estimated through the Boore-Atkinson (Boore and Atkinson, 2008) attenuation law. For this purpose, the shear wave velocity in the upper most 30 m (V_{S30}) for the city of Turin is assumed to model the soil characteristics. The

V_{S30} map is obtained via USGS website (USGS, 2013) at the link http://earthquake.usgs.gov/hazards/apps/vs30/ and saved in the database. Equivalent shear wave velocity in the uppermost 30 m ($V_{s30,eq}$) is evaluated at each building location, whereas moment magnitude, epicenter distance, equivalent shear wave velocity in the uppermost 30 m, and fault mechanism are used as input parameters of the Boore-Atkinson attenuation model (Boore and Atkinson, 2008). A set of scale factors, which identify the peak's attenuation of the acceleration time history at each building location are calculated. The frequency content variation is not considered in the simplified seismic scenario definition.

As first order evaluation of the damage assessment of the virtual city is provided by consider the geometrical attenuation only.

6.3. Approach 2: definition of a seismic scenario suitable for estimating the buildings' vulnerability

Current seismic guidelines and recommendations focus on the quantitative assessment of buildings susceptibility to damage by future seismic events. Vulnerability or "Damageability" is defined as the possible damage sustained by the building from a potential external influence such as a seismic event (Azar et al., 2004). In this context, fragility analysis method is widely used in Performance-Based Design to provide fragility functions associated with a given Damage State (DS) by assuming different seismic scenario described through a set of Intensity Measure (IM) parameters. Therefore, the selection of an appropriate seismic input, representative of different HLs associated with the considered site, plays a key role in the fragility analysis of buildings.

Different set of ground motions in both horizontal directions are assumed as seismic input for *IDEAL CITY*. Each selected set of motions is associated with a given HL. Detailed information on seismic input selection is provided in the following subsections.

6.3.1 Seismic hazard parameters

The design response spectrum at the reference site has been defined using Peak Ground Acceleration (*PGA*), maximum magnification factor for horizontal acceleration spectrum (F_0), and initial constant velocity period range (T_c*) adopted in NTC08 (2008). Three HLs associated with Damage Control (DC), Life Safety (LS), and Collapse Prevention (CP) performance levels have been adopted. Table 23 lists the macrozoning values of *PGA*, F_0, and T_c* at the reference site for each HL which is expressed through its exceedance probability in 50 years according to NTC08 (2008) for a rigid soil site.

Table 23. Performance levels and associated hazard parameters for the reference rigid soil site.

Performance Level	DC	LS	CP

Hazard Level	63%	10%	5%
PGA [g]	0.13	0.32	0.40
F_0 [-]	2.20	2.30	2.40
T_C^* [s]	0.30	0.40	0.45

The equivalent soil amplification has been accounted based on the shear wave velocity in the upper most 30 m (V_{s30}) map obtained via USGS website (USGS, 2013) at the link http://earthquake.usgs.gov/hazards/apps/vs30/ for the city of Turin. As illustrative example Figure 71 depicts the V_{s30} spatial distribution within *IDEAL CITY*.

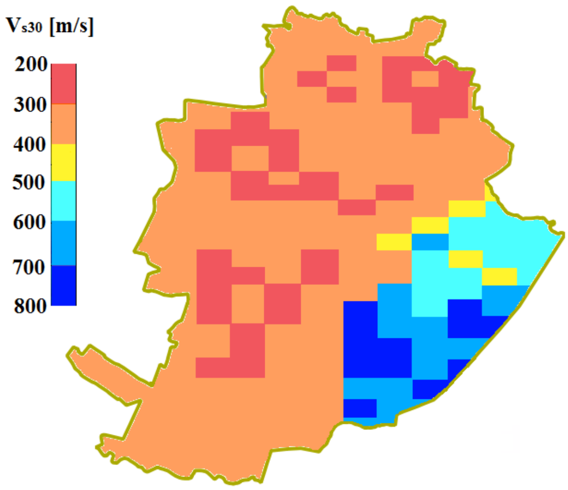

Figure 71. Vs30 spatial distribution within IDEAL CITY

The equivalent soil amplification factor ($S_{S,eq}$) and the equivalent coefficient associated with the period of constant velocity ($C_{C,eq}$) have been defined based on the soil seismic classification provided by NTC08 (Table 3.2.V, 2008). The reference soil used in the Boore-Atkinson attenuation model (Boore and Atkinson, 2008) is the class *B* of the NEHRP site classification (Dobry et al., 2000) which is identified through a V_{S30} low than 1500 m/s and greater than 760 m/s. As first order evaluation of equivalent soil amplification factors, the site class *A* of NTC08 has been considered equivalent to the soil class *B* of NEHRP. Table 24 resumes for each HL the simplified equivalent soil amplification factors associated with the soil category.

Table 24. Simplified equivalent soil amplification factors ($S_{S,eq}$) and equivalent coefficient associated with the period of constant velocity ($C_{C,eq}$), associated with the soil category for each HL.

Soil Category		A	B	C	D
V_{s30} [m/s]		760-1500	360 - 760	180- 360	< 180
$S_{S,eq}$ [-]	63 % in 50 years	1.00	1.20	1.57	1.34
	10 % in 50 years	1.00	1.15	1.22	1.11

	5 % in 50 years	1.00	1.11	1.04	1.02
$C_{C,eq}$ [-]	63 % in 50 years	1.00	1.40	1.56	2.28
	10 % in 50 years	1.00	1.32	1.42	1.98
	5 % in 50 years	1.00	1.26	1.32	1.77

Furthermore, the seismogenic characteristics of the considered site have been also assessed according to the de-aggregation study of the reference site (available at the link: http://esse1-gis.mi.ingv.it/). Table 25 lists the moment magnitude and source-to-site distance assumed for each HL based on the de-aggregation study of the reference site (Barani et al., 2009).

Table 25. De-aggregation values in terms of moment magnitude-epicenter distance parameters.

Hazard Level	**63%**	**10%**	**5%**
Moment magnitude M_w [-]	4.0 – 6.0	4.5 - 7.0	5.0 - 7.5
Epicenter distance R_{epi} [km]	0 - 40	0 - 30	0 - 30

6.3.2 Ground motion selection

Accessibility of a vast amount of real ground motion data, recorded over the past decades, contributes in successfully performing time–history structural analysis. Nowadays the trend is using real ground motion records instead of the artificial accelerograms because real earthquakes are usually distortion-free and have a more realistic energy content. Generally, the target spectrum is obtained considering the seismic hazard information at the site of interest, while the structural behavior is described by the predominant period. This constitutes the foundation of the ground motion selection. Current approaches of Ground Motion Selection and Modification (GMSM) are based on: scenario, time, and hazard intensity (ATC, 2011). Intensity-based GMSM methods are performed to match the IM parameter obtained from the probabilistic seismic hazard analysis (PSHA) (Cornell 1968). This is performed by scaling real ground motion records in order to match the target response spectrum. The spectral acceleration that is consistent with the fundamental period of the structure (with 5% damping ratio) is the most commonly used IM parameter for single structure. In case of large scale performance assessment of buildings, different IM parameters may be considered to describe the seismic scenario such as peak parameters (PGA, PGV, PGD), energy-based parameters (Arias intensity), or seismigenic-based parameters (moment magnitude). PGA is commonly used as seismic hazard indicator for large scale problems. This measure is directly connected with the inertial forces which appear in the structure especially for stiff systems. On the contrary, PGA is not a reliable indicator for flexible structures (high-rise buildings).

A set of seven real ground motions in both horizontal directions for each HL are selected and assumed as representative of the seismic input. A seismic energy-based GMSM is used to select the set of motions to be used in the nonlinear dynamic analyses. The GMSM procedure emerges from comparing a set of horizontal ground motions at various ranges of frequency with the target frequency content (Marasco, 2018).

The selected records are compatible with the seismic site in terms of the spectral acceleration at the period of reference and seismigenic parameters (M_w - R_{epi}). Numerical results showed that the selected group of ground motion records causes an identical elastic seismic action and approximately equal plastic dissipation on the structure. This in turn leads to significantly affect the structural response estimation and the structural damage prediction.

Target spectrum definition

The horizontal design spectra for each soil category (NTC08, 2008) are defined and assumed as target spectra for each selected HL. The software OPENSIGNAL (Cimellaro & Marasco, 2015) is used to obtain the design spectra in the reference site.

Scaling procedure

PGA is selected as target parameter, therefore, the records scaling procedure allows to have elastic response spectra matching the target spectrum at the referenced period $T_{ref}=0$. This scaling approach considers records resulting in the same PGA without taking into account the energy content of the records. Then, each record is additionally scaled based on the Housner intensity of the motion within a considered range of period (Marasco, 2018). This scaling approach leads to assume ground motion records matching the target Pseudo Velocity Spectrum (PSV) in a given period range. The selection of the range of period in which the spectrum compatibility needs to be verified is dependent on the modal characteristics of the buildings. The fundamental period of a regular building may be evaluated as $0.1 \cdot n_{st}$, where n_{st} refers to the number of story. Based on the building stock of *IDEAL CITY*, the most part of the residential buildings ranges from 2 stories to 8 stories. According to this observation, it is reliable to consider 0.8 s as period's upper bound limit. Thus, PGA is assumed as IM parameter, while the period range 0-0.8 s is considered for spectrum compatibility process and scaling procedure. Then, ground motion records are modified in order to have:

a) same PGA of the target;
b) same Housner intensity in the period range 0-0.8s of the target.

Considering the generic i^{th} ground motion record, the scale factor related to the condition *a)* ($SF_{I,i}$) is given in Equation (66).

$$SF_{I,i} = \frac{PGA_T}{PGA_i} \tag{66}$$

where PGA_T and PGA_i represent the PGA of the target and the i^{th} record, respectively. Equation (67) expresses the sale factor associated with the condition *b)* ($SF_{II,i}$).

$$SF_{II,i} = \frac{HI_T(\Delta T)}{HI_i(\Delta T)} \tag{67}$$

where HI_T and HI_i represent the Housner intensity of the target and the i^{th} record, respectively. ΔT refers to the assumed range of period which is equal to 0-0.8 s.

Selection procedure

Ground motions selection is performed considering the ground motion having equal values for SF_I and SF_{II}. Given the limited number of motions available in the available strong motion database, a small deviation between the two values of the scale factors may be accepted (<15%). The selection procedure is also based on the research of records characterized by seismogenic parameters compatible with the de-aggregation values (Table 25).

Among the compatible records which respect the aforementioned conditions, only seven records are selected by comparing the energy content of each compatible record with the target energy content. Then, the seven groups of motions which are the most representative of the target energy content are selected as seismic input. The same procedure is repeated for each target spectrum based on a given HL and soil amplification effects. The GMSM procedure is performed through OPENSIGNAL software (Cimellaro & Marasco, 2015). Table 26, Table 27, and Table 28 resume the main characteristics of the selected record for each HL at rigid soil site.

Table 26. Selected records representative of the hazard level with exceedance probability of 63 % in 50 years at rigid soil site.

63 % in 50 years				
Record ID	Description	Event date	M_w	R_{epi} [km]
1	Northern California	1975/08/01	5.2	10.4
2	Imperial Valley (aftershock)	1979/08/06	5.0	12.6
3	Anza, Horse Canyon	1980/02/25	5.2	12.7
4	Mammoth Lakes (aftershok)	1980/05/25	4.8	11.6
5	Coalinga (aftershock)	1983/05/02	5.1	13.1
6	Northridge (aftershok)	1994/01/17	5.1	21.5
7	Anza	2001/10/30	4.9	24.7

Table 27. Selected records representative of the hazard level with exceedance probability of 10 % in 50 years at rigid soil site.

10 % in 50 years

Record ID	Description	Event date	M_w	R_{epi} [km]
1	Mammoth Lakes	1980/05/25	6.1	10.9
2	Coalinga	1983/05/02	6.2	10.0
3	Whittier Narrows	1978/10/01	6.0	15.3
4	Biga	1983/07/05	6.1	17.7
5	Umbria Marche	1997/09/26	6.0	27.0
6	Northwest China	1997/01/21	6.1	19.1
7	Taiwan (aftershock)	1999/09/21	6.2	10.1

Table 28. Selected records representative of the hazard level with exceedance probability of 5 % in 50 years at rigid soil site.

5 % in 50 years				
Record ID	Description	Event date	M_w	R_{epi} [km]
1	Parkfield	1966/06/28	6.2	32.6
2	Imperial Valley	1979/08/06	6.5	27.6
3	Mammoth Lakes	1980/05/25	5.9	18.5
4	Coalinga	1983/05/02	6.2	16.2
5	Chalfant Valley	1986/07/21	6.2	14.3
6	Loma Prieta	1989/10/17	6.9	27.2
7	Norcia	2016/10/30	6.5	5.4

As illustrative example, Figure 72 depicts the mean spectrum compatibility for the case of 5 % exceedance probability in 50 years for a rigid soil site.

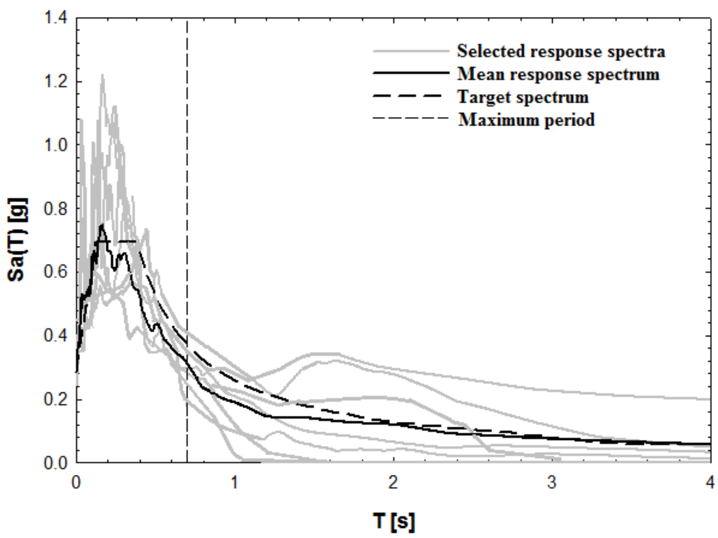

Figure 72. Mean spectrum compatibility associated with an exceedance probability of 5 % in 50 years at rigid soil site.

The mean spectrum-compatibility is satisfactory verified into the reference range of period (0-0.8 s).

Chapter 7

Damage assessment

7.1 Introduction

Structural performance is assessed based on static or dynamic methods of analysis suitable for multistory buildings. Since the earthquake excitation is a dynamic action, the dynamic approach provides more accurate results than the static one. Furthermore, the mechanical nonlinearities need to be included in the analysis in case of moderate and high severity seismic loading (nonlinear methods). However, the choice of the methods of analysis employed in assessing building performance depends on the requested degree of accuracy and on the complexity of the geometric configuration.

Static nonlinear methods may be used to estimate the seismic vulnerability of a structural system based on the concept of structural performance (Fajfar, 2000). This analysis is also called pushover analysis and it is a simplified tool that permits the estimation of the capacity of a structure subjected to a given external lateral increasing load (demand). An invariant horizontal force distribution is commonly assumed. This assumption can lead to inconsistent results for irregular structures (predominance of higher modes) or for very dissipative systems. In fact, the redistribution of the internal actions due to the plasticization of some members will be such as to vary the force applied at each story level. In addition, the influence of the dynamic characteristics of the ground motions (e.g. durations, velocity pulses, frequency content, etc.) cannot be taken into account. To overcome these limitations, nonlinear dynamic methods may be adopted to assess the building's performance. In this case, the structure is subjected to an acceleration time history, while the seismic response is obtained through the integration of the nonlinear equations of motion (Nonlinear Time History Analysis, NTHA).

In Performance-Based Design (Priestley, 2000) the structural performance objectives are defined as the *coupling of expected performance level with expected levels of seismic ground motions*. Furthermore, the performance levels are basically defined based on the experienced range of damage. According to HAZUS (FEMA, 2011) the seismic damage to buildings is classified into five levels (none, slight, moderate, extensive, and complete damage). Based on that, various indicators are used to quantify the damage to buildings caused by seismic activity such as local and global damage indicators (Azar et al., 2004). These indicators are named as Engineering Demand Parameters (EDPs) and are used to predict the Damage States (DSs) of structural and nonstructural components (ATC, 2011).

Generally, seismic damage of buildings is assessed through deformation-based criteria which better describe the post-elastic response of a building, where the deformation varies considerably even for small force variation. Maximum inter-story drift is widely adopted as EDP, because it is capable of characterizing the dynamic response of a building. Many researches have been conducted to estimate the average inter-story drifts associated with each DS.

Ghobarah (2004) defined the performance levels of RC buildings in terms of generic capacity curve. The structure is undamaged up to concrete cracking. A global stiffness reduction occurs between the concrete cracking and the steel's first yield and the building is considered reparable. Beyond steel yield the costs associated with the repair is high and the building is assumed irreversibly damaged. The ratio between the collapse displacement and the displacement associated with the global yield of the building represent the ductility of the system. The materials and the structural system affect the ductility of the system itself. For this purpose, Ghobarah (2004) focused on the definition of inter-story drift thresholds associated with ductile and non-ductile RC Moment Resisting Frames (MRF), MRF with masonry infills, and ductile and squat walls. The inter-story drift thresholds were estimated based on experimental data and theoretical analyses. Furthermore, Hazus methodology (FEMA, 2011) proposed a set of inter-story drift ratios and related structural DS threshold based on the building type and seismic design level. Other researchers adopted the spectral displacement as EDP and they defined the corresponding median values associated with the threshold of each DS both for RC (with or without infill walls) and unreinforced masonry buildings (Kappos et al., 2010, D'Ayala et al., 2012).

The DSs of the building portfolio of *IDEAL CITY* is assessed based on the inter-story drift threshold proposed by Ghobarah (2004) since they are reliable for existing RC and masonry buildings.

In order to investigate the effects of different level of seismic demand, it is common practice to estimate the probability of incurring a given level of damage based on the imposed demand (fragility functions). Fragility functions may be derived based on the statistical analysis of damage recorded in past earthquakes, simulated in analytical or numerical methodologies, expert judgment elicitations, or on a combination of these methodologies, which are named hybrid approach (Maio, 2015).

Analytical approach defines a direct relationship between the structural response and the damage effects (Rossetto et al., 2013). Numerical models are capable of taking into account detailed mechanical and geometrical characteristics. A large amount and high computational efforts is required in the assessment of the fragility function of the building stock of an urban environment. Analytical methodologies are used in estimating fragility function of single or of a reduced number of structures.

On the contrary, empirical approaches may be adopted to assess the seismic vulnerability of buildings at large geographical scales. Empirical approaches are based on the statistical analysis of the post-earthquake damage observation data which are interdependent with the macroseismic intensity. Epistemic uncertainties affect the empirical approach due to the lack of collected data of damage to the buildings, and inefficiency in the characterization of the ground motion intensity.

Expert judgments are required in assessing the seismic vulnerability of buildings in case the available data are poor. Systematic approach based on providing formal protocols, procedures, and guidelines may be adopted to estimate unknown variables and then provide a measure of buildings' vulnerability (Winkler et al., 1992).

Hybrid damage approaches combine post-earthquake damage statistics with analytical methodologies. These approaches may be useful to estimate the building stock vulnerability of a large scale environment in case the collected damage data is not adequate and the use of simulation requires a high computational effort. Then, a combination of analytical simulations, post-earthquake surveys, and expert judgments may result an efficient approach. Kappos et al. (1998) generated fragility functions of the typical Greek building stock through a combination of statistical and nonlinear dynamic analyses for all the existing RC building typologies.

An analytical approach, based on the result of the nonlinear time history analyses, has been adopted to assess the fragility functions of the buildings located within *IDEALCITY*.

7.2 Nonlinear time history analysis through SAP2000

Direct integration time history analysis is performed in SAP2000 (CSI, 2018) for evaluating the buildings' performance. According to Figure 69, each building is modeled as a multi-linear plastic element by setting the force-displacement function and the hysteresis behavior. Different independent properties may be defined for each deformational degree. In other words, the internal deformations are independent. Only the elastic and plastic properties simulating the horizontal response of a building are set, whereas the other DOFs are fixed.

Force-displacement relationships refer to the median backbone curves derived through the proposed physical model, while the hysteresis behavior is modeled based on the Takeda model (Takeda et al., 1970). Figure 73 illustrates an example of properties setting of a multi-linear plastic element in SAP2000 (CSI, 2018).

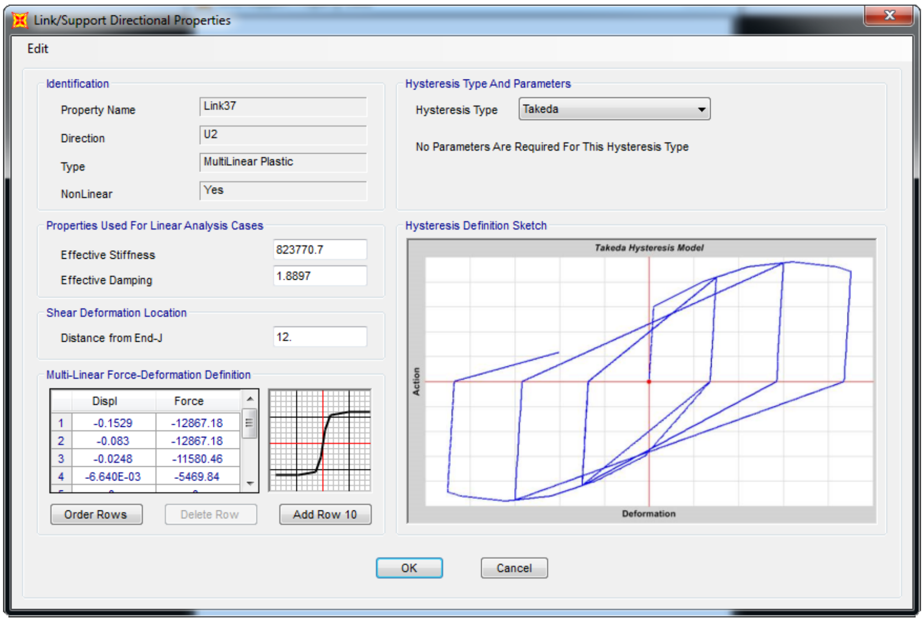

Figure 73. Multi-linear plastic link element setting (CSI, 2018).

The median force-displacement relationship is set in the associated table (Down-left in Figure 73), while the Takeda hysteresis model is selected through the related pop-up-menu (Up-right in Figure 73). In addition, the initial stiffness value is fixed based on the elastic stiffness, whereas the equivalent damping is evaluated according to the Rayleigh formulation. The equivalent mass is concentrated on the top of each element, whereas the seismic base excitation is defined in terms of displacement time history.

Then, the maximum absolute top displacements of each link element are estimated and considered as seismic demand.

7.3 Global to local conversion of seismic response

The capacity of each building is provided for the equivalent SDOF system corresponding to the real building. Furthermore, the response of each building is estimated through the time history analyses, which provide a set of absolute maximum top displacements. This parameter needs to be converted into the maximum inter-story drift that better characterizes the dynamic response of the building. These conversions entail passage from global response (SDOF) to local response (MDOF) through a simplified response model. This model is based on the definition of the lateral displacement distribution which identifies the response of the MDOF system ($\{u_{MDOF}\}$) that is evaluated as the sum of an elastic $\{u_e\}$ and a plastic $\{u_p\}$ contributions (Figure 74).

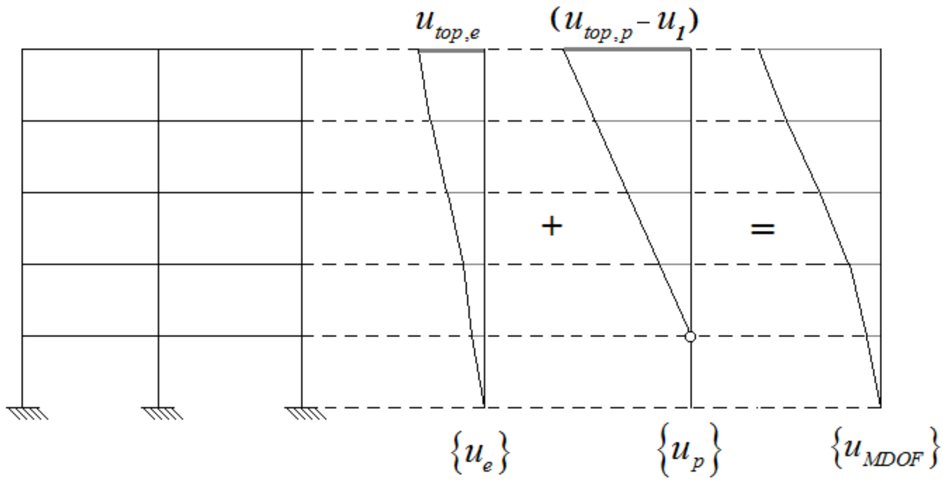

Figure 74. Elastic and plastic displacements distributions

Figure 74 shows an illustrative example of the estimation of the lateral absolute displacement distribution based on the calculated top displacement. The elastic and plastic contribution of the equivalent SDOF system are represented by $u_{top,e}$ and $u_{top,p}$, respectively, and the following conditions are provided (Equation (68)).

$$\begin{aligned} &u_{top,e} \leq u_1 \quad for: \mathrm{R}C,\ URM,\ and\ \ RM\ \ buildings \\ &u_1 < u_{top,p} \leq u_4 \quad for: \mathrm{R}C\ \ buildings \\ &u_1 < u_{top,p} \leq u_3 \quad for: URM\ \ and\ \ RM\ \ buildings \end{aligned} \tag{68}$$

7.3.1 Lateral elastic displacement distribution

The global capacity curve is estimated based on the pushover analysis. Furthermore, the seismic action is assimilated to a lateral invariant force distribution ($\{F\}$) proportional to the equivalent modal shape of the structure. According to the elasticity theory, the roof displacement distribution is assessed (Equation (69)).

$$\{u_e\} = \alpha \cdot \{\Phi_{eq}\} = \alpha \cdot \{F\} \cdot \left[K_{BT_R}\right]^{-1} \tag{69}$$

where $\left[K_{BT_R}\right]$ represents the stiffness matrix of the structure, while $\{u_e\}$ is the vector containing the lateral roof displacements. When the first plastic hinge occurs in the weakest vertical frame member, the direct proportionality between the stiffness matrix and the lateral force distribution is not valid anymore.

7.3.2 Lateral plastic displacement distribution

The definition of the maximum shear is based on the limit analysis. Therefore, the kinematic configuration associated with the collapse of the building is known. Herein, it is reliably assumed that the lateral displacement distribution beyond the global yield point is directly proportional to the displacement distribution represented by the collapse mechanism $\{u_p\}$.

7.4 Damage Level

According to the model depicted in Figure 74, the maximum absolute inter-story drift is identified and compared with the thresholds values of inter-story drift proposed by Ghobarah (2004) to assess the damage level (Table 29).

Table 29. Threshold values of inter-story drift proposed by Ghaborah (2004).

Damage state	Ductile MRF	Nonductile MRF	Ductile Walls	Nonductile Walls
No Damage	< 0.2%	< 0.1%	< 0.2%	< 0.1%
Slight	0.4%	0.2%	0.4%	0.2%
Moderate	<1.0%	<0.5%	<0.8%	<0.4%
Extensive	1.8%	0.8%	1.8%	0.7%
Complete	> 3.0%	> 1.0%	> 2.5%	> 0.8%

Figure 75 resumes the procedure adopted to assess the seismic response of a building and then the associated damage level.

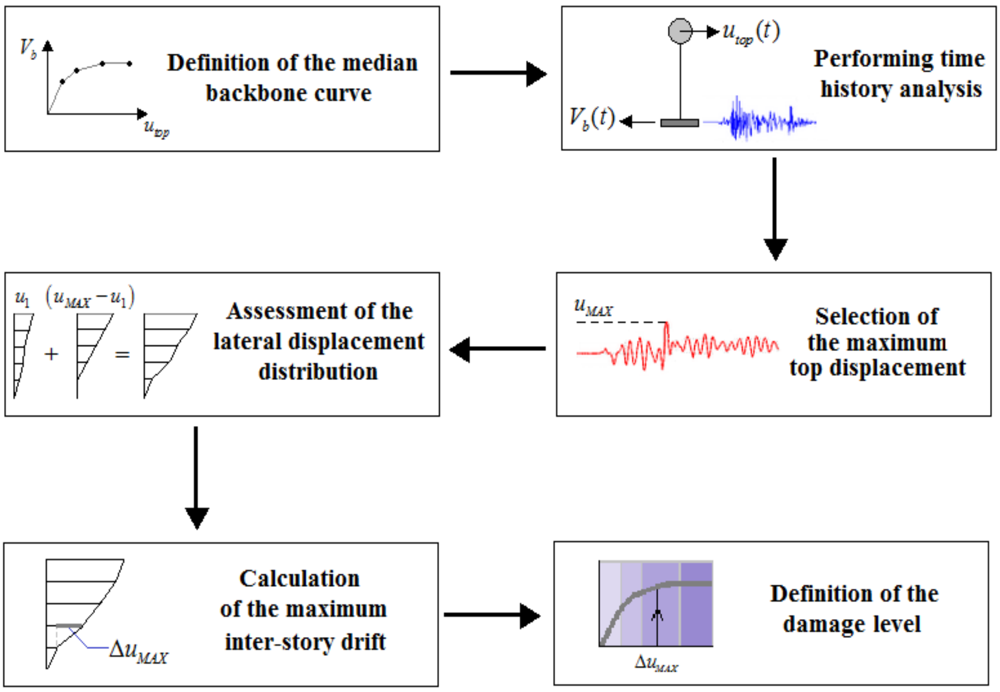

Figure 75. Proposed procedure to assess the damage to the buildings.

Chapter 8

Analysis implementation and simulation

8.1 Introduction

Simulating the seismic response of a large scale building portfolio is accomplished by modeling the physical system and then solving the equation of motions through fixed numerical methods by taking into account its main features according to the requested degree of accuracy. Furthermore, the modeling procedure is based on the available data which provide useful physical and statistical information. Therefore, the collected data needs to be manipulated and translated into computer recognizable format. Model translation process combines three essential features: information storage, algorithm development, and visualization tool. The application of these simulation stages represents the core of the simulation by itself that are named as implementation.

Implementation for simulation of large scale systems may be performed at different hierarchical levels such are simulation packages, simulation languages, and programming in general purpose languages. Several simulation tools were developed in the domain of natural disasters aimed to coordinate the decision making activities (Mustapha et al., 2013). Agent-Based Disaster Simulation Environment (ABDiSE) is a framework providing a complete tools for simulation different types of hazards (e.g. fires, floods and debris flows). This simulation package describes the agent's movement and interaction within the environment. Dynamic Discrete Disaster Decision Simulation System (D4S2) is a simulation tool addressed to predict the large-scale system's response to a natural disaster and provide support to decision makers in the emergency phase.

Simulation language refers to specialized programming language used to define the desired model. Special purpose algorithmic languages may have advantages in terms of efficiency and effectiveness of use (Shannon, 1997). Bauer et al. (2001) developed a set of Unified Modeling Language (UML) described through idioms and extensions. The agent interaction protocols adopted in the agent-based programming field were differently described to represent the internal behavior of an agent within the environment. Furthermore, simulation may be performed through general purpose languages. Many general purpose programming languages have been developed over the years, while the use of one specific language is dependent on the goal and variables involved into the particular application. Different algorithms may be adapted to represents a sequence of actions to be performed in a finite amount of space and time through a general computer formal language.

An integrated environment for seismic damage simulation of large scale building portfolio is implemented using MATLAB (MATLAB, 2018) language and SAP2000 (CSI, 2018) Application Programming Interface (API) tool. Simulation results are visualized by using both visualization environment tool of SAP2000 (CSI, 2018) which provides the real time dynamic response and Geographical Information System (GIS) (Goodchild, 2009) that is able to show the map of damage for a given seismic scenario.

8.2 Analysis flow

Figure 76 resumes the proposed step-by-step procedure adopted for large scale seismic simulation.

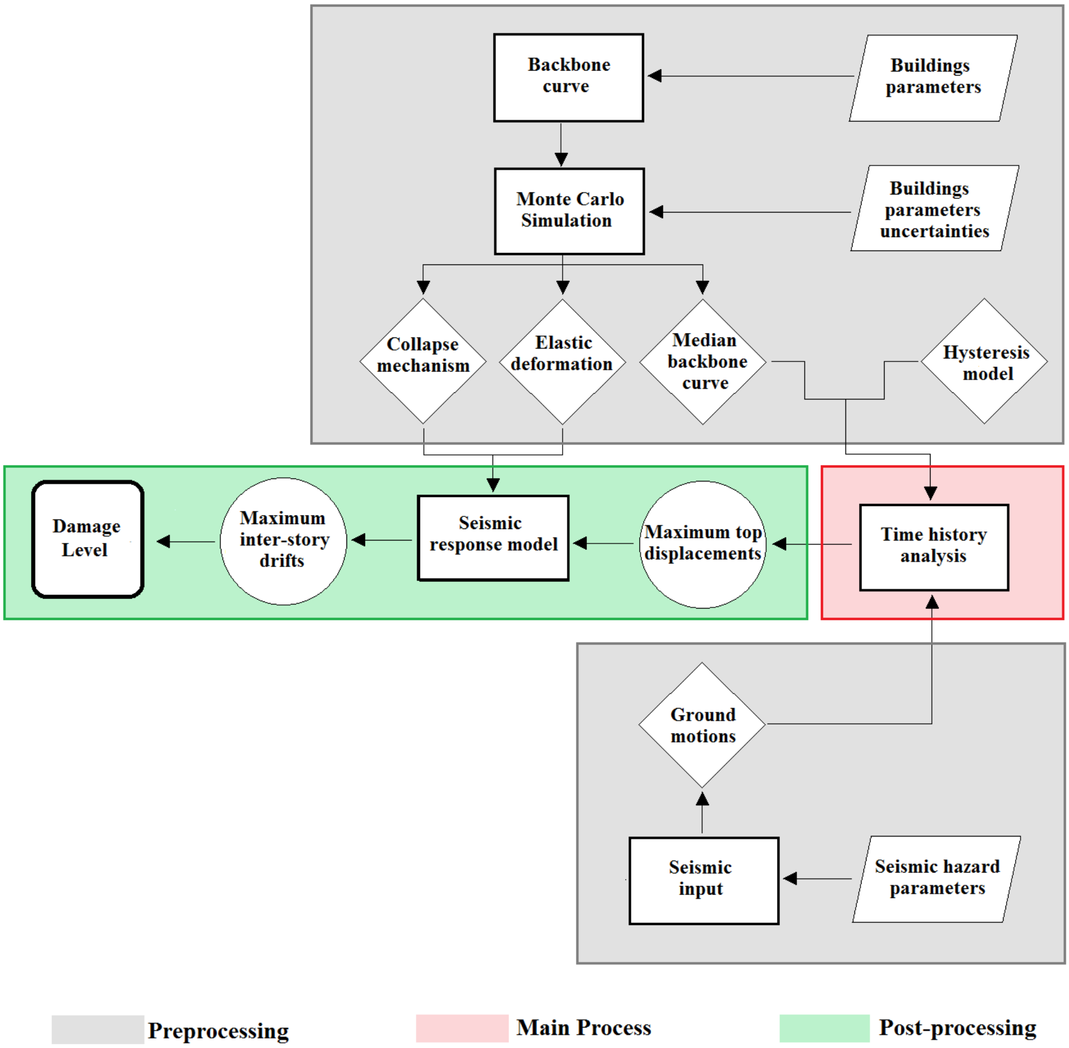

Figure 76. Schematic representation of the proposed large scale simulation process.

All the data required for the analysis implementation are identified by the parallelepiped shape elements shown in Figure 76. The rectangular shape elements refer to the modeling processes, while the rhombus shape elements identify the physical outcomes needed to evaluate the buildings' performance. The circular shape elements represent the building response results.

Four modeling processes are used to implement the proposed approach, which are:

- physical modeling of the global capacity of each building by considering the uncertainties ("*Backbone curve*" and "*Monte Carlo Simulation*" in Figure 76);
- approximated large scale seismic input definition ("*Seismic input*" in in Figure 76);
- nonlinear global dynamic response analysis ("*Time history analysis*" in Figure 76).
- assessment of the inter-story drifts which represent the EDPs ("*Seismic response model*" in Figure 76).

The physical results requested for assessing the buildings' response under a given seismic scenario are:

- median backbone curve and related dispersion parameter;
- elastic deformation of the buildings associated with the horizontal floor displacements;
- collapse mechanism.
- set of ground motions which are representative of the seismic hazard of the urban area;
- hysteresis model.

Time history analysis may be considered as the main process (red background in Figure 76) in assessing the buildings' performance. Therefore, all the modeling processes addressed to estimate the global capacity of each building and the seismic input are considered as data preprocessing (grey background in Figure 76). The modeling processes aimed to manage and arrange the outcomes of the time history analysis represents the post-processing (green background in Figure 76).

The entire analysis flow is controlled through a dedicated software tool developed in MATLAB (MATLAB, 2018) that is arranged into different algorithms. A physical algorithm is developed in MATLAB programming language to assess the median backbone curve and the hysteresis model. Furthermore, a simplified MATLAB-based algorithm is developed to define the simplified seismic scenario at urban level. All the physical data resulted from the preprocessing phase are remotely set in SAP2000 (CSI, 2018) and controlled by MATLAB by using the API software library available in SAP2000. Time history analysis has been performed and the results are remotely and automatically controlled by MATLAB. A third physical algorithm is implemented for converting the global response of each building to the desired EDP. Then, the damage levels are estimated for each single building within *IDEAL CITY*.

The computational procedures are performed through a Rack Server with no. 2 Intel Xeon (E5-2698 v4 2.2GHz,50M Cache,9.60GT/s QPI,Turbo,HT,20C/40T (135W) Max Mem 2400MHz) and 256 Gb RAM (8x32GB RDIMM, 2400MT/s, Dual Rank, x4 Data Width).

8.3 Preprocessing implementation

The building inventory of *IDEAL CITY*, containing all the information (such as material, geometry and mechanical properties), is developed with the aim of representing the typical Italian residential building stock. All the collected and manipulated information are allocated on an external server named as *IDEAL SERVER*. The storage is arranged by no. 4 x 1.2TB disks with a data storage virtualization technology (RAID) 5, with data redundancy purposes.

Moreover, the global soil characteristics and seismic hazard properties for the considered urban area are contained into the database.

8.3.1 Given seismic scenario definition

Earthquake scenario can be defined by the user as acceleration time histories in both horizontal directions (North-South, and East-West directions). Location of the epicenter and magnitude of the earthquake have to be additionally fixed by the user. A simplified algorithm is implemented to estimate the geometrical attenuation at any building location within the virtual city by calculating the source-to-site distances. The geometrical attenuation of the seismic excitation is estimated through the Boore-Atkinson (Boore and Atkinson, 2008) attenuation model. The algorithm is capable to evaluate the equivalent shear wave velocity in the uppermost 30 m ($V_{s30,eq}$) at each building location considering the $V_{s,30}$ map information stored into the database.

The acceleration time histories at each building location are evaluated by multiplying the assumed accelerations recorded in the epicenter by the associated scale factors which considered the geometrical attenuation.

8.3.2 Median backbone curve and hysteresis model definition

A physical algorithm is developed to evaluate the median characteristic points of the backbone curves. Aleatory uncertainties in the input model parameters are taken into account through the implementation of MCS. A number of 100 experimental input samples are set in the simulation which provides an adequate estimation of the outputs. Random input sampling is performed based on the standard deviation values defined for mechanical, geometrical, and construction element parameters.

Due to the large amount of processed data, parallel computing process is implemented using the MATLAB Parallel Computing Toolbox which allows the use of multicore processors. The algorithm is run on *IDEAL SERVER* and the outputs are automatically saved. The algorithm provides a set of deterministic output below resumed:

- median backbone curves' properties which refers to the base shear-top displacement values associated with the generalized points of the curve in both horizontal directions;
- total dispersion of the backbone curves represented by the lognormal standard deviation associated with each point of the curve.
- mean input sampled data such as: material strength, percentage of reinforcement, and equivalent mass;
- equivalent modal shapes in both horizontal directions. This information is useful to define the roof displacement distributions;
- collapse mechanism data which refers to the type of mechanism (global or local) and the weakest story.

A schematic overview on the algorithm flow is provided in Figure 77.

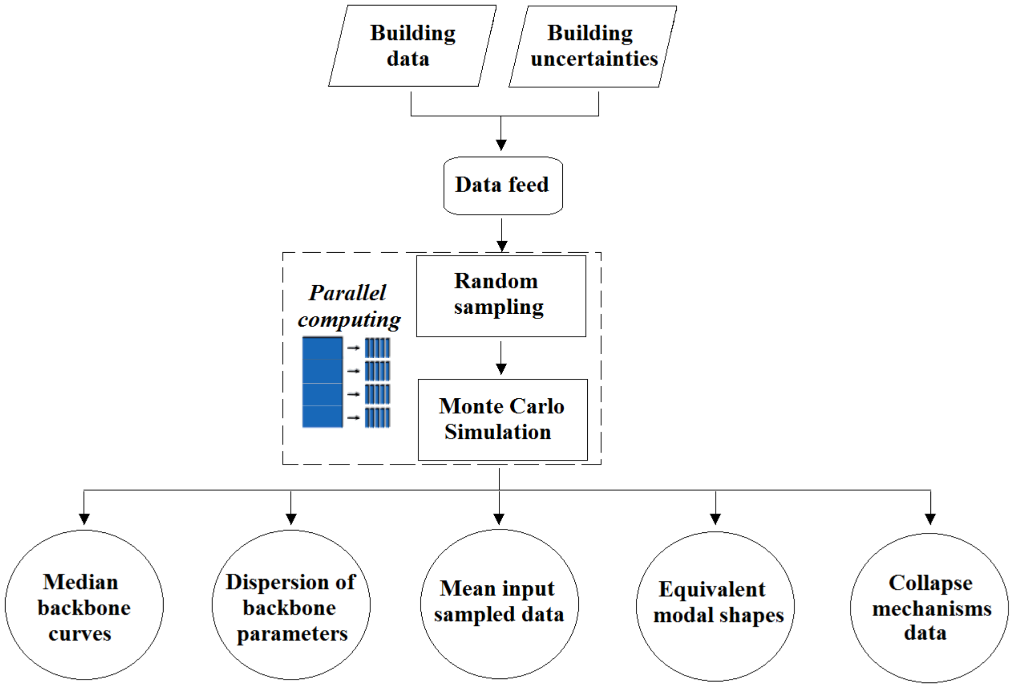

Figure 77. Algorithm flow for estimating the median backbone curve.

Due to the unavailability of detailed data, the dynamic degradation of the buildings is modeled according to the Takeda hysteresis model (Takeda et al., 1970).

8.4 Main process

The set of physical parameters estimated in the preprocessing phase are automatically imported in SAP2000 through the API tool provided by Computer Structure Inc. (CSI). The SAP2000 API is a programming tool that offers efficient access to the analysis and design technology of the SAP2000 structural analysis software. A direct interaction with third-party applications is allowed during run-time analysis. The API software library provides access to a collection of objects and functions capable of remotely controlling the data exchange and setting data in SAP2000. Each building is modeled in as a multi-linear plastic element by setting the force-displacement functions and the hysteresis behavior. Data exchange is managed by a MATLAB algorithm aimed to automatically set the parameters below resumed for each multi-linear plastic element:

1) nonlinear properties;
2) elastic stiffness and equivalent damping coefficient;
3) hysteresis model;
4) equivalent mass concentrated on the top;
5) seismic base excitation in terms of ground displacement histories.

Thus, direct integration time history analysis is performed on the *IDEAL SERVER* by parallelizing the processes performed through SAP2000. Multiple-cores processes are automatically executed by SAP2000 for non-linear direct integration time history analyses for any type of link elements. The outputs are automatically saved in terms of maximum absolute top displacement of each multi-linear plastic element. The results are arranged into tabular file by specifying the file name and the format. The derived outcomes are remotely controlled by MATLAB. The described algorithm flow is resumed in Figure 78.

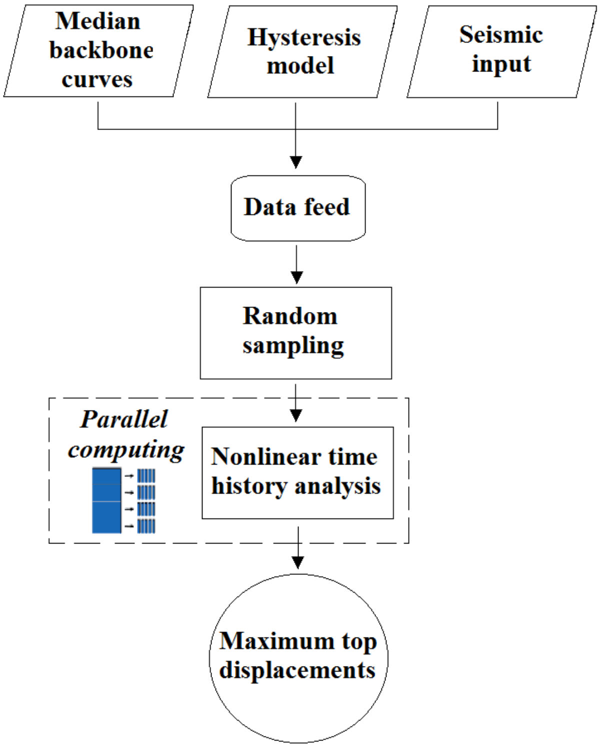

Figure 78. Algorithm flow for assessing the maximum top displacements of the buildings.

This algorithm is able to significantly reduce the time requested for performing nonlinear analysis and manage the outcomes. Simplified building modeling allows reducing the computational effort required to evaluate the dynamic buildings' response. SAP2000 parallel processing also reduces the run time analysis by taking advantage on the multi-cores structure of the *IDEAL SERVER*.

8.5 Post-processing

The outcomes of the nonlinear time history analysis are automatically processed through a MATLAB algorithm which converts the equivalent SDOF response in maximum inter-story drifts. These EDPs are suitable for assessing the damage level of each building within *IDEAL CITY*. The algorithm is also able to associate the level of damage experienced by the building based on the damage limits proposed by Ghobarah (2004). The results in terms of DSs are saved into the *IDEAL SERVER* database. Figure 79 illustrates the algorithm flow associated with the post-processing.

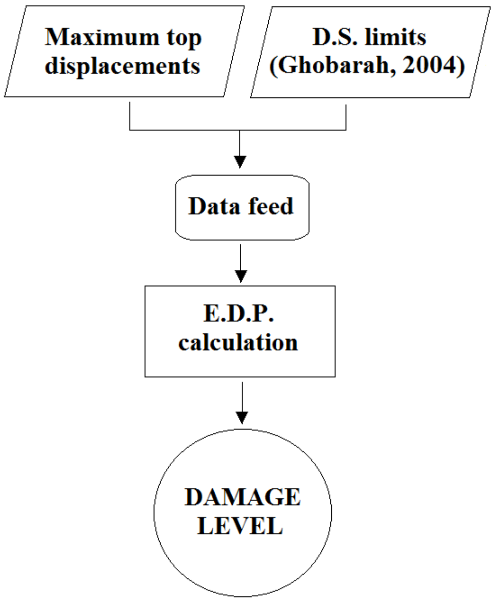

Figure 79. Algorithm flow for evaluating the level of damage of each building.

8.5.1 Visualization

2D or 3D visualization of the damage experienced by the buildings represent the simplest approach. Different color may be adopted to illustrate the damage level of the built environment through a 2D map or a more sophisticated 3D view.

SAP2000 visualization tool (real time visualization)

3D visualization is also provided by taking advantage on the multi-step animation video tool of SAP2000. This tool allows showing the movement of the built environment after a time history analysis and save the generated video in *avi* format. 3D visualization is obtained by extruding the buildings according to their planar layout. The 2D map of *IDEAL CITY*, which is available in .dwg format, is imported in SAP2000. Thus, each building is considered as a frame element having a cross section equal to its planar layout. The height of the buildings are imported in SAP2000 by using the interactive database command and then applied to the buildings. The generated 3D frame elements identify the buildings within the virtual city. The mechanical characteristics and the cross section geometrical parameters are set to zero. Moreover, the rigid links are defined to model the connection between the top of the frame and the link elements. In this case the frame elements are representative of the 3D city visualization and the time history are then applied only on the link elements which simulate the seismic behavior of the buildings.

The real time visualization of the seismic response of *IDEAL CITY* under a given scenario is represented by the top displacement histories of the frame elements.

GIS visualization tool (static visualization)

Visualization of different attributes of the analyzed building stock is also provided through the software Quantum GIS (Goodchild, 2009). Different colors are adopted to show different possible features of each building within the built environment. 3D-GIS visualization is generated through the 2D-GIS data in conjunction with the height attributes collected for each building. In detail, the building exterior polygons are identified and then mapped with its corresponding attribute collected into the database. This allows a simple and clear static 3D visualization that may be useful for decision making process. Furthermore, the results of the simulation in terms of level of damage are visualized taking advantage on the GIS capabilities. Therefore, different colors are associated with each level of damage experienced by the buildings. In addition, all of the building's attributes are assigned and plotted into a specific dialog box that is accessible by the user.

8.6 Integrated simulation environment

An integrated environment for seismic damage simulation of large scale building portfolio is implemented using MATLAB language and SAP2000 API tool. Simulation results are visualized by using the visualization environment tool of SAP2000 and GIS. The inner data flow of the developed integrated environment is shown in Figure 80.

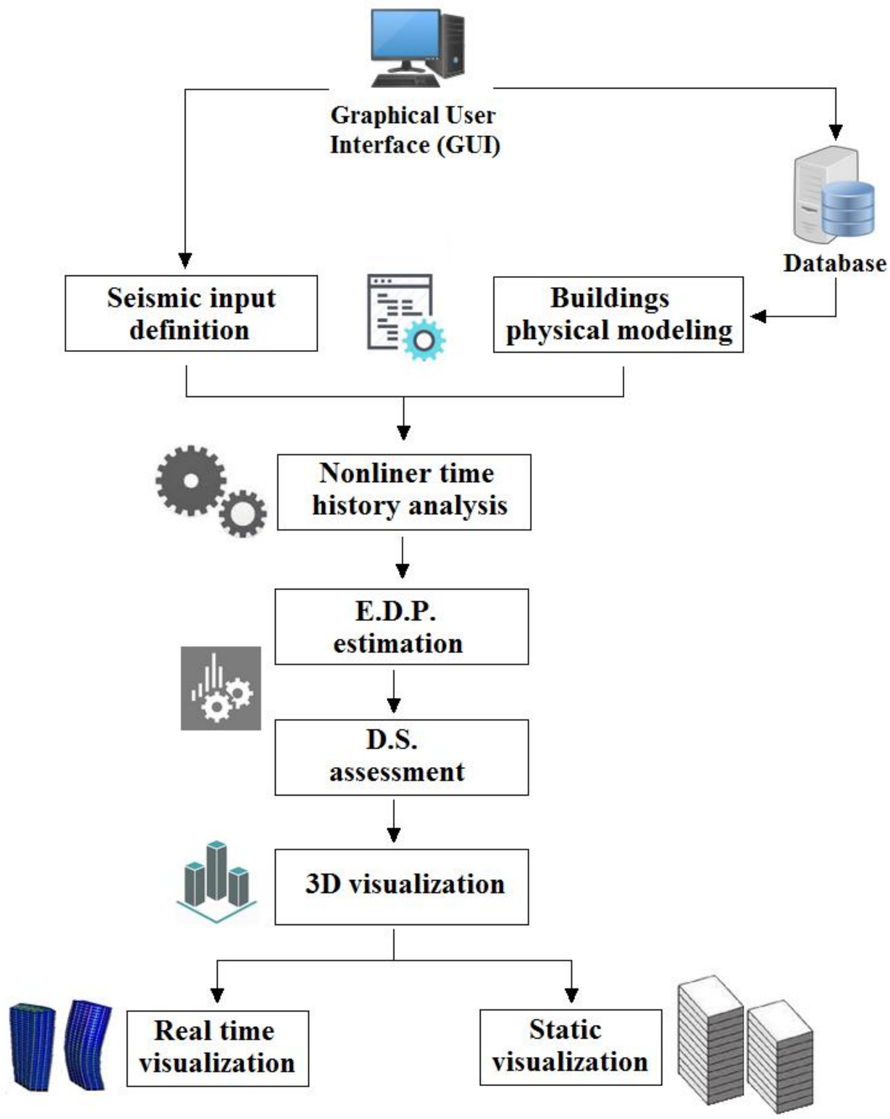

Figure 80. Complete data flow of the large scale simulation environment.

The interactive Graphical User Interface (GUI) allows the selection the earthquake scenario in the virtual city (magnitude, epicenter location, representative ground motion). Furthermore, the building stock data, allocated into the database, are accessible for the preprocessing phase (seismic input definition and buildings physical modeling). Then, the dynamic buildings' response is assessed through nonlinear time history analysis and the EDPs are estimated. The last step of the simulation consists in evaluating the DSs. 3D visualization tool allows to display the movement of the built environment after the time history analysis. Furthermore, a map of the damage experienced by the built environment is provided as outcome of the simulation.

Chapter 9

Case study and model verification

9.1 Introduction

Whatever modeling approach and methodology is used, the performance measures of the model will be expressed by the degree of accuracy in the representation of the real system. Generally, a model is more abstract than the system that represents. Thus, the abstraction process leads to eliminate unnecessary details focusing on the elements within the system which are important from a performance point of view. On the other hand, the abstraction process introduces a certain degree of inaccuracy. The reliability of the inaccuracy must be judged based on additional consideration such as running time, allowable resources, and output efficiency. In case of unavailability of powerful technological resources, a certain degree of inaccuracy may be justified. Furthermore, reducing the elapsed time is another advantage to be considered in the evaluation of the efficiency of a simulation model.

Model validation is necessary to judge how the assumptions which have been made are reasonable with respect to the real system. Therefore, verification represents the task of demonstrating that the model reproduces the system behavior with enough fidelity to satisfy analysis objectives. Based on this definition, comparison with a real system is the most reliable technique to verify a simulation model. In some cases, this approach may be unfeasible because the measurements on the real system would be expensive or impossible to be carried out. Furthermore, it is often costly and time consuming to determine that a model is absolutely valid or applicable. In these cases, the reliability and efficiency of the model may be checked through the judgment of the output results. Then, a simulation model may be verified when the simulation results respects given rules or are coherent with the expected ones.

First, the proposed simulation model will be applied considering a given seismic scenario and the associated output will be discussed. Then, the fragility assessment of the building stock of *IDEAL CITY* will be provided and some of the results will be shown. Finally, the verification of the proposed large scale simulation model will be carried out focusing on the physical model abstraction and the fragility assessment.

9.2 Damage assessment for a given seismic scenario

The seismic input definition has been set in terms of epicenter location, magnitude, and time history recorded in the epicenter. The epicenter distance associated with the center of gravity of the downtown is 9 km. Geometrical attenuation at any building location has been estimated through the dedicated algorithm.

The horizontal acceleration time histories recorded during the Central Italy earthquake (6.5 M_w, 2016/10/30) in the station of Norcia (NRC) have been assumed as representative of the seismic accelerations (Figure 81) recorded in the zone close to the epicenter. Since a 6.5 moment magnitude earthquake is capable of breaking tens of km of fault, the ground motion parameters recorded within the projection area of the rupture fault on the surface have been considered constant. This assumption leads to consider the same selected horizontal acceleration time history for the zone close to the epicenter.

Figure 81.a depicts the North-South component of the acceleration time history recorded in the station of Norcia.

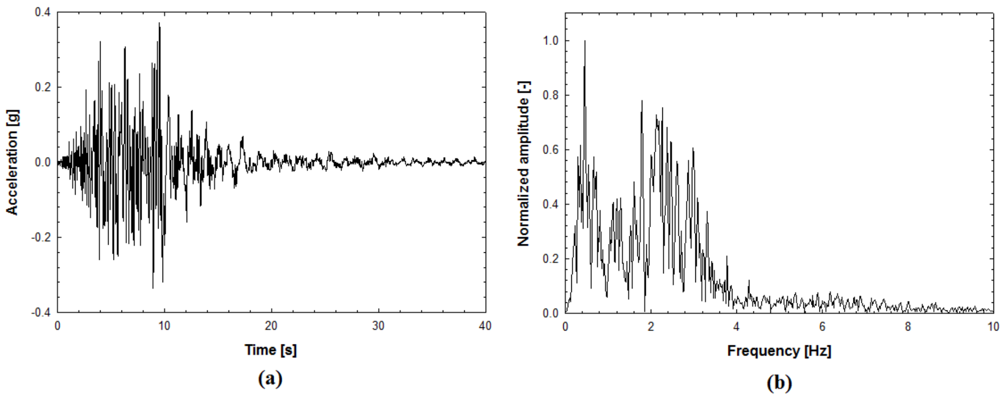

Figure 81. North-South acceleration time history recorded in Norcia during the Central Italy earthquake (a), and associated frequency content (b).

A PGA value of 0.37 g has been recorded, while Figure 81.b illustrates the Fourier transform of the ground motion. The selected ground motion shows a wide frequency bandwidth (0.4-3.3 Hz) which leads to cause significant dynamic amplification on the structure. Figure 82 shows the elastic acceleration response spectrum of the considered ground motion.

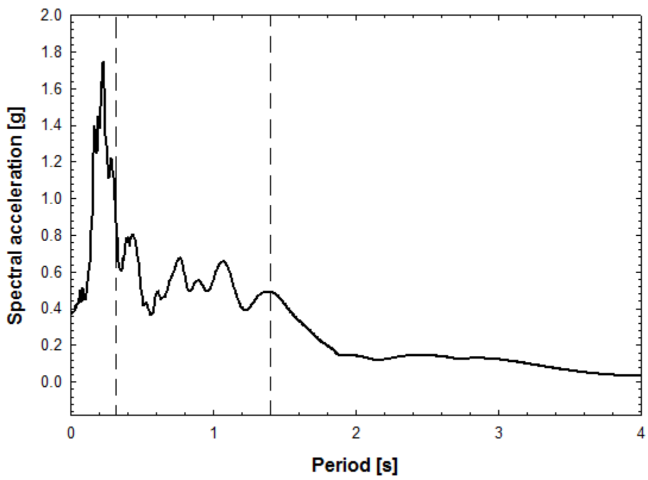

Figure 82. Elastic acceleration response spectrum of the considered ground motion.

The maximum amplitude is given for structure with period less than 0.3 s (rigid structures), whereas a dynamic amplification which ranges from 0.4 g to 0.7 g is observed for structure with period between 0.3 s and 1.4 s. This range of periods is mostly representative of the fundamental periods of the residential building stock of *IDEAL CITY*. This in turn leads to consider a seismic input which causes a similar maximum elastic response on the building within the virtual city.

The physical building modeling has been obtained through the dedicated algorithm and the dynamic characteristics of the building portfolio have been set on SAP2000 environment. A number of 50 iterations have been set to perform MCS and assess the median backbone curve for each building.

The computational procedures have been performed through the Rack Server named as *IDEAL SERVER* whose technical characteristics are resumed in *chapter 8*. The measured absolute elapsed time has been estimated in 162 minutes for 50 MCS iterations and 23420 buildings, which corresponds to 0.02 s/building/iteration of absolute elapsed time.

Ground displacements time histories have been derived and applied at the base of each building model. The geometrical attenuation of the seismic excitation has been estimated through the Boore-Atkinson (Boore and Atkinson, 2008) attenuation model by estimating the equivalent shear wave velocity in the uppermost 30 m ($V_{s30,eq}$) at each building location. Figure 83 depicts the 2D map of PGA values calculated by taking into account the geometrical attenuation, while the epicenter location is represented by the red star.

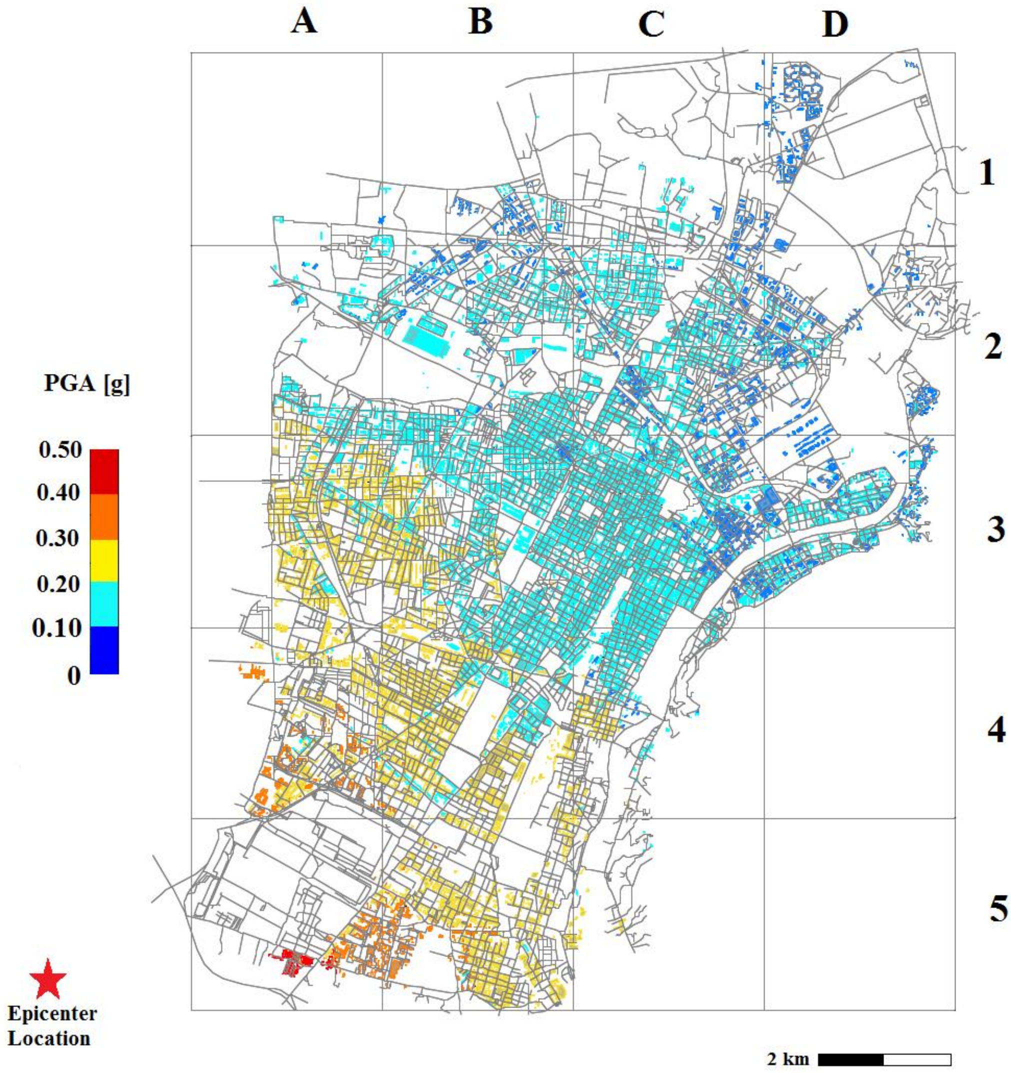

Figure 83. PGA map of IDEAL CITY.

Time history analysis has been performed and the dynamic building response of *IDEAL CITY* has been estimated. The measured running time has been estimated in 72 minutes for entire *IDEAL CITY* by using between 62 % and 78 % of maximum CPUs capacity. The outputs have been automatically saved in terms of maximum absolute top displacement of each multi-linear plastic element. The results have been arranged into tabular file by specifying the file name and the format. The top displacement of each element have been derived and used to define the related maximum inter-story drift according to the proposed seismic response model (*paragraph 7.3*). Thus, the building damage levels have been derived based on the threshold of inter-story drifts proposed by Ghobarah (2004).

Figure 84 depicts the 2D visualization of the damage level for the entire *IDEAL CITY*.

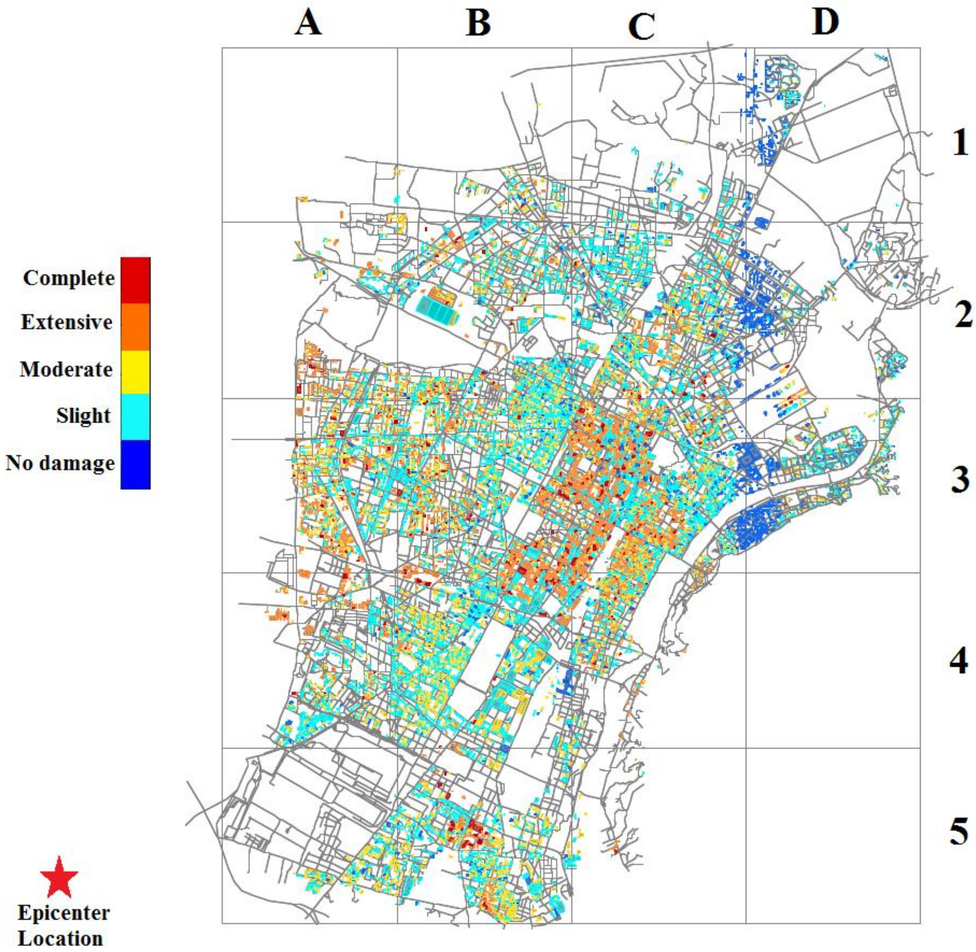

Figure 84. 2D visualization of the damage level to the buildings within *IDEAL CITY*.

The total percentages of buildings associated with each DS have been calculated and illustrated in Figure 85.

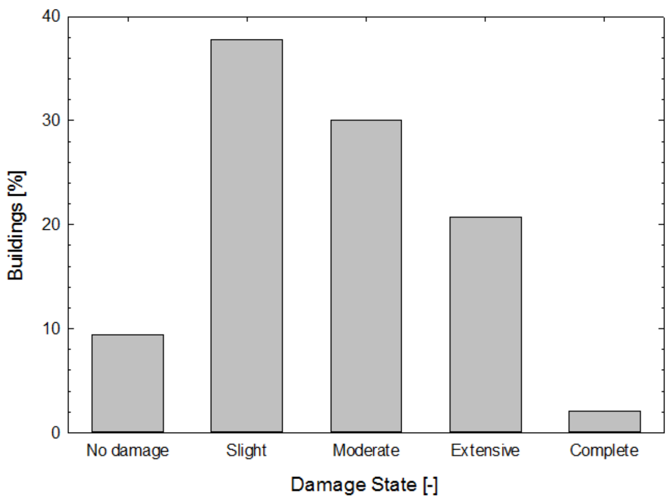

Figure 85. Buildings' damage distribution within *IDEAL CITY*.

Most part of the buildings has experienced slight DS (about 38 %), while 30 % and 22 % of the buildings have a moderate and extensive DS, respectively. Only 2 % of the buildings are collapsed, whereas the remaining part is undamaged (about 9 %). The distribution of DSs based on the year of construction is depicted in Figure 86.

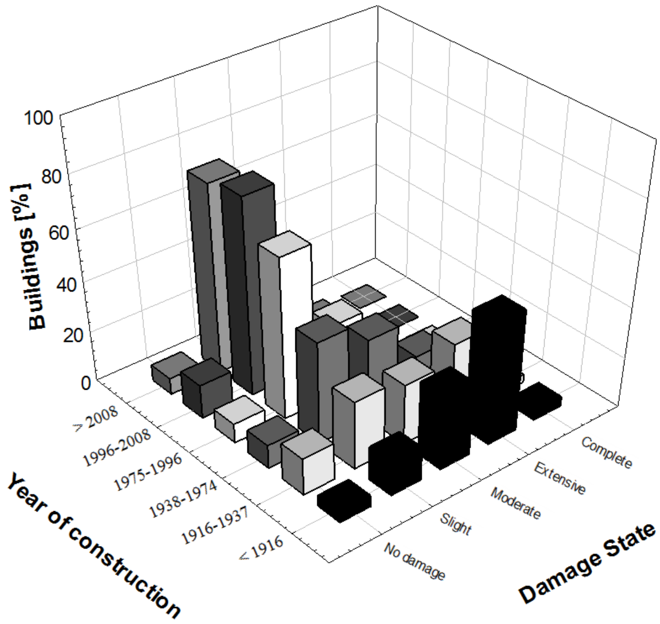

Figure 86. Building percentage distribution based on the DSs and year of construction.

Figure 86 shows how the most part of the buildings built before 1916 have experienced extensive and moderate DSs. The same trend is recorded for the category of building identified by the range 1916-1937. A dominant slight damage is observed for the buildings which have been built after 1975. These results are consistent with the newest seismic design procedures which aim to enhance the structural performance under seismic loads.

The downtown of the city is mainly composed by old masonry buildings that may experiences a large damage in comparison with modern RC buildings. According to Figure 84, it is possible to observe that the highest percentage of complete and extensive damaged buildings is located in the downtown (*C3*) and in the old neighborhoods of the city (*B3*, *B2*, *C2*). Furthermore, Figure 87 depicts a 3D damage visualization of the downtown area obtained through SAP2000 tool.

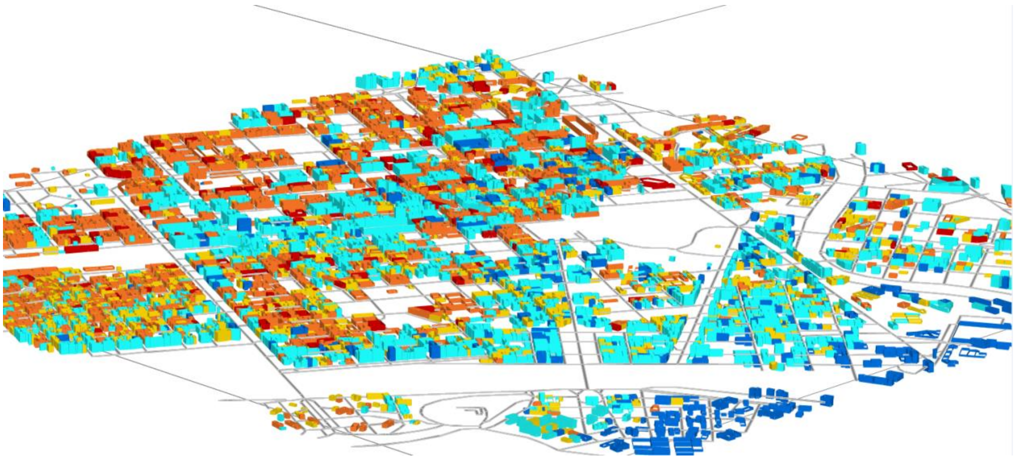

Figure 87. 3D damage visualization of the IDEAL CITY downtown (*C3* in the grid of Figure 84).

Extensive and complete damage are also observed in zones more close to the epicenter (*B5*) or in zone where a high percentage of old building are located (*A2, A3*). The North-East zone of *IDEAL CITY* is far from the epicenter and then a high percentage of undamaged building has been identified. Furthermore, the South-West part of the city represents the modern housing zone. Despite this area is the closest one to the epicenter, the buildings are moderately or slightly damaged due to the higher structural performance.

The real time visualization of the seismic response of *IDEAL CITY* under given seismic scenario has been obtained through the multi-step animation tool of SAP2000. Figure 88 shows a 3D visualization of a small part of *IDEAL CITY* for four different time steps.

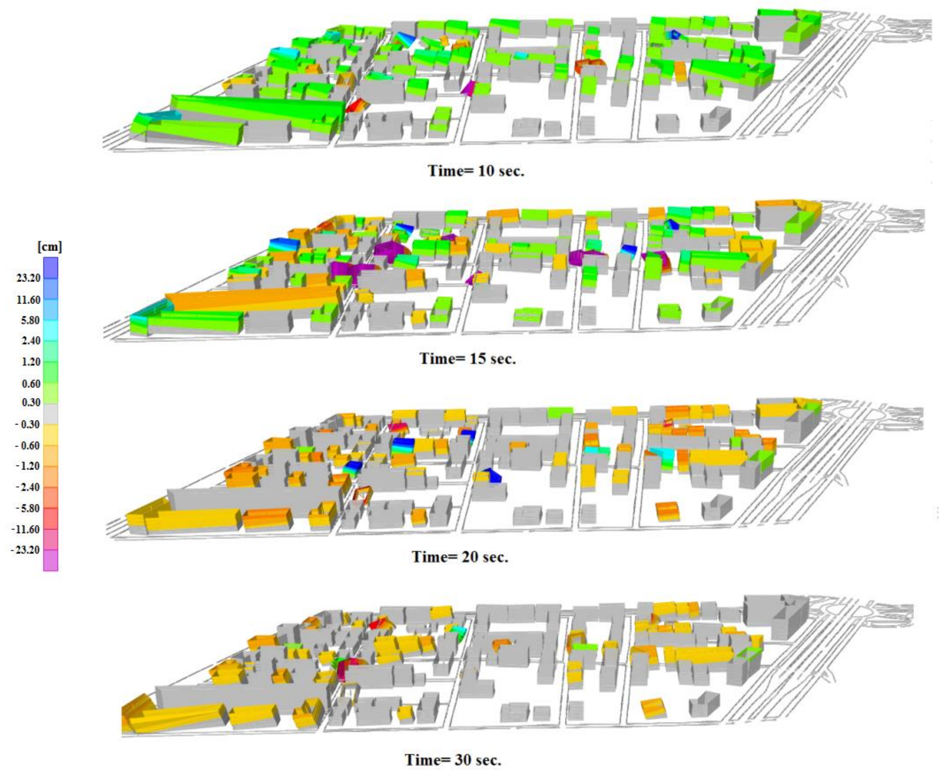

Figure 88. 3D visualization of a part of IDEAL CITY for four different time steps.

It is also interesting to visualize the input and output data using current computing technology and interactive GIS. As illustrative example, Figure 89.a shows a static map of the level of structural damage related to a part of the building stock of *IDEAL CITY*. Furthermore, a zoomed view of the static map is depicted in Figure 89.b.

(a)

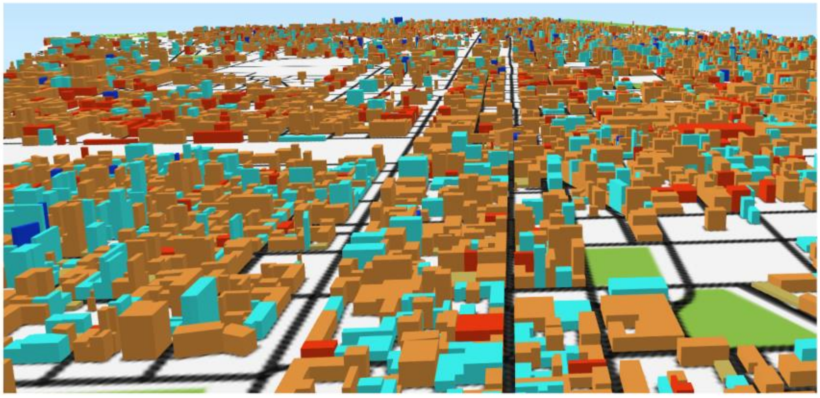

(b)

Figure 89. 3D-GIS visualization of the DSs for part of IDEL CITY (a) and its zoomed view (b).

9.3 Fragility curves of building portfolio

The type and extent of damage that a structural component may experiences is uncertain. ATC 21 (2017) observed that the nonlinear building response, defined through an EDP, at a given earthquake scenario is lognormally distributed and the best approximation of the building's dynamic response is the median of the lognormal distribution (θ). The median parameter is substantially equal to the geometric mean of the building' response that is represented by the selected EDP. These observations are valid for a given seismic scenario which is identified through a specific IM parameter. Various parameters may be used to describe the seismic scenario such as peak parameters (PGA, spectral acceleration at the reference period), energy content (Arias intensity), earthquake intensity (moment magnitude), etc. IM represents a link between the earthquake properties (magnitude, source-to-site distance R, faulting style and soil type) and the assessment of the structure behavior (Pejovic et al., 2015). Unfortunately, all the possible selected IMs are not capable to provide an estimation of the response of the structure which is not affected by uncertainties. According to the ATC-58-1 (2011) provisions, the measure of dispersion of the building's response (β) at a given earthquake scenario, is represented by the standard deviation of the lognormal distribution associated to the building's response. The two statistical parameters above discussed are then used to identify the fragility function that represents statistical distributions that indicate the conditional probability of exceeding a certain DS for different IM values (ATC, 2011).

An analytical approach has been adopted to assess the fragility functions of the buildings located within *IDEALCITY*. The derived fragility functions are associated with the four considered DSs which are: slight, moderate, extensive, and complete.

Given the geographical scale and the variety of the buildings' characteristics within *IDEAL CITY*, the PGA has been selected as IM parameter. This measure is directly connected with the inertial forces and which appears in the structure especially for stiff systems. Peak parameters do not take into account the frequency and energy content of the ground motion which influences the dynamic response of the structure. In order to overcome these limitations, the GMSM proposed by Marasco et al. (2018) has been used to select a set of seven ground motions in both horizontal directions for each HL which is representative of the seismic intensity that may occurs in the reference site.

The seismic scenario has been defined through a set of seven motions for each HL. Then, the dynamic response of the buildings have been obtained through nonlinear time history analysis in SAP2000, while the output have been automatically saved in terms of maximum absolute top displacement. The results have been arranged into tabular file by specifying the file name and the format.

The measured time history running time has been estimated in 265 minutes for entire *IDEAL CITY* and for 21 ground motions by using an between 62 % and 78 % of maximum CPUs capacity.

The top displacement of each element has been converted into the maximum inter-story drift according to the proposed seismic response model. Finally, the fragility curves in terms of PGA have been derived based on the threshold of inter-story drifts proposed by Ghobarah (2004) and the median θ and dispersion β parameters identifying all the four considered DSs have been assessed.

A database containing all the median and dispersion parameters associated with the slight, moderate, extensive, and complete DS has been created for both horizontal directions of the buildings within *IDEAL CITY*.

The median PGA is used as the representative parameter of the seismic vulnerability of individual building. The 2D visualization of the median values of PGA associated with a slight (Figure 90a), moderate (Figure 90b), extensive (Figure 90c), and complete (Figure 90d) DS is provided for the building stock of *IDEAL CITY*.

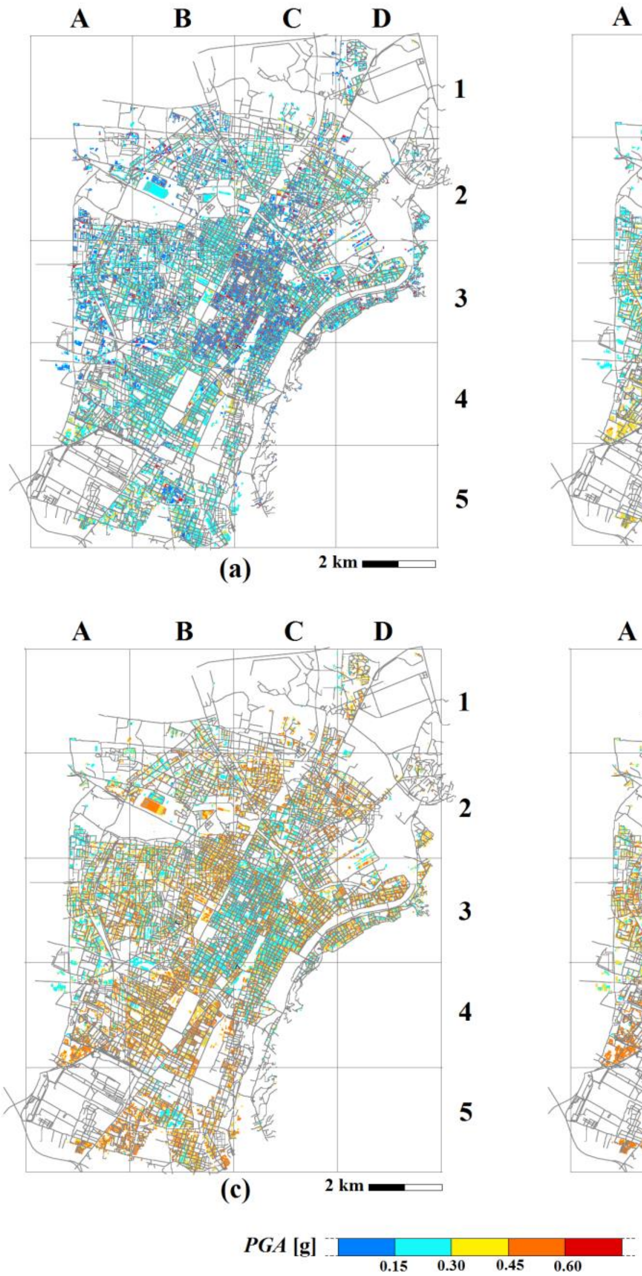

Figure 90. 2D visualization of the median drift ratio associated with a complete DS.

According to Figure 90, the downtown of IDEAL CITY (*C3*) is the most vulnerable zone. The spatial distribution of the building archetypes (Figure 91.a) and year of construction (Figure 91.b) confirm that the vulnerability distribution is higher in the zones where the old buildings are located.

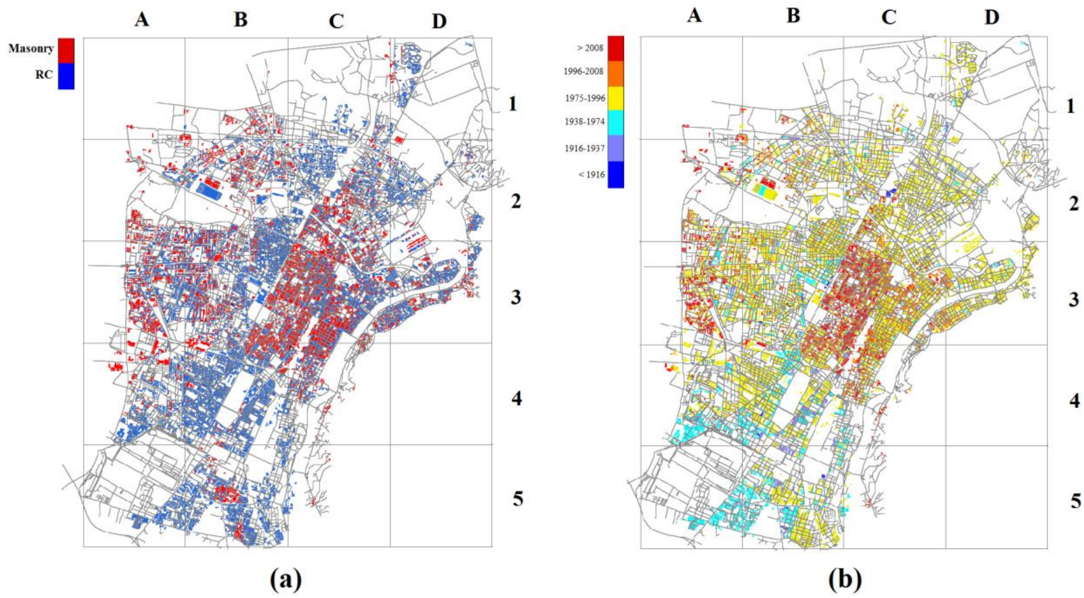

Figure 91. Spatial distribution of building archetype (a) and year of construction (b).

In addition, it is worth mentioning that the masonry buildings represent the most vulnerable archetype of the analyzed building portfolio.

To better analyze the outcomes of the simulations, the percentage of buildings associated with the four DSs (N_{DB}) has been calculated and normalized with respect to the number of buildings built in the same period of construction. Figure 92 depicts the percentage of damaged building per year of construction based on the related DSs.

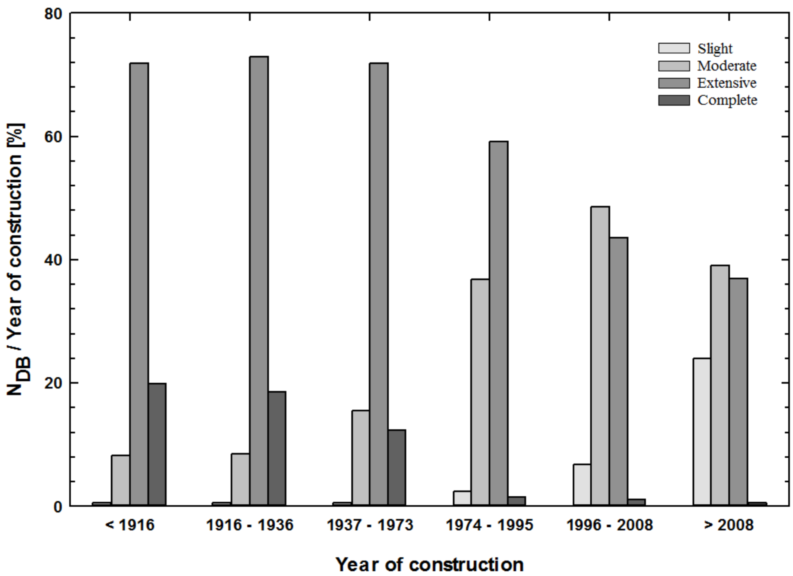

Figure 92. Percentage of buildings associated with the four DSs normalized with respect to the number of buildings built in the same period of construction.

The percentage of buildings with complete DS is inversely proportional to the age of the buildings. In other words, older buildings experienced a greater irreversible damage, whereas slight and moderate DSs are predominant for new buildings. In detail, 20 % of buildings built before 1916 have experienced complete DS and about 72 % are extensively damaged. The percentage of building with slight DS is increasing up to 22% for building built after 2008. For the same year of construction, the percentage of buildings with moderate damage reaches the value of 40 %. Thus, reversible damage is mostly observed for new buildings. This trend is consistent with the newest seismic design procedures which aim to enhance the structural performance under seismic loads.

Vulnerability of the building portfolio has been also investigated by considering the distribution of buildings with certain DS for low-rise, mid-rise and high-rise configurations. According to Hazus methodology (FEMA, 2011), buildings are categorized in different types based on the number of stories. RC Moment Resisting Frames with number of story from 1 to 3 are considered as low-rise structures, between 4 and 7 refer to mid-rise buildings, and more than 7 stories represent high-rise buildings. Masonry buildings are classified as low-rise (from 1 to 2 stories), medium-rise (3 stories) and high-rise (more than 3 stories). The percentage of buildings associated with the four DSs have been calculated and normalized with respect to the number of low, mid, and high-rise masonry (Figure 93.a) and RC (Figure 93.b) buildings.

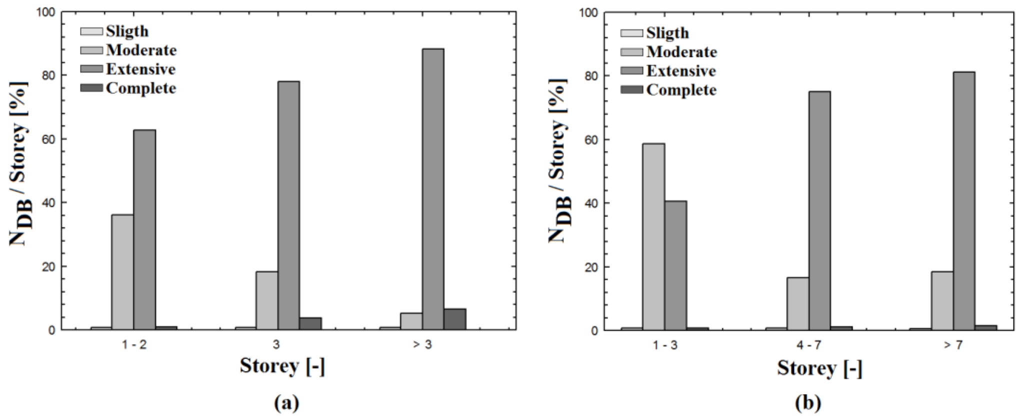

Figure 93. Percentage of buildings associated with the four DSs normalized with respect to the number of low, mid, and high-rise masonry (a) and RC (b) buildings.

Irreversible damage (extensive and complete DSs) increases with the number of stories of both RC and masonry buildings. Simultaneously, slight and moderate DSs are greater for low-rise buildings. Therefore, seismic vulnerability increases with the number of stories of buildings. This consideration is confirmed by Hazus methodology (FEMA, 2011), which provides median values of structural DS thresholds higher for low-rise buildings and lower for high-rise buildings.

Furthermore, the percentage of masonry buildings that have experienced irreversible DSs is always greater than that one associated with RC buildings.

This observation emphasizes that masonry buildings are more vulnerable than RC buildings.

9.4 Methodology verification

In order to test the proposed simulation model and the associated fragility functions assessment, two RC buildings have been assumed as case studies (Figure 94).

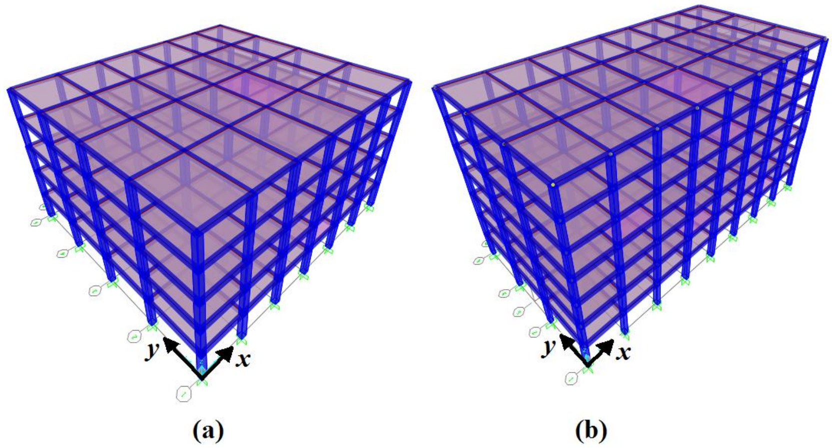

Figure 94. Five story (a) and seven story (b) case study buildings.

The first case study building (Figure 94.a) is a five story building with a square planar layout, whereas Figure 94.b depicts a seven story building having a rectangular planar layout. Both buildings have a span length of 4.40 m in *x* direction and 6.00 m in *y* direction, whereas a story height of 3.00 m is used. The structural members have been designed according to the Italian seismic regulations (NTC08, 2008). Figure 95 illustrates the designed member sections for the two case study buildings.

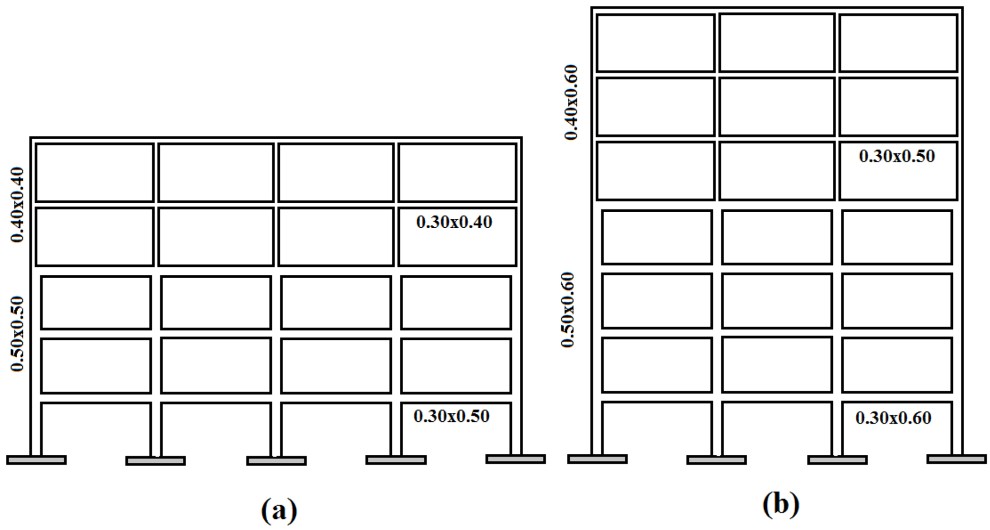

Figure 95. Five story (a) and seven story (b) 2D frame and related dimensions of the structural elements.

A symmetric reinforcement arrangement has been designed for the beams and columns. A strength class C 30/37 has been chosen for the concrete, whereas the B450C strength class has been considered for the steel bars.

The seismic hazard has been selected to be representative of a high seismic hazard level of the national territory. For this purpose, the city of Soveria Mannelli, Italy (Lat: 39.0833, Long: 16.3667) has been selected as reference site.

The software SAP2000 (CSI, 2018) has been used to build the FEM models of the structures. Concentrated plasticity model (FEMA 356 type P-M2-M3 for columns and M2-M3 for beams) has been chosen to account for the nonlinearity in the structural components. A 5% damping ratio has been assigned to the frames according to Rayleigh formulation.

The mechanical and geometrical parameters used to define the FEM models have been used as representative of the median input variables of the proposed physical model. Each of those parameters has been considered as aleatory variables and the associated dispersion values have been assumed. MCS have been executed by assuming a number of iterative steps equal to 100, and then the median backbone curves have been assessed for both horizontal principal directions. A comparison between the capacity curves obtained through the pushover analysis performed in SAP2000 and the median backbone curves estimated using the proposed physical model is shown in Figure 96 (first case study building) and Figure 97 (second case study building).

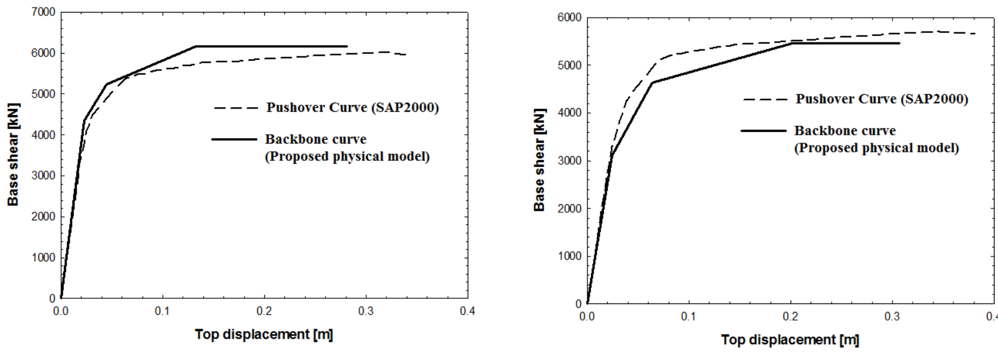

(a) (b)

Figure 96. Comparison between capacity curves obtained through the pushover analysis and the median backbone curves estimated using the proposed physical model in x direction (a) and y direction (b) for the first case study building.

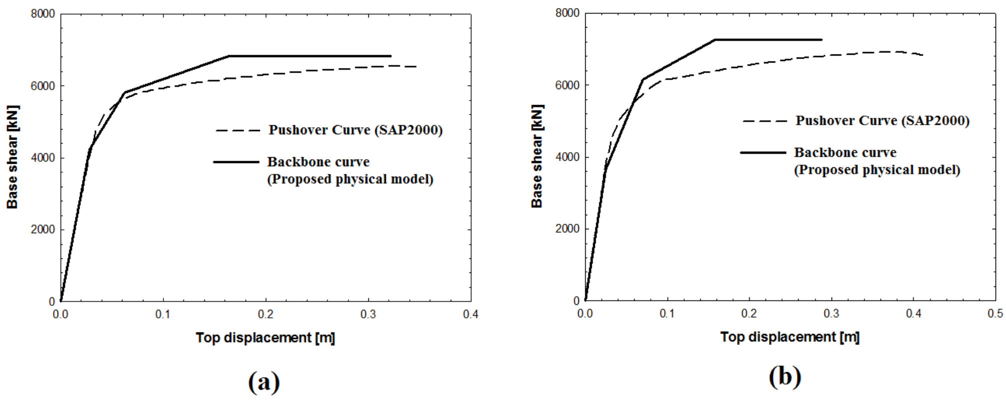

Figure 97. Comparison between capacity curves obtained through the pushover analysis and the median backbone curves estimated using the proposed physical model in *x* direction (a) and *y* direction (b) for the second case study building.

For both case study buildings, the median backbone curves provide comparable and reliable results in the two horizontal directions. Moreover, the collapse top displacements of the median backbone curve are always lower than those ones obtained through the pushover analysis performed on the FEM model. Furthermore, the estimated maximum shear capacity tends to be equal or, in some cases, greater than the expected one. This is due to the application of the kinematic theorem of the limit analysis, which provides an upper bound limit of the structural capacity in terms of force. This in turn, leads to assume a stiffer behavior than the real one.

The same set of seven ground motions in both horizontal directions for the HLs listed in Table 23 have been adopted as seismic input. The direct integration dynamic nonlinear analyses have been performed in SAP2000 and the PGA has been assumed as EDP. According to Ghobarah (2004), the fragility curves for each DS have been derived and compared with those ones obtained through the proposed simulation approach. Figure 98 depicts the comparisons of the fragility curves associated with moderate (Figure 98.a) and complete (Figure 98.b) DSs for the first case study building.

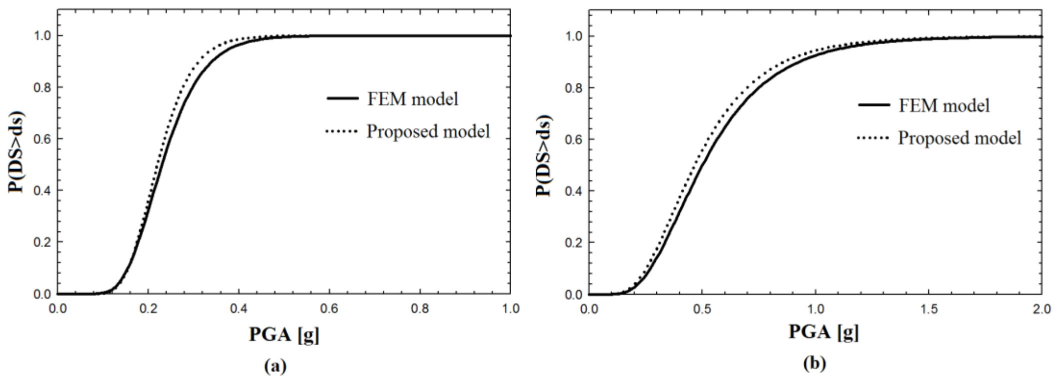

Figure 98. Comparison between fragility curves obtained through the time history analysis performed for the FEM model and the proposed physical model

associated with the moderate (a) and the complete (b) DSs for the first case study building.

The fragility functions associated with the moderate DS are similar in terms of median demand and dispersion. Considering the complete DS, the median PGA obtained through the proposed model is lower than the PGA estimated by using the FEM model.

Figure 99.a illustrates the comparisons of the fragility curves associated with moderate DS, whereas Figure 99.b refers to the complete DS for the second case study building.

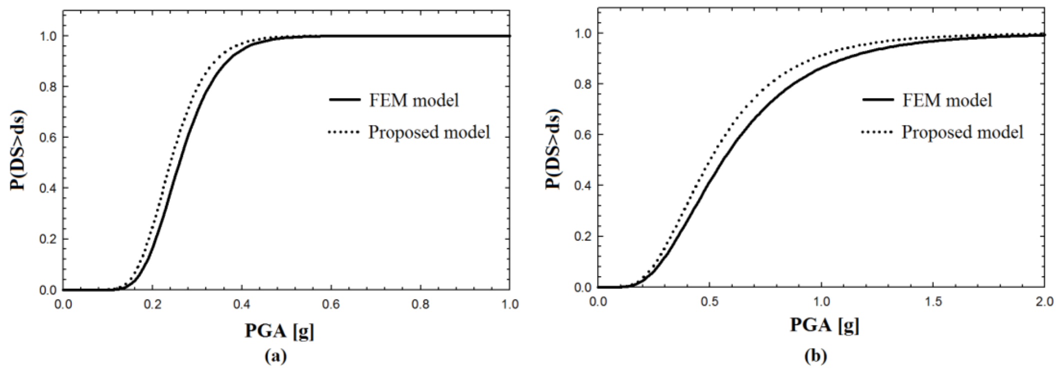

Figure 99. Comparison between fragility curves obtained through the time history analysis performed for the FEM model and the proposed physical model associated with the moderate (a) and the complete (b) DSs for the second case study building.

Similarly to the first case study building, the fragility functions associated with the moderate DS of the second case study building are similar. Regarding the complete DS, the proposed model provides a fragility function more conservative than the fragility curve obtained by using the FEM model. In any case, the median PGA associated with the two fragility functions are similar.

Thus, the proposed model tends to provide more conservative results for higher damage level. Moreover, it is possible to claim that the proposed simulation model provides comparable results in terms of fragility function with the FEM model. Furthermore, the proposed seismic simulation approach is able to provide reliable fragility functions specific for individual building.

Conclusion

The prediction of physical damage and the impact of natural hazards on building stock is always a challenge to community developers and decision makers. However, damage assessment for large-scale cities is more complicated than a single site due to the buildings spatial distribution and uncertainties in building attributes for different hazard intensities. Moreover, the concept of virtual city is attracting the interest of researchers due to the ease in testing the simulation models while taking into account the main features of existing building portfolio.

In this research a simulation model to assess the damage to the building portfolio of a large-scale area under a given seismic scenario was proposed. A large scale city (*IDEAL CITY*) was envisioned as being representative of the typical Italian residential building stock. Furthermore, a typological approach was adopted to estimate the average mechanical, geometrical, and construction elements parameters, while the structural configurations were determined based on the current seismic design rules of the year of construction. The intensive data collection and processing led to build a comprehensive exposure database of typical Italian housing portfolio with a high level of granularity. Furthermore, the assumption of random input variables prompted to investigate different input dataset representative of the typical building portfolio and then providing a set of possible damage scenarios. The definition of the exposure building database of *IDEAL CITY* is one of the strength of this research because it allows increasing the accuracy and consistency of the simulation results.

The seismic capacity of the building stock was estimated through an efficient physical simulation model that takes into account the aleatory uncertainties associated with the building attributes. Monte Carlo Simulation was performed by repeating random input sampling to obtain different numerical outputs in terms of global capacity curve for individual buildings. Then, median global capacity and related dispersion were assessed as representative of the seismic behavior of each building. It is worth mentioning how the physic nature of the proposed mode in assessing the parameters of the capacity curve allows taking into consideration both global and local collapse mechanisms. Therefore, this approach enhances the accuracy in estimating the global shear resistance of buildings.

Different case studies buildings (RC and masonry) demonstrated the accuracy and effectiveness of the capacity model in reproducing the global seismic behavior of individual building. Furthermore, the proposed capacity model, suitable both for RC and masonry buildings, leads to accurately identify the capacity curve for individual building rather than assess the capacity of groups of buildings. In addition, the proposed capacity model is able to provide a set of possible seismic behaviors for each building.

A simplified seismic scenario was identified to test the proposed simulation model. Then, the building performance was obtained through nonlinear time history analyses, where each building was modeled as equivalent SDOF system. The dynamic characteristics of any individual building were derived from the median capacity curve, while the equivalent damping ratio was estimated according to the Rayleigh formulation. In addition, the dynamic degradation was modeled based on the Takeda hysteretic model.

The proposed building modeling and the use of nonlinear dynamic analysis lead to limit the computational efforts without losing accuracy and consistency with the expected results.

A simplified seismic response model is also proposed to convert the global seismic response to local response that is more suitable for the damage assessment procedures. Then, the entire simulation model was tested both in terms of capacity model and damage assessment for a given seismic scenario and through different set of time histories aimed to estimate the fragility curves for the considered building portfolio.

The reliability of the proposed simulation model was demonstrated by the results of the seismic scenario-based simulation. First of all, the results of the large-scale simulation showed a direct proportionality between the experienced damage to the buildings and their age. Furthermore, the assessed Damage States also revealed that older buildings experienced a greater irreversible damage, whereas slight and moderate DSs were predominant for new buildings. These results are consistent with the newest seismic design procedures which aim to enhance the structural performance under seismic loads by limiting the structural damage.

Moreover, masonry buildings were found to be more vulnerable than RC buildings. This observation is in line with the global behavior of the two building archetypes. In fact, the intrinsic fragility of masonry buildings leads to experience a higher level of damage. In addition, the simulation outcomes showed how irreversible damage increases with the number of stories of both RC and masonry buildings. This consideration is in line with the Hazus methodology, which provides median values of structural DS thresholds higher for low-rise buildings and lower for high-rise buildings. Furthermore, the percentage of masonry buildings that have experienced irreversible DSs was always greater than that one associated with RC buildings. This observation emphasizes that masonry buildings are more vulnerable than RC buildings.

The simulation results satisfactory verified the entire simulation model. Therefore, it is possible to claim that the developed simulation model provides an efficient perspective to estimate the potential seismic vulnerability of building portfolio that is representative of the Italian housing stock. Furthermore, the proposed simulation model significantly reduces the computational effort while analyzing different set of input variables that allows exploring a set of possible damage scenarios. This methodology may support decision-maker to explore how their community responds to a disruptive event, quantify the performance of buildings due to hazard occurrence, and to plan the better resilience-building strategies to minimize both loss and recovery time.

The entire proposed simulation model was implemented in an integrated environment that offers to the user a simple and useful tool. Furthermore, a visualization tool was implemented to show the simulation results both in real time and static map. The visualized simulation results provide a powerful tool to investigate the response of the system and to take decisions about it.

Future work

Many different adaptations and improvement have been left for the future due to lack of time (i.e. data collection, processing information, and running analysis are usually very time consuming). Future work concerns deeper analysis in seismic scenario definition and creation of a detailed building exposure database. I would have like to extend my research by applying the proposed simulation model to a medium real urban environment. In detail, future work will focus on three main issues:

1. Definition of a comprehensive and harmonized building exposure database. It could be interesting to define criteria for the development of a building taxonomy to describe and classify uniformly the building portfolio of urban areas. This can lead to a better estimation of seismic vulnerability of certain area. The basic idea to collect all the available information and manipulate them to define the main building attributes such as dynamic characteristics, strength properties, nonstructural properties, etc. For this purpose, different sources may be exploited. Whatever vibration analyses and testing are available, the dynamic characteristics of a building can be estimated through the Experimental Modal Analysis (EMA). Furthermore, in some cases, the aforementioned attributes can be assessed by using the Ambient excitation Measurement (AEM). Moreover, satellite images and available GIS inventory data may be used to detect general building information. In addition, existing in-situ data and design documents may be adopted to evaluate the strength and mechanical properties of the building. When no information is accessible or available, it may be useful to have a direct line with customers, stakeholders, and any other subject of the community. They have to be involved in the data collection process in different ways such as providing photos or other illustration, filling questionnaire related to the private or public building stock, and create or share building reports. All the above mentioned data acquisition approach could be managed and standardized to define an exhaustive and comprehensive building exposure database.

2. Definition of seismic scenario at urban level. In this research, a simplified method was adopted to estimate the seismic input to be used in the nonlinear analysis. This procedure was merely used to test and verify the proposed simulation model. The future work could concern the estimation of the seismic microzonation of real urban site through the analysis of the available borehole data. The goal could be the estimation of an urban map of Intensity Measure parameters (e.g. PGA, response spectrum parameters, simplification parameters, etc.) through a soil site response model.

3. Simulation of the dynamic behavior of building based on its global capacity model. In this research, nonlinear time history analyses were performed to assess the dynamic behavior of the building stock. Therefore, these analyses require a huge computational effort in comparison with the other step of the proposed simulation model. Therefore, future work could aim to the estimation of the dynamic building behavior based on the knowledge of the backbone curve. For this purpose, SPO2IDA methodology (Vamvatsikos and Cornell, 2006) could be adopted. It provides a direct connection between the static pushover (SPO) curve and the results of incremental dynamic analysis (IDA). Furthermore, since the proposed capacity model provides a set of backbone curves, the application of the SPO2IDA approach could be a feasible approach for accounting the uncertainties in the simulation results.

4. Development of a technical resilience framework to quantitatively represent the response of physical system under assigned scenario. Definition of a resilience framework of physical systems can help decision makers to identify critical areas of weakness, and to identify actions and programs to improve the resilience at urban level.

References

An, Dawn, Kim, Nam H, & Choi, Joo-Ho. (2015). Practical options for selecting data-driven or physics-based prognostics algorithms with reviews. Reliability Engineering & System Safety, 133, 223-236.

ATC (2012). Seismic Performance Assessment of Buildings. ATC-58, Applied Technology Council, Redwood City, CA.

ATC21. (2017). Rapid visual screening of buildings for potential seismic hazards: A handbook. Federal Emergency Management Agency, US: Government Printing Office.

ATC. (2009). Quantification of Building Seismic Performance Factors. FEMA: Federal Emergency Management Agency.

Azar, H. S., Meskouris, K., & Azar, M. S.. (2004). Probabilistic seismic risk and damageability assessment.

Barani, Simone, Spallarossa, Daniele, & Bazzurro, Paolo. (2009). Disaggregation of probabilistic ground-motion hazard in Italy. Bulletin of the Seismological Society of America, 99(5), 2638-2661.

Bauer, Bernhard, Müller, Jörg P, & Odell, James. (2001). Agent UML: A formalism for specifying multiagent software systems. International journal of software engineering and knowledge engineering, 11(03), 207-230.

Bazzurro, Paolo, & Cornell, C Allin. (2004). Ground-motion amplification in nonlinear soil sites with uncertain properties. Bulletin of the Seismological Society of America, 94(6), 2090-2109.

Boore, David M, & Atkinson, Gail M. (2008). Ground-motion prediction equations for the average horizontal component of PGA, PGV, and 5%-damped PSA at spectral periods between 0.01 s and 10.0 s. Earthquake Spectra, 24(1), 99-138.

Bosher, Lee. (2008). Hazards and the built environment: attaining built-in resilience: Routledge.

Box, George EP. (1979). Robustness in the strategy of scientific model building Robustness in statistics (pp. 201-236): Elsevier.

Brzev, S., Greene, M., Arnold, C., Blondet, M., Cherry, S., Comartin, C., Pantelic, J. (2004). The web-based world housing encyclopedia: housing construction in high seismic risk areas of the world. In 13th world conference on earthquake engineering, Paper (No. 1677).

Bruneau, Michel, Chang, Stephanie E, Eguchi, Ronald T, Lee, George C, O'Rourke, Thomas D, Reinhorn, Andrei M, Von Winterfeldt, Detlof. (2003). A framework to quantitatively assess and enhance the seismic resilience of communities. Earthquake spectra, 19(4), 733-752.

Bruneau, Michel, & Reinhorn, Andrei. (2007). Exploring the concept of seismic resilience for acute care facilities. Earthquake Spectra, 23(1), 41-62.

Bucchi, F.;, Arangio, S.;, & Bontempi, F. (2013). Seismic Assessment of an Historical Masonry Building using Nonlinear Static Analysis. Paper presented at the 14th International Conference on Civil, Structural and Environmental Engineering Computing, Sardinia, Italy.

Cimellaro, Gian Paolo. (2006). Quantification of seismic resilience of health care facilities.

Cimellaro, Gian Paolo, & Marasco, Sebastiano. (2015). A computer-based environment for processing and selection of seismic ground motion records: OPENSIGNAL. Frontiers in Built Environment, 1, 17.

Cimellaro, Gian Paolo, & Marasco, Sebastiano. (2018). Introduction to Dynamics of Structures and Earthquake Engineering (Vol. 45): Springer.

Cimellaro, Gian Paolo, Reinhorn, Andrei M, & Bruneau, Michel. (2010). Framework for analytical quantification of disaster resilience. Engineering Structures, 32(11), 3639-3649.

Cimellaro, Gian Paolo, Reinhorn, Andrei M, & Bruneau, Michel. (2010). Seismic resilience of a hospital system. Structure and Infrastructure Engineering, 6(1-2), 127-144.

Coburn, Andrew W, Spence, Robin JS, & Pomonis, Antonios. (1992). Factors determining human casualty levels in earthquakes: mortality prediction in building collapse. Paper presented at the Proceedings of the First International Forum on Earthquake related Casualties. Madrid, Spain, July 1992.

Cornell, C Allin. (1968). Engineering seismic risk analysis. Bulletin of the seismological society of America, 58(5), 1583-1606.

Corrado, Vincenzo, Ballarini, Ilaria, & Corgnati, Stefano Paolo. (2012). National scientific report on the TABULA activities in Italy: Politecnico di Torino.

CSI. (2018). Integrated Finite Element Analysis and Design of Structures Basic Analysis Reference ManualComputers and Structures, Inc., Berkeley, California, USA.

Cutter, Susan L, Ash, Kevin D, & Emrich, Christopher T. (2014). The geographies of community disaster resilience. Global environmental change, 29, 65-77.

Cyx, W, Renders, N, Van Holm, M, & Verbeke, S. (2011). IEE TABULA-typology approach for building stock energy assessment. Mol, Belgium.

D'Ayala, D., & Kishali, E. (2012). Analytically derived fragility curves for unreinforced masonry buildings in urban contexts. In 15th world Conference of Earthquake Engineering (paper 5266). Lisbon, Portugal.

Destegül, Umut. (2004). Sensitivity Analysis of Soil Site Response Modelling in Seismic Microzonation for Lalitpur, Nepal.

Dobry, R., Borcherdt, R. D., Crouse, C. B., Idriss, I. M., Joyner, W. B., Martin, G. R., & Seed, R. B. (2000). New site coefficients and site classification system used in recent building seismic code provisions. *Earthquake spectra*, *16*(1), 41-67.

DOLCE, M., “Schematizzazione e modellazione per azioni nel piano delle pareti”, Corso sul consolidamento degli edifici in muratura in zona sismica, Ordine degli Ingegneri, Potenza, 1989 (in italian).

Dolce, Mauro, Kappos, Andreas, Masi, Angelo, Penelis, Gregory, & Vona, Marco. (2006). Vulnerability assessment and earthquake damage scenarios of the building stock of Potenza (Southern Italy) using Italian and Greek methodologies. Engineering Structures, 28(3), 357-371.

EC2. (2004). Eurocode 2: Design of concrete structures-Part 1-2: General rules-Structural fire design. European Standards, London.

EC6. (2005). Eurocode 6: Design of Masonry Structures—Part 1-1: General Rules for Reinforced and Unreinforced Masonry Structures. Comité Européen de Normalisation: Brussels, Belgium.

EC8. (2005). Eurocode 8: Design of structures for earthquake resistance-Part 1: General rules, seismic actions and rules for buildings. Brussels: European Committee for Standardization.

El Ezz, Ahmad Abo, Nollet, Marie-José, & Nastev, Miroslav. (2015). Assessment of earthquake-induced damage in Quebec city, Canada. International journal of disaster risk reduction, 12, 16-24.

Eleftheriadou, Anastasia K, & Karabinis, Athanasios I. (2013). Evaluation of damage probability matrices from observational seismic damage data. International Journal of Earthquakes and Structures, 4(3).

Ellingwood, Bruce R, Rosowsky, David V, & Pang, Weichiang. (2008). Performance of light-frame wood residential construction subjected to earthquakes in regions of moderate seismicity. Journal of structural engineering, 134(8), 1353-1363.

Fajfar, Peter. (2000). A nonlinear analysis method for performance-based seismic design. Earthquake spectra, 16(3), 573-592.

Fajfar, Peter, & Gašperšič, Peter. (1996). The N2 method for the seismic damage analysis of RC buildings. Earthquake Engineering & Structural Dynamics, 25(1), 31-46.

FEMA273. (1997). NEHRP guidelines for the seismic rehabilitation of buildings Federal Emergency Management Agency, (Council, Building Seismic Safety ed.). Washington, DC: Building Seismic Safety Council.

FEMA (1998). Handbook for the seismic evaluation of buildings-a prestandard, FEMA 310, Washington D.C.

FEMA (1998). Rapid visual screening of buildings for potential seismic hazards: a handbook, FEMA 154, Washington D.C.

FEMA (2000). Prestandard and Commentary for the Seismic Rehabilitation of Buildings. FEMA 356, Federal Emergency Management Agency, Washington, D.C.

FEMA (2011). Hazus FEMA’s methodology for estimating potential losses from disasters, FEMA Federal Emergency Management Agency, Washington, D.C.

Freeman, S. A. (1998). The capacity spectrum method. In Proceedings of the 11th European conference on earthquake engineering, Paris.

Frumento, S, Giovinazzi, S, Lagomarsino, S, & Podestà, S. (2006). Seismic retrofitting of unreinforced masonry buildings in Italy.

Gamba, P., Dell'Acqua, F., & Lisini, G. (2009). BREC: the Built-up area RECognition tool. In Urban Remote Sensing Event, 2009 Joint (pp. 1-5). IEEE.

GB. (2001). Code for seismic design of buildings [GB 50011-2001]. China Architectural and Building Press, China Google Scholar.

Grossi, P., Kunreuther, H., & Windeler, D. (2005). An introduction to catastrophe models and insurance. In *Catastrophe modeling: A new approach to managing risk* (pp. 23-42). Springer, Boston, MA.

Ghobarah, Ahmed. (2004). On drift limits associated with different damage levels. Paper presented at the Performance-Based Seismic Design Concepts and Implementation: Proceedings of the International Workshop, Bled, Slovenia.

Goodchild, M. F. (2009). Geographic information system. In Encyclopedia of Database Systems (pp. 1231-1236). Springer, Boston, MA.

Hori, M, Ichimura, T, & Oguni, K. (2006). Development of Integrated Earthquake Simulation for estimation of strong ground motion, structural responses and human actions in urban areas.

Inel, Mehmet, & Ozmen, Hayri Baytan. (2006). Effects of plastic hinge properties in nonlinear analysis of reinforced concrete buildings. Engineering structures, 28(11), 1494-1502.

Isukapalli, Sastry S. (1999). Uncertainty analysis of transport-transformation models.

Jaiswal, K., Wald, D., & Porter, K. (2010). A global building inventory for earthquake loss estimation and risk management. *Earthquake Spectra*, *26*(3), 731-748.

Kappos, AJ, Stylianidis, KC, & Pitilakis, K. (1998). Development of seismic risk scenarios based on a hybrid method of vulnerability assessment. Natural Hazards, 17(2), 177-192.

Kappos, A. J., & Panagopoulos, G. (2010). Fragility curves for reinforced concrete buildings in Greece. Structure and Infrastructure Engineering, 6(1-2), 39-53.

Katsanos, Evangelos I, Sextos, Anastasios G, & Manolis, George D. (2010). Selection of earthquake ground motion records: A state-of-the-art review from a structural engineering perspective. Soil Dynamics and Earthquake Engineering, 30(4), 157-169.

Korkmaz, KA. (2009). Seismic safety assessment of unreinforced masonry low-rise buildings in Pakistan and its neighbourhood. Natural Hazards and Earth System Sciences, 9(3), 1021.

Kumar, M., Stafford, P. J., & Elghazouli, A. Y. (2013). Influence of ground motion characteristics on drift demands in steel moment frames designed to Eurocode 8. Engineering Structures, 52, 502-517.

Lagomarsino, Sergio, Penna, Andrea, Galasco, Alessandro, & Cattari, Serena. (2013). TREMURI program: an equivalent frame model for the nonlinear seismic analysis of masonry buildings. Engineering Structures, 56, 1787-1799.

Lee, T. H., & Mosalam, K. M. (2006). Probabilistic Seismic Evaluation of Reinforced Concrete Structural Components and Systems. Pacific Earthquake Engineering Research Center No 2006/04.

Lu, Xinzheng, & Guan, Hong. (2017). Earthquake disaster simulation of civil infrastructures: from tall buildings to urban areas: Springer.

Magenes, G., Calvi, G.M. (1996). Descrizione del metodo SAM e prime applicazioni (in italian).

Maheri, Mahmoud R, & Najafgholipour, MA. (2012). In-plane shear and out-of-plane bending capacity interaction in brick masonry walls. Paper presented at the 15th World Conference on Earthquake Engineering, Lisbon, Portugal.

Maio, Rui, & Tsionis, Georgios. (2015). Seismic fragility curves for the European building stock. Review and evaluation of analytical fragilitycurves.

Mannakkara, Sandeeka, & Wilkinson, Suzanne. (2013). Build back better principles for post-disaster structural improvements. Structural Survey, 31(4), 314-327.

Marasco, Sebastiano, & Cimellaro, GP. (2018). A new energy-based ground motion selection and modification method limiting the dynamic response dispersion and preserving the median demand. Bulletin of Earthquake Engineering, 16(2), 561-581.

MATLAB. (2018). MATLAB Version 2018b, Version 2012b Edition. Natick, MA: The MathWorks Inc.

McAllister, T.P. (2015). Community Resilience Planning Guide for Buildings and Infrastructure Systems, (Vol. 1): NIST SP.

Mirza, S. A., & MacGregor, J. G. (1979). Variability of mechanical properties of reinforcing bars. *Journal of the Structural Division*, *105*(ASCE 14590 Proceeding).

Mouroux, P., & Le Brun, B. (2006). Presentation of RISK-UE project. Bulletin of Earthquake Engineering, 4(4), 323-339.

Mustapha, Karam, Mcheick, Hamid, & Mellouli, Sehl. (2013). Modeling and simulation agent-based of natural disaster complex systems. Procedia Computer Science, 21, 148-155.

NIST. (2015). Community Resilience Planning Guide for Buildings and Infrastructure Systems, Volume I.

Norris, Fran H, Stevens, Susan P, Pfefferbaum, Betty, Wyche, Karen F, & Pfefferbaum, Rose L. (2008). Community resilience as a metaphor, theory, set of capacities, and strategy for disaster readiness. American journal of community psychology, 41(1-2), 127-150.

NTC-08 (2008) Nuove Norme Tecniche per le Costruzioni (NTC08). Consiglio Superiore dei Lavori Pubblici, Ministero delle Infrastrutture, Gazzetta Ufficiale della Repubblica Italiana, n. 29 (in Italian).

Oberkampf, William L, DeLand, Sharon M, Rutherford, Brian M, Diegert, Kathleen V, & Alvin, Kenneth F. (2002). Error and uncertainty in

modeling and simulation. Reliability Engineering & System Safety, 75(3), 333-357.
Ordonez, G. A. (2000). SHAKE2000: A computer program for the 1D analysis of geotechnical earthquake engineering problems. Geomotions, LLC, USA.
Ozcebe, G., Sucuoglu, H., Yucemen, M. S., Yakut, A., & Kubin, J. (2006). Seismic Risk Assessment of Existing Building Stock in Istanbul a Pilot Application in Zeytinburnu District. In Proceedings of 8th US national conference on earthquake engineering, San Fransisco.
Pejovic, Jelena, & Jankovic, Srdjan. (2015). Selection of Ground Motion Intensity Measure for Reinforced Concrete Structure. Procedia Engineering, 117, 588-595.
Pfefferbaum, Rose L, Pfefferbaum, Betty, Nitiéma, Pascal, Houston, J Brian, & Van Horn, Richard L. (2015). Assessing community resilience: An application of the expanded CART survey instrument with affiliated volunteer responders. American Behavioral Scientist, 59(2), 181-199.
Pitilakis, K., Crowley, H., & Kaynia, A. M. (2014). SYNER-G: typology definition and fragility functions for physical elements at seismic risk. Geotechnical, Geological and Earthquake Engineering, 27.
Priestley, M. J. N. (2000). Performance based seismic design. Bulletin of the New Zealand society for earthquake engineering, 33(3), 325-346.
Renschler, Chris S, Frazier, Amy E, Arendt, Lucy A, Cimellaro, Gian Paolo, Reinhorn, Andrei M, & Bruneau, Michel. (2010). A framework for defining and measuring resilience at the community scale: The PEOPLES resilience framework: MCEER Buffalo.
Rizzano, Gianvittorio, Sabatino, Riccardo, & Zambrano, Manuela. (2009). L'influenza delle fasce di piano sulla resistenza di pareti in muratura (in italian).
Rojahn, Christopher, & Sharpe, Roland L. (1985). Earthquake damage evaluation data for California: Applied technology council.
Rose, Adam, & Liao, Shu-Yi. (2005). Modeling regional economic resilience to disasters: A computable general equilibrium analysis of water service disruptions. Journal of Regional Science, 45(1), 75-112.
Rossetto, T, Ioannou, I, & Grant, DN. (2013). Existing empirical fragility and vulnerability relationships: compendium and guide for selection. Pavia, Italy: GEM Foundation.
Schlesinger, S. (1979). Terminology for model credibility. SIMULATION, 32(3), 103-104. doi: 10.1177/003754977903200304.
Shannon, Robert E. (1977). Introduction to simulation languages. Paper presented at the Proceedings of the 9th conference on Winter simulation-Volume 1.
Smith, Neil, & O'Keefe, Phil. (1980). Geography, Marx and the concept of nature. Antipode, 12(2), 30-39.
Steelman, Joshua S, & Hajjar, Jerome F. (2009). Influence of inelastic seismic response modeling on regional loss estimation. Engineering Structures, 31(12), 2976-2987.

Tagawa, H., Miyamura, T., Yamashita, T., & Kohiyama, M. (2015). Detailed Finite Element Analysis of Full-scale Four-story Steel FrameStructure. International Journal of High-Rise Buildings, 1.

Takeda, Toshikazu, Sozen, Mete Avni, & Nielsen, N Norby. (1970). Reinforced concrete response to simulated earthquakes. Journal of the Structural Division, 96(12), 2557-2573.

Tang, Baoxin, Lu, Xinzheng, Ye, Lieping, & Shi, Wei. (2011). Evaluation of collapse resistance of RC frame structures for Chinese schools in seismic design categories B and C. Earthquake engineering and engineering vibration, 10(3), 369.

Terán-Gilmore, A., Zuñiga-Cuevas, O., & Ruiz-García, J. (2009). Displacement-based seismic assessment of low-height confined masonry buildings. Earthquake Spectra, 25(2), 439-464.

Tomazevic, M. (1978). The Computer Program POR Report ZRMK. Ljubljana, Slovenian.

Turnsek V., & Cacovic, F. (1971). Some Experimental Results on the Strength of Brick Masonry Walls. Zavod za Raziskavo Materiala, Konstrukcij, Ljubljana, Yugoslavia.

USGS (2013). "Seismic Hazard Analysis tools. U.S. Geological Survey." < http://earthquake.usgs.gov/hazards/designmaps/grdmotion.php>.

Vamvatsikos, D., & Cornell, C. A. (2002). Incremental dynamic analysis. Earthquake Engineering & Structural Dynamics, 31(3), 491-514.

Vicente, R., Parodi, S., Lagomarsino, S., Varum, H., & Silva, J. A. R. (2008). Seismic vulnerability assessment, damage scenarios and loss estimation: case study of the old city centre of Coimbra, Portugal.

Vrouwenvelder, T. (1997). The JCSS probabilistic model code. *Structural Safety*, *19*(3), 245-251.

Wells, D. L., & Coppersmith, K. J. (1994). New empirical relationships among magnitude, rupture length, rupture width, rupture area, and surface displacement. *Bulletin of the seismological Society of America*, *84*(4), 974-1002.

Whitman, R.V. (1973). Damage Probability Matrices for Prototype buildings; Seismic Design Decision Analysis. Cambridge, Massachusetts: Massachusetts Institute of Technology.

Winkler, RL, Hora, SC, & Baca, RG. (1992). The Quality of Experts' Probabilities Obtained Through Formal Elicitation Techniques. Center for Nuclear Waste Regulatory Analyses CNWRA. San Antonio (TX), USA.

Xu, Zhen, Lu, Xinzheng, Guan, Hong, Han, Bo, & Ren, Aizhu. (2014). Seismic damage simulation in urban areas based on a high-fidelity structural model and a physics engine. Natural hazards, 71(3), 1679-1693.

Yucemen, MS, & Askan, A. (2003). Estimation of earthquake damage probabilities for reinforced concrete buildings Seismic Assessment and Rehabilitation of Existing Buildings (pp. 149-164): Springer.